

INFORMATION TO USERS

This manuscript has been reproduced from the microfilm master. UMI films the text directly from the original or copy submitted. Thus, some thesis and dissertation copies are in typewriter face, while others may be from any type of computer printer.

The quality of this reproduction is dependent upon the quality of the copy submitted. Broken or indistinct print, colored or poor quality illustrations and photographs, print bleedthrough, substandard margins, and improper alignment can adversely affect reproduction.

In the unlikely event that the author did not send UMI a complete manuscript and there are missing pages, these will be noted. Also, if unauthorized copyright material had to be removed, a note will indicate the deletion.

Oversize materials (e.g., maps, drawings, charts) are reproduced by sectioning the original, beginning at the upper left-hand corner and continuing from left to right in equal sections with small overlaps.

ProQuest Information and Learning
300 North Zeeb Road, Ann Arbor, MI 48106-1346 USA
800-521-0600

UMI[®]

University of Alberta

A NOVEL SIGNALLING SCHEME BASED ON TRANSMITTED REFERENCE
FOR UWB COMMUNICATIONS

by

Alfred Lee



A thesis submitted to the Faculty of Graduate Studies and Research in partial
fulfillment of the requirements for the degree of **Master of Science**.

Department of Electrical and Computer Engineering

Edmonton, Alberta
Spring 2005



Library and
Archives Canada

Bibliothèque et
Archives Canada

Published Heritage
Branch

Direction du
Patrimoine de l'édition

395 Wellington Street
Ottawa ON K1A 0N4
Canada

395, rue Wellington
Ottawa ON K1A 0N4
Canada

Your file *Votre référence*

ISBN:

Our file *Notre référence*

ISBN:

NOTICE:

The author has granted a non-exclusive license allowing Library and Archives Canada to reproduce, publish, archive, preserve, conserve, communicate to the public by telecommunication or on the Internet, loan, distribute and sell theses worldwide, for commercial or non-commercial purposes, in microform, paper, electronic and/or any other formats.

The author retains copyright ownership and moral rights in this thesis. Neither the thesis nor substantial extracts from it may be printed or otherwise reproduced without the author's permission.

AVIS:

L'auteur a accordé une licence non exclusive permettant à la Bibliothèque et Archives Canada de reproduire, publier, archiver, sauvegarder, conserver, transmettre au public par télécommunication ou par l'Internet, prêter, distribuer et vendre des thèses partout dans le monde, à des fins commerciales ou autres, sur support microforme, papier, électronique et/ou autres formats.

L'auteur conserve la propriété du droit d'auteur et des droits moraux qui protègent cette thèse. Ni la thèse ni des extraits substantiels de celle-ci ne doivent être imprimés ou autrement reproduits sans son autorisation.

In compliance with the Canadian Privacy Act some supporting forms may have been removed from this thesis.

Conformément à la loi canadienne sur la protection de la vie privée, quelques formulaires secondaires ont été enlevés de cette thèse.

While these forms may be included in the document page count, their removal does not represent any loss of content from the thesis.

Bien que ces formulaires aient inclus dans la pagination, il n'y aura aucun contenu manquant.


Canada

To my parents

Abstract

The demands for higher data rates in wireless personal area networks have led to the current interest and development of the ultra-wideband (UWB) communication technology. An ultra-wideband (UWB) channel has the potential to provide both low cost and high speed wireless devices with its extensive spectrum resources. However, how to design an efficient, reliable, low complexity transmission technology for UWB channels is still a big question. In this thesis, a novel dual pulse (DP) transmission scheme that improves the data rate of a popular and simple technique called transmitted reference (TR) is proposed. A complete system including the transmitter and receiver for the DP scheme is presented and extensively studied. Three receiver designs based on non-coherent general selection combining (GSC), absolute threshold-GSC (AT-GSC), and normalised threshold-GSC (NT-GSC) of a front-end autocorrelator are proposed and their performances are analysed and simulated thoroughly in UWB channels. Furthermore, an improved version of the DP scheme called improved DP (*iDP*) is also proposed. The new DP designs offer a range of advantages over the traditional TR system, such as doubled data rate, more immunity to channel variation, less detection delay and ease of implementing delay units, etc., while maintaining similar performance and complexity.

Acknowledgements

I would like to express my gratitude to my supervisor, Dr. Xiaodai Dong, for her patient guidance, insightful technical advice and continuous encouragement throughout my study at the University of Alberta. Most of the ideas in this thesis was inspired by Dr. Xiaodai Dong.

I thank Lei, Zhengang, Mohsen, Yue and many others in the department for their technical comments and suggestions. I thank Teresia Ng for her continuous support and encouragement through my master degree program. Special thanks to Lei Xiao for providing suggestions and help on my thesis.

This work made use of the infrastructure and resources of CNS (Computing and Network Services) and the University of Alberta.

Table of Contents

1	Introduction	1
1.1	Background	1
1.2	History and Regulation of UWB	4
1.3	UWB Fading Environments	5
1.4	Current UWB Developments	7
1.5	Thesis Outline	9
2	The Transmitted Reference system	11
2.1	Introduction	11
2.2	TR System Overview	13
2.3	Receiver Performance	15
2.3.1	Autocorrelation Receiver	16
2.3.2	Autocorrelator with Noise Averaging	19
2.4	IEEE channel model	23
2.5	Simulation Results and Discussion	25
2.5.1	Simulation Setup	27
2.5.2	The effect of T_{tr} on basic Autocorrelation Receiver	29
2.5.3	The effect of T_{tr} on noise averaging Autocorrelation Receiver	34
2.5.4	The effect of N_p on noise averaging Autocorrelation Receiver	34
2.6	Conclusion	44
3	The DP - Dual Pulse system	45
3.1	Introduction	45
3.2	DP Transmitter System	46
3.3	DP Receiver Performance	49
3.3.1	Known path delay τ_k 's	49
3.3.2	Known path delay τ_k 's with noise averaging	51
3.3.3	Receiver design for unknown path delay τ_k 's	54
3.3.3.1	Generalised Selection Combining (GSC)	56
3.3.3.2	Absolute Threshold GSC (AT-GSC)	61

3.3.3.3	Normalised Threshold (NT-GSC)	63
3.3.4	Noise averaging applied on unknown path delay τ_k 's	66
3.4	Simulation Results and Discussion	68
3.4.1	Simulation setup	69
3.4.2	The effect of L on the basic GSC Receiver	69
3.4.3	The effect of L on the GSC Receiver with noise averaging	70
3.4.4	The effect of N_p on GSC Receiver with noise averaging	75
3.4.5	The effect of D_{th} on the basic AT-GSC Receiver	79
3.4.6	The effect of D_{th} on the AT-GSC Receiver with noise averaging	84
3.4.7	The effect of N_p on the AT-GSC Receiver with noise averaging	92
3.4.8	The effect of η_{th} on the basic NT-GSC Receiver	92
3.4.9	The effect of η_{th} on the NT-GSC Receiver with noise averaging	92
3.4.10	The effect of N_p on the NT-GSC Receiver with noise averaging	101
3.4.11	The effect of T_{dp-int} on the basic DP-Int Receiver	101
3.4.12	The effect of T_{dp-int} on the DP-Int Receiver with noise averaging	110
3.4.13	Performance Comparison between TR, GSC, AT-GSC, NT-GSC and DP-Int Receivers	115
3.5	Conclusion	119
4	The Improved DP System	125
4.1	Introduction	125
4.2	Improved DP System Overview	126
4.3	Receiver Design	128
4.4	Simulation Results and Discussion	130
4.4.1	Simulation Setup	131
4.4.2	Comparison between Improved DP systems of various combining schemes and the TR system	132
4.4.3	Comparison between Improved DP and DP systems	132
4.5	Conclusion	137
5	Summaries and Conclusion	143
5.1	Conclusion	143
5.2	Suggestions for Future Work	145
	Bibliography	146

List of Figures

1.1	FCC defined indoor UWB spectrum mask	5
2.1	The binary PAM modulated TR system signal pair	14
2.2	TR system transmitter block diagram	14
2.3	TR autocorrelation receiver block diagram	16
2.4	The channel response of a simple 20 path test channel	19
2.5	Performance of autocorrelation receiver in a 20 path channel	20
2.6	TR autocorrelation receiver with noise averaging block diagram	21
2.7	Performance of autocorrelation receiver with noise averaging in a 20 path channel	23
2.8	Sample channel realization of CM1	26
2.9	Sample channel realization of CM4	26
2.10	The pulse shape of the 2 nd derivative Gaussian pulse $p(t)$	27
2.11	The frequency response of the 2 nd derivative Gaussian pulse $p(t)$	28
2.12	Effect of T_{tr} on TR systems with autocorrelation receiver in CM1	30
2.13	Effect of T_{tr} on TR systems with autocorrelation receiver in CM2	31
2.14	Effect of T_{tr} on TR systems with autocorrelation receiver in CM3	32
2.15	Effect of T_{tr} on TR systems with autocorrelation receiver in CM4	33
2.16	Effect of T_{tr} on TR systems with noise averaging autocorrelation receiver in CM1	35
2.17	Effect of T_{tr} on TR systems with noise averaging autocorrelation receiver in CM2	36
2.18	Effect of T_{tr} on TR systems with noise averaging autocorrelation receiver in CM3	37
2.19	Effect of T_{tr} on TR systems with noise averaging autocorrelation receiver in CM4	38
2.20	Effect of N_p on TR systems with noise averaging autocorrelation receiver in CM1	40
2.21	Effect of N_p on TR systems with noise averaging autocorrelation receiver in CM2	41
2.22	Effect of N_p on TR systems with noise averaging autocorrelation receiver in CM3	42

2.23	Effect of N_p on TR systems with noise averaging autocorrelation receiver in CM4	43
3.1	Illustration of OOK and binary PAM modulated DP signal $g_{dp}(t)$	47
3.2	Binary PAM modulated DP system transmitter block diagram	48
3.3	Block diagram for DP known τ receiver design	50
3.4	Numerical analysis and simulation comparison for known τ receiver	52
3.5	Block diagram for DP known τ receiver design	53
3.6	Numerical analysis and simulation comparison for noise averaging known τ receiver	55
3.7	Block diagram for DP unknown τ receiver design	55
3.8	The impulse response of a simple 5 path test channel	61
3.9	Numerical analysis and simulation comparison for DP GSC scheme	62
3.10	The channel response of a simple 10 path test channel	63
3.11	Numerical analysis and simulation comparison for DP AT-GSC scheme	64
3.12	Numerical analysis and simulation comparison for DP NT-GSC scheme	67
3.13	Effect of L on DP-GSC systems in CM1	71
3.14	Effect of L on DP-GSC systems in CM2	72
3.15	Effect of L on DP-GSC systems in CM3	73
3.16	Effect of L on DP-GSC systems in CM4	74
3.17	Effect of L on DP-GSC systems with noise averaging in CM1 .	75
3.18	Effect of L on DP-GSC systems with noise averaging in CM2 .	76
3.19	Effect of L on DP-GSC systems with noise averaging in CM3 .	77
3.20	Effect of L on DP-GSC systems with noise averaging in CM4 .	78
3.21	Effect of N_p on DP-GSC systems with noise averaging in CM1	80
3.22	Effect of N_p on DP-GSC systems with noise averaging in CM2	81
3.23	Effect of N_p on DP-GSC systems with noise averaging in CM3	82
3.24	Effect of N_p on DP-GSC systems with noise averaging in CM4	83
3.25	Effect of D_{th} on DP AT-GSC systems in CM1	84
3.26	Effect of D_{th} on DP AT-GSC systems in CM2	85
3.27	Effect of D_{th} on DP AT-GSC systems in CM3	86
3.28	Effect of D_{th} on DP AT-GSC systems in CM4	87
3.29	Effect of D_{th} on DP AT-GSC systems with noise averaging in CM1	88
3.30	Effect of D_{th} on DP AT-GSC systems with noise averaging in CM2	89
3.31	Effect of D_{th} on DP AT-GSC systems with noise averaging in CM3	90

3.32	Effect of D_{th} on DP AT-GSC systems with noise averaging in CM4	91
3.33	Effect of N_p on DP AT-GSC systems with noise averaging in CM1	93
3.34	Effect of N_p on DP AT-GSC systems with noise averaging in CM2	94
3.35	Effect of N_p on DP AT-GSC systems with noise averaging in CM3	95
3.36	Effect of N_p on DP AT-GSC systems with noise averaging in CM4	96
3.37	Effect of η_{th} on DP NT-GSC systems in CM1	97
3.38	Effect of η_{th} on DP NT-GSC systems in CM2	98
3.39	Effect of η_{th} on DP NT-GSC systems in CM3	99
3.40	Effect of η_{th} on DP NT-GSC systems in CM4	100
3.41	Effect of η_{th} on DP NT-GSC systems with noise averaging in CM1	102
3.42	Effect of η_{th} on DP NT-GSC systems with noise averaging in CM2	103
3.43	Effect of η_{th} on DP NT-GSC systems with noise averaging in CM3	104
3.44	Effect of η_{th} on DP NT-GSC systems with noise averaging in CM4	105
3.45	Effect of N_p on DP NT-GSC systems with noise averaging in CM1	106
3.46	Effect of N_p on DP NT-GSC systems with noise averaging in CM2	107
3.47	Effect of N_p on DP NT-GSC systems with noise averaging in CM3	108
3.48	Effect of N_p on DP NT-GSC systems with noise averaging in CM4	109
3.49	Effect of T_{dp-int} on DP-Int systems in CM1	111
3.50	Effect of T_{dp-int} on DP-Int systems in CM2	112
3.51	Effect of T_{dp-int} on DP-Int systems in CM3	113
3.52	Effect of T_{dp-int} on DP-Int systems in CM4	114
3.53	Effect of T_{dp-int} on DP-Int systems with noise averaging in CM1	115
3.54	Effect of T_{dp-int} on DP-Int systems with noise averaging in CM2	116
3.55	Effect of T_{dp-int} on DP-Int systems with noise averaging in CM3	117
3.56	Effect of T_{dp-int} on DP-Int systems with noise averaging in CM4	118
3.57	Comparison between TR and proposed DP systems for CM1 .	120
3.58	Comparison between TR and proposed DP systems for CM2 .	121
3.59	Comparison between TR and proposed DP systems for CM3 .	122
3.60	Comparison between TR and proposed DP systems for CM4 .	123
4.1	Illustration of binary PAM modulated i DP signal set $g_1(t)$ and $g_2(t)$	127
4.2	Block diagram for i DP receiver design	129

4.3	Block diagram for <i>i</i> DP receiver design with noise averaging . .	130
4.4	Comparison between TR and proposed <i>i</i> DP systems for CM1 .	133
4.5	Comparison between TR and proposed <i>i</i> DP systems for CM2 .	134
4.6	Comparison between TR and proposed <i>i</i> DP systems for CM3 .	135
4.7	Comparison between TR and proposed <i>i</i> DP systems for CM4 .	136
4.8	Comparison between DP and <i>i</i> DP systems for CM1	138
4.9	Comparison between DP and <i>i</i> DP systems for CM2	139
4.10	Comparison between DP and <i>i</i> DP systems for CM3	140
4.11	Comparison between DP and <i>i</i> DP systems for CM4	141

List of Symbols

Symbol	Definition
A	Number of multipaths considered ($\leq K$)
A_i	Subspace of \mathcal{S}_D
b_i	The i th modulated binary bit $\in \{-1, 1\}$
\mathcal{B}_i	Subspace of \mathcal{S}_D
D	Decision variable
D_k	Autocorrelator output of the k th path
D_l	The l th sub-decision variable
D_{th}	Decision threshold
$erfc(x)$	Complementary error function
E_b	Average received energy per bit
$f(x)$	Probability density function of x
$F(x)$	Cumulative distribution function of x
$g_1(t)$	First DP pulse set for the i DP system
$g_2(t)$	Second DP pulse set for the i DP system
$g_{dp}(t)$	Ultra-wideband pulse for the DP system
$g_{idp}(t)$	Ultra-wideband pulse set for the i DP system
$g_{rx}(t)$	Received ultra-wideband pulse shape for the TR system
$g_{tr}(t)$	Ultra-wideband pulse for the TR system
$h(t)$	UWB multipath channel impulse response
I_i	Index set for subspace A_i
K	Total number of multipaths
L	Number of autocorrelator outputs summed
L_t	Total number of possible paths
M	Length of Hamming window
N_0	One-sided power spectrum density of white Gaussian noise
N_p	Number of frames averaged
N_s	Repetition rate of an information signal transmitted
\tilde{n}	Zero mean additive white Gaussian noise
n	Low-pass filtered Gaussian noise
$p(t)$	Transmitted sub-pulse of a dual pulse
$p_{rx}(t)$	Received pulse shape corresponding to $p(t)$

$R(\tau)$	Autocorrelation function of the signal pulse
$R_n(\tau)$	Noise autocorrelation function
$\tilde{r}_{dp}(t)$	Received DP signal
$r_{dat}(t)$	Received IPI free data signal in the i DP scheme
$r_{dp}(t)$	Low-pass filtered received DP signal
$r_{ref}(t)$	Received IPI free reference signal in the i DP scheme
$\tilde{r}_{tr}(t)$	Received TR signal
$r_{tr}(t)$	Low-pass filtered received TR signal
S_D	Probability space of (D_1, \dots, D_{L_t})
$s_1(t)$	First sub-pulse of the DP scheme
$s_2(t)$	Second sub-pulse of the DP scheme
$s_{dp}(t)$	Transmitted DP signal
$s_{tr}(t)$	Transmitted TR signal
$T(x)$	Testing function
T_d	Time delay between two transmitted pulses
T_f	Transmission time frame length
$T_{m ds}$	Maximum delay spread of the channel
T_{tr}	Autocorrelator integration length
T_w	Pulse duration
W	One-sided bandwidth of the lowpass filter
$w[n]$	Hamming window coefficients
α_k	Amplitude of the k_{th} path
α	Channel amplitude vector
μ	Mean of a random variable
$\Phi(s)$	Moment generating function
$\Psi_l(s)$	Incomplete MGF of the first kind
$\tilde{\Psi}_l(s)$	Incomplete MGF of the second kind
σ^2	Variance of a random variable
σ_n^2	The variance of the noise to noise term
τ_k	Delay of the k_{th} path
τ	Channel delay vector

List of Abbreviations

Acronym	Definition
3G	Third Generation
AT-GSC	Absolute Threshold Generalised Selection Combining
AWGN	Additive White Gaussian Noise
BER	Bit Error Rate
CDF	Cumulative Distribution Function
CDMA	Code Division Multiple Access
CM	Channel Model
DP	Dual Pulse
DP-Int	Dual Pulse Integrator
DS-CDMA	Direct-Sequence Code Division Multiple Access
EIRP	Effective Isotropic Radiated Power
FCC	Federal Communications Commission
GPS	Global Positioning System
GSC	Generalised Selection Combining
GSM	Global System for Mobile Communications
iDP	Improved Dual Pulse
i.n.d.	Independent and Non-identically Distributed
I&D	Integrate-and-Dump
IEEE	Institute of Electrical and Electronics Engineers
IPI	Inter-Path Interference
ISI	Inter-Symbol Interference
ISM	Industrial, Scientific, and Medical
LOS	Line-Of-Sight
MGF	Moment Generating Function
MMS	Multimedia Messaging Service
NLOS	Non-Line-Of-Sight
NT-GSC	Normalised Threshold Generalised Selection Combining
OFDM	Orthogonal Frequency Division Multiplex
OOK	On-Off Keying
PAM	Pulse Amplitude Modulation
PDA	Personal Digital Assistant
PDF	Probability Density Function

PHY	Physical Layer
PPM	Pulse Position Modulation
PRAKE	Partial RAKE
R.V.	Random Variable
s.t.	Such that
SMS	Short Message Service
SNR	Signal-to-Noise Ratio
STDL	Stochastic Tapped-Delay-Line
TH-CDMA	Time-Hopping Code Division Multiple Access
TR	Transmitted Reference
USB	Universal Serial Bus
UWB	Ultra-WideBand
WCDMA	Wideband Code Division Multiple Access
WiFi	Wireless Fidelity
WLAN	Wireless Local Area Network
WPAN	Wireless Personal Area Network

Chapter 1

Introduction

1.1 Background

Driven by the increasing market demand, wireless communications has maintained as one of the fastest growing segments in telecommunications industry. The mobile market in the United States has seen an addition of 14 million new mobile subscribers in 2003, an increase from 12 million in 2002 [1]. The total voice revenue reported in the United States cellular market for year 2003 was 90 billion dollars. While revenues from voice calls still account for the majority of the income for wireless operators, the use of wireless data services such as short message service (SMS), multimedia messaging service (MMS), and wireless internet has increased substantially in the past few years. It was predicted that by year 2010, over 50% of the mobile revenue will come from mobile data service in North America and Europe [2].

As the wireless traffic migrates away from voice orientated networks into networks that support both voice and data, the demand for high speed wireless networks increases. The third generation (3G) cellular network holds promise to provide high data rate access for wireless data services of up to 2 Mb/s rate [3]. However, the cost of the dedicated spectrum required for 3G networks is extremely high; a 20 year 3G spectrum license cost United Kingdom operator Vodafone 5.964 billion pounds in the year 2000 auction [4]. With the high cost and relatively low throughput compared to wireless fidelity (WiFi)

of the Institute of Electrical and Electronics Engineers (IEEE) 802.11x's standards used in wireless local area network (WLAN), wireless hotspot based on WLAN technology has quickly emerged to be the cost effective way to provide fast wireless internet/data access in a low mobility environment. When operates in IEEE 802.11a or 802.11g standards which utilise unlicensed industrial, scientific, and medical (ISM) bands [5] of 5 GHz and 2.4 GHz respectively, WLAN is able to provide speed of upto 54 Mb/s [6].

At the time of WLAN development, a new network named wireless personal area network (WPAN) is also under development. WPAN is specified in IEEE 802.15 standards, where Bluetooth is the current technology used in WPAN [7,8]. WPAN is developed as a technology to connect electronic devices within a personal's radius together, and to replace the wired connections for such devices. Like the WLAN, as the technology matures, more and more companies have realised the potential of WPAN and we see an increasing number of products having Bluetooth build-in. Some of the products with Bluetooth build-in are cellphones [9], headsets, personal digital assistants (PDAs), and various computer devices [10,11]. With the new legislation to prevent drivers from talking on cellphone without a handsfree device, handsfree headsets are becoming a standard requirement. This has helped turning Bluetooth into a new feature for car manufacturers. Luxury manufacturers such as Acura, BMW, Lexus have made this feature available [12] on their cars, enabling Bluetooth cellphones to integrate into the audio system. The demand for WPAN is ever increasing. Recent study by In-Stat/MDR addressed that in 2003 the worldwide Bluetooth chipset shipments reached 69 million and predicted sales of more than 700 million units in 2008 [13].

With the increasing popularity of wireless connection between different devices, the demand for high speed connection between devices has also increased. Bluetooth technology group [8] has recently released Bluetooth 2.0, which increases its transfer rate by 3 to 10 times. Apple Computer Inc. has released new notebooks that support such transfer rate of up to 3 Mb/s based

on Bluetooth 2.0 technology [10]. However, Bluetooth's data rate is still far too slow as a replacement for universal serial bus (USB) and Firewire connections for items such as external hard drives, external DVD readers, and portable music players.

In order to integrate USB and Firewire connection into WPAN, the wireless connection has to be able to support transfer speed of over 500 Mb/s. The IEEE 802.15.3a WPAN working group has found ultra-wideband (UWB) a possible technology that can support data rate of over 500 Mb/s in future WPAN products [14]. In fact, the UWB development firm Alereon has recently released a UWB evaluation kit designed as a USB cable replacement. The evaluation kit is capable of supporting a data rate of 480 Mb/s over a UWB wireless link [15]. With the early development of UWB devices already capable of supporting such a high data rate, UWB has positioned itself as a promising physical layer candidate for high-speed WPAN. This would allow WPAN to be implemented in a new range of products with a high speed requirement that Bluetooth is not able to support. However, the usage of UWB technology does not stop at the application of WPAN. The UWB technology has also found home in vehicular radar systems and imaging systems. The application of UWB technology in these systems improves resolution and sensitivity [16]. Another application of UWB is in the sensor networks, where aside from the high data rate capability of the UWB technology, the low power and low implementation cost of UWB are also very attractive properties [16].

The UWB technology provides a lot of promises, but it is still in early development. The properties of UWB channels are not yet well known. There are also other concerns, such as how UWB will coexist with "narrowband" signals and what is the most cost effective design for UWB transmitters and receivers. In this thesis, we propose efficient transmitter and receiver techniques for UWB and analyse their performance in realistic UWB channels.

This chapter is organised as follows. A brief history of UWB and the spectrum regulation for UWB transmission is presented in Section 1.2. In

Section 1.3, the UWB fading environment is discussed with channel modelling attempt presented by various researchers. Section 1.4 contains a brief overview of current UWB developments. The outline of the thesis is given in Section 1.5.

1.2 History and Regulation of UWB

UWB signals are defined as baseband pulses with very short duration, typically in nanosecond range and occupy a large frequency range from near DC to a few gigahertz [17]. The official definition of UWB given by Federal Communications Commission (FCC) refers to transmission systems with a bandwidth greater than 500 MHz or have a fractional bandwidth in excess of 20%. The fractional bandwidth is defined as B/f_c , where B represents the -10 dB bandwidth and f_c is the center frequency [18]. Use of very large bandwidth for communication can be dated back to the start of wireless transmission, where signal was generated by spark-gap transmitters. Such wireless communication system was used by Guglielmo Marconi who successfully completed the first wireless transmission between St. John's Newfoundland and Cornwall, England in 1901 [19]. Since then, government regulations have limited the bandwidth usage to limit the interference between communication systems, and thus promoted the development of narrowband communication systems. However, with the increasing demand of communication capacity, a shift to wider bandwidth has been observed in the wireless industry in order to provide high speed data transmission and improved capacity.

Before the United State Department of Defense applied the term UWB in 1989 [16, 20], the UWB technology were referred to as carrier-free, baseband or impulse technology. Impulse radio was developed as far back as 1940's when several impulse radio system patents were filed [21]. The patent filed by Ross and Robbins in 1973 is the first milestone for UWB communication which set up the foundation for UWB communication developments [22]. On

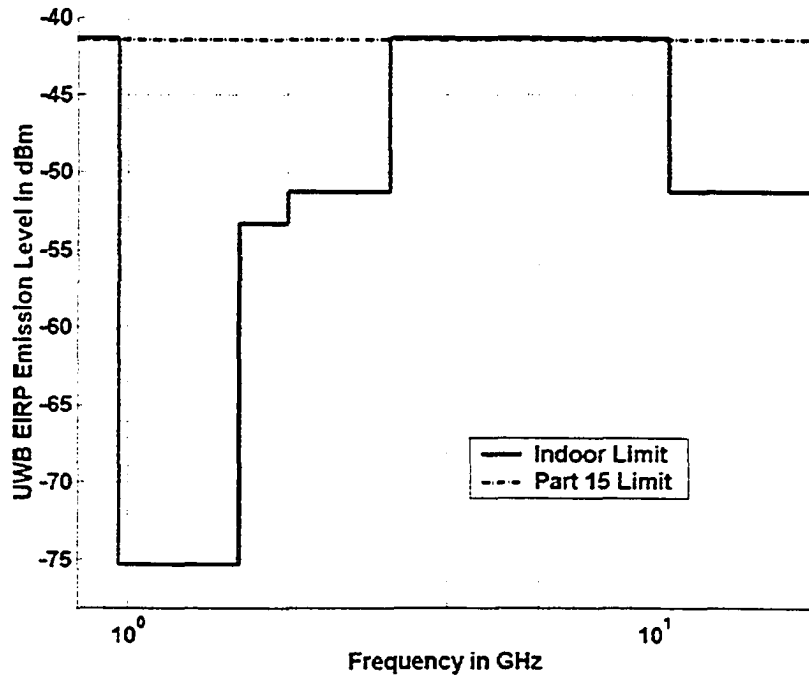


Figure 1.1: FCC defined indoor UWB spectrum mask

April 22, 2002, FCC issued UWB regulations under Part 15 of Commission's Rules, which outlined the -10 dB bandwidth of UWB signal to be within 3.1 GHz to 10.6 GHz and effective isotropic radiated power (EIRP) limit defined as -41.3 dBm [18]. Fig. 1.1 is a graphical representation of the FCC UWB spectral mask for indoor channels under rule Part 15. The UWB regulation set by FCC not only legalised the UWB research, but also provided a defined specification, gave researchers a standardised UWB frequency range to work with.

1.3 UWB Fading Environments

One of the challenges ultra-wideband researchers face is the lack of a well defined channel propagation model. While the "narrowband" channel has been investigated extensively for a long time and well understood, with the large

bandwidth and short pulse duration of the UWB signal, more structures of the channel is exposed, and thus the UWB communication channel has largely been unknown to researchers. Since UWB is aimed at providing wireless connection in the indoor environment, the channel behaviour is even more complicated and less understood. This leads to modelling of the UWB channel from experimental measurements by researchers.

In UWB research, since there was no well known UWB statistical channel model, the analyses were done with additive white gaussian noise (AWGN) channel with or without multipath as the UWB channel [23–25]. In the first published finding of UWB channels, Win *et al.* [26] conducted an UWB signal propagation experiment with bandwidth in excess of 1 GHz, in 14 different locations in a modern office building. The finding from the experiment showed an increased noise floor from offices at the edge of building with large windows. It also found that the effect of office doors and large computer monitors were minimal, and results in [26] showed that UWB signal does not suffer much from fades.

Intel also started projects to characterise the UWB channel. Leslie *et al.* [27] analysed the UWB channel from 2 GHz to 8 GHz range in a residential area. With the 612 different transmit and receive location combinations, they observed that non-line of sight (NLOS) paths contained five times as much multipath fragmentation as line of sight (LOS) paths. In an effort to characterise different channel models, Intel counted the number of paths that are within 10 dB of the peak return path. A mean of 7 paths for LOS and 35 paths for NLOS with standard deviation of 5 and 30 paths respectively were observed. This finding indicated that in NLOS channels, the channel energy are separated into more paths than in LOS channel.

Cassioli *et al.* [28] analysed the extensive UWB channel measurements for a typical modern office building and formed the stochastic tapped-delay-line (STDLD) model for the UWB indoor channel. The measurements procedure separated the large scale and small scale fading. For large scale fading which

referred to parameter affected by switching from one room to another, the model determines that the average power decays exponentially with the decay constant determined statistically. It is also found that the total received energy experienced a lognormal shadowing around the mean energy given by the path-loss power law. For small scale fading which defines small location change within the room, the energy gain followed a Gamma distribution with m factor decreasing with increasing excess delay. This model provided a detailed representation of the UWB channels, but the statistical value it depends on is site specific.

There are many other UWB channel models and evaluations presented by others, which were all taken into consideration when the IEEE 802.15.3a task group established the standard UWB channels [29, 30]. The standard UWB channels were established to provide an easy to use channel model and a common ground for comparison between different transmission methods. The IEEE 802.15 standard model is based on a modified Saleh-Valenzuela model [31] with a lognormal amplitude distribution, and a shadowing term to account for total received multipath energy variation that results from blockage of LOS path. It also assumes the channel stays either completely static or changes completely from one data burst to the next. The model was proposed with four sets of parameters designed to simulate different channel scenarios from LOS to NLOS. The detailed description of the channel model can be found in Section 2.4.

1.4 Current UWB Developments

In the beginning of the UWB development, the most common modulation method proposed for UWB was pulse-position modulation (PPM) [32-35]. Another modulation scheme that is also used in UWB communications is on-off keying (OOK) [36]. With multiuser in mind, modulations such as time-hopping code division multiple access (TH-CDMA) [37], direct-spread code

division multiple access (DS-CDMA) [38], orthogonal frequency division multiplex (OFDM) [39] are often investigated in UWB research. In fact, in the establishment of the IEEE 802.15.3a standard, the two remaining proposals in the running are the one based on OFDM modulation and the other based on DS-CDMA modulation [14].

Besides the modulation scheme, coexistence of UWB with the current narrowband and wideband systems such as the global positioning system (GPS), GSM and WCDMA is a subject of plenty study [40]. The pulse shaping [41,42] of the UWB signals is also very important, since maximizing the transmitted power of a UWB signal while satisfying the FCC spectrum mask has a direct impact on the system performance. The UWB pulse normally has a duration in the order of nanosecond, and accurate timing acquisition becomes critical and challenging [43]. Other on-going research effort focused on receiver designs and signalling schemes. Some of the UWB receiver designs presented including various rake receiver designs [44–48] and suboptimal design such as autocorrelation receivers [49]. The signalling scheme used also determines the type of receiver used. For example, autocorrelation receivers are often used with transmitted reference (TR) signalling scheme [49]. Another signalling scheme used for UWB is the pilot symbol signalling scheme [50]. While the current development of UWB covers more areas than that mentioned here, these topics provided a good indication of some areas that the UWB development is heading.

The UWB technology has also been adopted as one of the physical layer candidates in the IEEE 802.15.4a which defines the WPAN for low rate applications [51]. The main focus of the IEEE 802.15.4a task group is to create a low cost and low power consumption devices for sensor networks or similar systems. At the time of writing of this thesis, the development of IEEE 802.15.4a standard is still at a very early stage with proposals being presented and selection process just started. In connection with all the on-going research in the UWB area, a new transmission scheme is proposed in this thesis that

retains the low complexity and robustness of the TR system but doubles the data rate, which makes it a good candidate for IEEE 802.15.4a applications. The new scheme also offers other benefits that are detailed in the subsequent chapters.

1.5 Thesis Outline

In Chapter 2, the conventional transmitted reference (TR) design is presented and its receiver performance is analysed. Two receiver variants are analysed here; one is a simple autocorrelation detector and the other is the autocorrelation detector with noise averaging applied to the reference signal. Details of the IEEE 802.15.3a channel models are presented, and these channel models are employed in the simulation. The performance of TR system with regular autocorrelation receiver and with noise averaging autocorrelation receiver under different channel models (CM1-CM4) are simulated. The efficiency of the noise averaging technique is also simulated.

A new scheme called dual pulse (DP) transmission is introduced in Chapter 3. Details of the DP system are presented and the receiver performances with channel path delay knowledge are analysed, followed by three receivers that require no priori channel knowledge at all. The receivers are based on non-coherent general selection combining (GSC), absolute threshold-GSC (AT-GSC), and normalised threshold-GSC (NT-GSC). Their performances are analysed and numerically evaluated with and without noise averaging applied. A simple autocorrelation receiver design is also introduced for the DP system. The new DP system with the three “GSC” receivers as well as the autocorrelation receiver are simulated extensively to obtain the effect of different design parameters on system performance in realistic UWB channels. The simulation results on the comparison between the DP system and the TR system are also compared in this chapter.

Chapter 4 introduces a modified version of the DP system called the im-

proved DP (*i*DP) system, that eliminates possible inter-pulse interference (IPI) in the DP system. The new system is then simulated and compared with the equivalent TR system. To show the *i*DP system's IPI elimination property, it is also compared with the DP system presented in Chapter 3.

Finally, the new schemes presented are concluded in Chapter 5, with the possible future work outlined.

Chapter 2

The Transmitted Reference system

2.1 Introduction

Many different transmitter and receiver designs have been proposed for the UWB channels. By far the most popular designs are based on the rake receiver structure [44-48]. Since a UWB channel has a large number of distinct paths, it creates an ideal situation for the application of rake type receivers. The “all-rake” receiver [44] which collects energy of all the paths of the UWB channel is the ideal receiver system. However, the large number of correlators needed in the “all-rake” receiver means extremely high complexity and thus an increase in power consumption, which makes it impossible to build the receiver in reality. Therefore, partial rake and selective rake receivers were proposed [44, 47]. The partial rake receiver collects the energy of the first X number of paths of the UWB channel. It is straightforward to see that when the number of collected paths increases, the performance improves for the partial rake receiver, because more channel energy is collected in the receiver [46]. An improved version of the partial rake receiver, called selective rake receiver is also proposed [47]. The selective rake receiver picks the X strongest paths of the UWB channel and decodes those paths. The selective rake receiver has an improved performance over the partial rake receiver but it is more complicated

to implement.

In general, rake receivers with a large number of fingers are very complex. They require perfect knowledge of the channel and accurate timing of each path in order to have good performance. Due to the large number of paths and the short pulse durations, estimating the UWB channel is not an easy task. Therefore the channel estimation process adds a lot of complexity to the overall rake receiver design. These complications will add up to a higher cost for the UWB devices, which is against the goal of UWB to provide cheap high speed wireless devices.

One of the receiver designs that have gained popularity recently is the autocorrelation receiver based on the transmitted reference (TR) signal design. The advantage of the TR autocorrelator technique is the elimination of the complicated channel estimation required in the rake receiver design. This will greatly reduce the overall complexity of the system, therefore a low cost UWB receiver is possible. The TR technique was first used in a UWB system by Hoctor *et al.* [52, 53]. The idea of applying TR systems to the UWB channel has since gained a lot of interest with publications analysing the performance of TR in multipath channels [34]. Chao *et al.* derived and analysed the optimal and suboptimal receivers [49]. The TR system was further studied in [54–56].

In this chapter, the bit error rate (BER) performance of a typical TR system with autocorrelation receiver is analysed. A noise averaging technique is then applied in the autocorrelation receiver to reduce the noise effect and thus improve the performance. The IEEE channel models are introduced and used to simulate the performance of two autocorrelation receivers. The effects of various parameters in the receiver design on the system performance are investigated.

2.2 TR System Overview

The TR signalling technique consists of an unmodulated reference signal and a modulated data signal for each information bit. In conventional TR systems, the modulated signal is transmitted after certain delay T_d following the unmodulated signal to ensure there is no interference between the two signals [49]. A binary pulse amplitude modulation (PAM) modulated TR signal pair is represented by

$$s_0(t) = g_{tr}(t) + b_0 g_{tr}(t - T_d) \quad (2.1)$$

where $g_{tr}(t)$ is represents an ultra-wideband pulse with a non-zero value in the interval $[0, T_w]$; the energy of $g_{tr}(t)$ is defined as $\frac{E_b}{2}$ and $b_0 \in \{-1, 1\}$. A binary PAM modulated TR signal pair is illustrated in Fig. 2.1, and a block diagram of the transmitter design is shown in Fig. 2.2. In this thesis, the delay T_d between the unmodulated and modulated pulses is set to equal to the data transmission time frame T_f . Therefore, TR signal pairs are transmitted in intervals of $2T_f$. To improve the transmission reliability, the same TR signal pair can be sent N_s times. A binary PAM modulated signal pair for transmission can be expressed as

$$s_{tr}(t) = \sum_{i=-\infty}^{\infty} g_{tr}(t - 2iT_f) + b_{\lfloor i/N_s \rfloor} g_{tr}(t - (2i + 1)T_f). \quad (2.2)$$

Since the unmodulated signal is transmitted together with the modulated signal as a pair on the same channel, the unmodulated signal will undergo the same channel distortion as the modulated signal assuming the channel remains unchanged during the period T_f . Thus, the received unmodulated signal can be used as a noisy reference for the detection of the modulated signal and avoid the need for explicit channel estimation. The received signal pair is expressed as

$$\begin{aligned} \tilde{r}_{tr}(t) = & \sum_{i=-\infty}^{\infty} g_{tr}(t - 2iT_f) * h(t) \\ & + b_{\lfloor i/N_s \rfloor} g_{tr}(t - (2i + 1)T_f) * h(t) + \tilde{n}(t) \end{aligned} \quad (2.3)$$

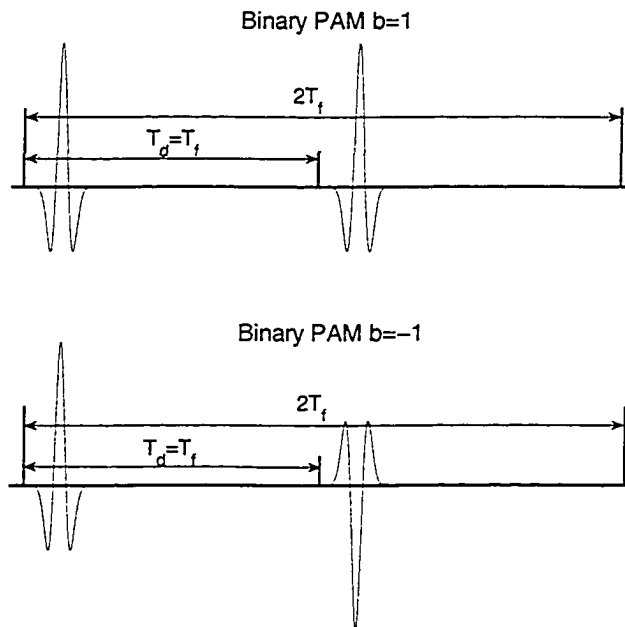


Figure 2.1: The binary PAM modulated TR system signal pair

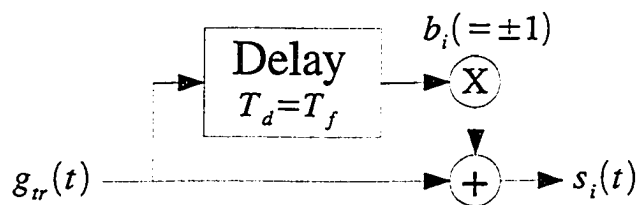


Figure 2.2: TR system transmitter block diagram

where $\tilde{n}(t)$ is the zero mean additive white Gaussian (AWGN) noise with variance $\frac{N_0}{2}$ and $h(t)$ represents the multipath channel impulse response. The UWB multipath channel response can be generalised as

$$h(t) = \sum_{k=1}^K \alpha_k \delta(t - \tau_k) \quad (2.4)$$

where K is the total number of multipath, α_k and τ_k are the amplitude and delay of the k_{th} path respectively. The multipath channel is assumed to have unit average power, i.e., $E[\sum_{k=1}^K |\alpha_k|^2] = 1$. The transmission time frame T_f is greater than the maximum channel delay τ_K plus the pulse duration T_w to ensure there is no inter-symbol interference (ISI) between the reference and data signal (i.e., $T_f \geq \tau_K + T_w$). At the receiver, the received signal is then passed through an ideal lowpass filter with a one-sided bandwidth of W and unit magnitude. The output of the lowpass filter at the i th symbol interval (with duration $2N_s T_f$) is given by

$$r_i(t) = \sum_{j=0}^{N_s-1} \sum_{k=1}^K [\alpha_k g_{rx}(t - 2jT_f - \tau_k) + \alpha_k b_i g_{rx}(t - (2j+1)T_f - \tau_k)] + n(t) \quad (2.5)$$

where $g_{rx}(t)$ corresponds to the received pulse shape. The use of different representations for pulses is to indicate the possible shape difference between the received $g_{rx}(t)$ and the transmitted pulse $g_{tr}(t)$ due to channel distortion. The bandwidth of the lowpass filter is designed to limit the white Gaussian noise to within the filter bandwidth and allow the pulse pair to pass through without distortion. The term $n(t)$ indicates the bandlimited noise. In the next section, two autocorrelation detectors and their performance analysis will be presented.

2.3 Receiver Performance

Two conventional TR receiver designs are analysed in this section: a basic autocorrelation receiver and an autocorrelation receiver with noise averaging

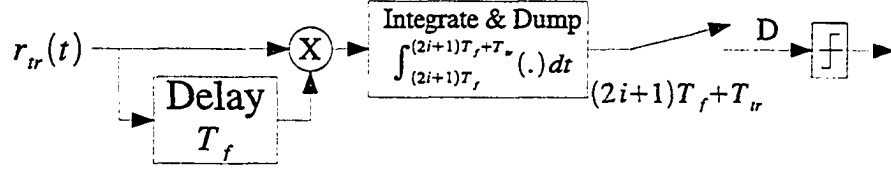


Figure 2.3: TR autocorrelation receiver block diagram

technique.

2.3.1 Autocorrelation Receiver

An autocorrelator is used to correlate the unmodulated reference signal with the modulated data signal to demodulate the data signal. The autocorrelator takes the received signal $r_{tr}(t)$ and multiply it with a T_f delayed received signal and intergrate it over a time period T_{tr} . A graphical representation of the autocorrelation receiver is shown in Fig. 2.3. The output of the autocorrelator for one symbol duration is given by

$$\begin{aligned}
 D &= \sum_{j=0}^{N_s-1} \int_{(2j+1)T_f}^{(2j+1)T_f+T_{tr}} r_i(t)r_i(t-T_f)dt \\
 &= \sum_{j=0}^{N_s-1} \int_{(2j+1)T_f}^{(2j+1)T_f+T_{tr}} \left\{ \left[\sum_{k=1}^K [\alpha_k g_{rx}(t-2jT_f-\tau_k) \right. \right. \\
 &\quad \left. \left. + \alpha_k b_i g_{rx}(t-(2j+1)T_f-\tau_k)] + n(t) \right] \right. \\
 &\quad \left. \cdot \left[\sum_{k=1}^K [\alpha_k g_{rx}(t-2jT_f-T_f-\tau_k) \right. \right. \\
 &\quad \left. \left. + \alpha_k b_i g_{rx}(t-(2j+1)T_f-T_f-\tau_k)] + n(t-T_f) \right] \right\} dt
 \end{aligned} \tag{2.6}$$

Let T_{tr} equal to AT_w , where A is a positive integer that is less than or equal to K . As defined earlier, $g_{rx}(t)$ is non-zero only for $t \in [0, T_w]$. Using a change

of variable $v = t - (2j + 1)T_f$, (2.6) can be rewritten as

$$\begin{aligned}
D &= N_s b_i \int_0^{T_{tr}} \sum_{k=1}^K \alpha_k^2 g_{rx}^2(v - \tau_k) dv \\
&+ \sum_{j=0}^{N_s-1} b_i \int_0^{T_{tr}} \sum_{k=1}^K \alpha_k g_{rx}(v - \tau_k) n(v + 2jT_f) dv \\
&+ \sum_{j=0}^{N_s-1} \int_0^{T_{tr}} \sum_{k=1}^K \alpha_k g_{rx}(v - \tau_k) n(v + 2jT_f + T_f) dv \\
&+ \sum_{j=0}^{N_s-1} \int_0^{T_{tr}} n(v + 2jT_f) n(v + (2j + 1)T_f) dv \\
&= X_1 + X_2 + X_3 + X_4
\end{aligned} \tag{2.7}$$

where the terms X_1 , X_2 , X_3 , and X_4 are defined as

$$X_1 = b_i N_s \int_0^{T_{tr}} \sum_{k=1}^K \alpha_k^2 g_{rx}^2(v - \tau_k) dv = b_i N_s R(0) |\boldsymbol{\alpha}|^2 \tag{2.8}$$

$$X_2 = b_i \sum_{j=0}^{N_s-1} \int_0^{T_{tr}} \sum_{k=1}^K \alpha_k g_{rx}(v - \tau_k) n(v + 2jT_f) dv \tag{2.9}$$

$$X_3 = \sum_{j=0}^{N_s-1} \int_0^{T_{tr}} \sum_{k=1}^K \alpha_k g_{rx}(v - \tau_k) n(v + 2jT_f + T_f) dv \tag{2.10}$$

$$X_4 = \sum_{j=0}^{N_s-1} \int_0^{T_{tr}} n(v + 2jT_f) n(v + (2j + 1)T_f) dv \tag{2.11}$$

where

$$R(\tau) = \int_0^{T_{tr}} g_{rx}(t) g_{rx}(t - \tau) dt \tag{2.12}$$

$$|\boldsymbol{\alpha}|^2 = \sum_{k=1}^A \alpha_k^2 \tag{2.13}$$

where $\boldsymbol{\alpha} = (\alpha_1, \alpha_2, \dots, \alpha_A)$. Conditioned on b_i , $\boldsymbol{\alpha}$ and $\boldsymbol{\tau} = (\tau_1, \tau_2, \dots, \tau_A)$, X_2 and X_3 can be modeled as zero mean Gaussian random variables (R.V.s) with variance equal to $\frac{N_0}{2} N_s R(0) |\boldsymbol{\alpha}|^2$. The noise to noise term X_4 can be approximated as Gaussian distributed from central limit theorem with zero

mean and variance

$$\sigma_{X_4}^2 = \mathbb{E}(X_4^2) = \sum_{a=0}^{N_s-1} \sum_{j=0}^{N_s-1} \int_0^{T_{tr}} \int_0^{T_{tr}} \mathbb{E}[n(v_1 + 2aT_f)n(v_1 + (2a+1)T_f) \\ n(v_2 + 2jT_f)n(v_2 + (2j+1)T_f)] dv_1 dv_2. \quad (2.14)$$

For zero-mean jointly Gaussian R.V.s y_1, y_2, y_3, y_4 and $\mathbb{E}[x_i x_j] = C_{ij}$, there is [57]

$$\mathbb{E}[y_1 y_2 y_3 y_4] = C_{12} C_{34} + C_{13} C_{24} + C_{14} C_{23} \quad (2.15)$$

Applying (2.15) to (2.14) yields

$$\sigma_{X_4}^2 = \sum_{a=0}^{N_s-1} \sum_{j=0}^{N_s-1} \int_0^{T_{tr}} \int_0^{T_{tr}} \{R_n^2(T_f) + R_n^2(v_2 - v_1 + 2(j-a)T_f) \\ + R_n(v_2 - v_1 + 2(j-a)T_f + T_f)R_n(v_2 - v_1 + 2(j-a)T_f - T_f)\} dv_1 dv_2 \quad (2.16)$$

where $R_n(\tau) = \mathbb{E}[n(t)n(t+\tau)] = N_0 W \text{sinc}(2W\tau)$ [58]. When $\tau \geq T_f$, $R(\tau)$ can be approximated as zero. Therefore, the variance exists when $a = j$, and (2.16) can be simplified to

$$\sigma_{X_4}^2 \approx \sum_{j=0}^{N_s-1} \int_0^{T_{tr}} \int_0^{T_{tr}} R_n^2(v_2 - v_1) dv_1 dv_2 \\ = N_s \int_0^{T_{tr}} \int_0^{T_{tr}} R_n^2(v_2 - v_1) dv_1 dv_2 \quad (2.17)$$

where (2.17) can be further simplified to [49]

$$\sigma_{X_4}^2 \approx N_s W \frac{N_0^2}{2} T_{tr}. \quad (2.18)$$

The decision variable D can then be approximated as a Gaussian R.V. conditioned on b_i, α and τ . Its mean and variance are given by

$$\mathbb{E}[D|b_i, \alpha, \tau] = b_i N_s R(0) |\alpha|^2 \quad (2.19)$$

$$\text{Var}[D|\alpha, \tau] = N_s N_0 R(0) |\alpha|^2 + \sigma_{X_4}^2. \quad (2.20)$$

The conditional probability of error for the autocorrelation receiver is given by

$$P(e|\alpha, \tau) = P(D < 0 | b_i = 1, \alpha, \tau) = Q\left(\frac{N_s R(0) |\alpha|^2}{\sqrt{N_s N_0 R(0) |\alpha|^2 + \sigma_{X_4}^2}}\right). \quad (2.21)$$

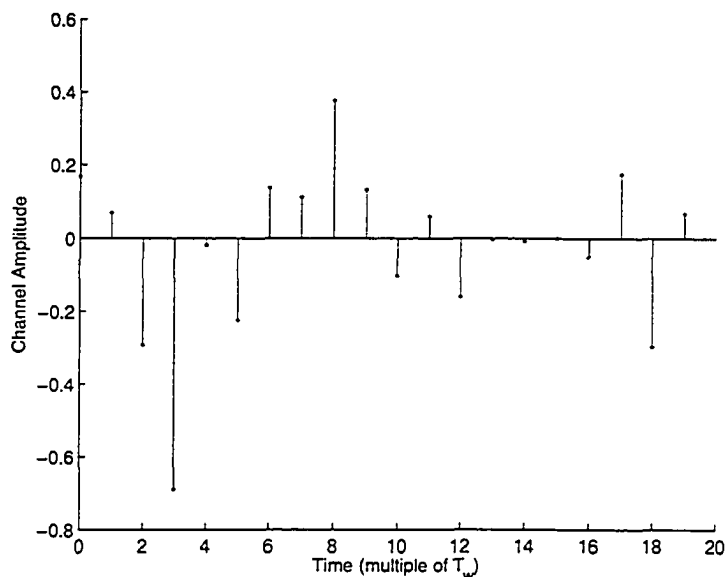


Figure 2.4: The channel response of a simple 20 path test channel

The numerical evaluation and simulation result of the autocorrelation receiver over a simple multipath channel are compared in Fig. 2.5 with $N_s = 1$. The unit gain channel used have 20 paths, with paths arriving every integer multiple T_w . The channel response is plotted in Fig. 2.4. As shown in Fig. 2.5, the analytical results closely match the simulation results for both $T_{tr} = 10T_w$ and $T_{tr} = 20T_w$ case. Therefore, it is evident that it is possible to model the system decision variable as a Gaussian R.V. under these circumstances.

2.3.2 Autocorrelator with Noise Averaging

To improve the performance of the TR system, a technique called noise averaging was applied [34]. Noise averaging is applied to the reference signal to improve the signal to noise ratio (SNR). This is achieved by adding the current reference signal with $N_p - 1$ delayed reference signal of previous signals, dividing the sum by N_p and using it as the reference signal for demodulation. A graphical representation of the system is presented in Fig. 2.6. Assuming

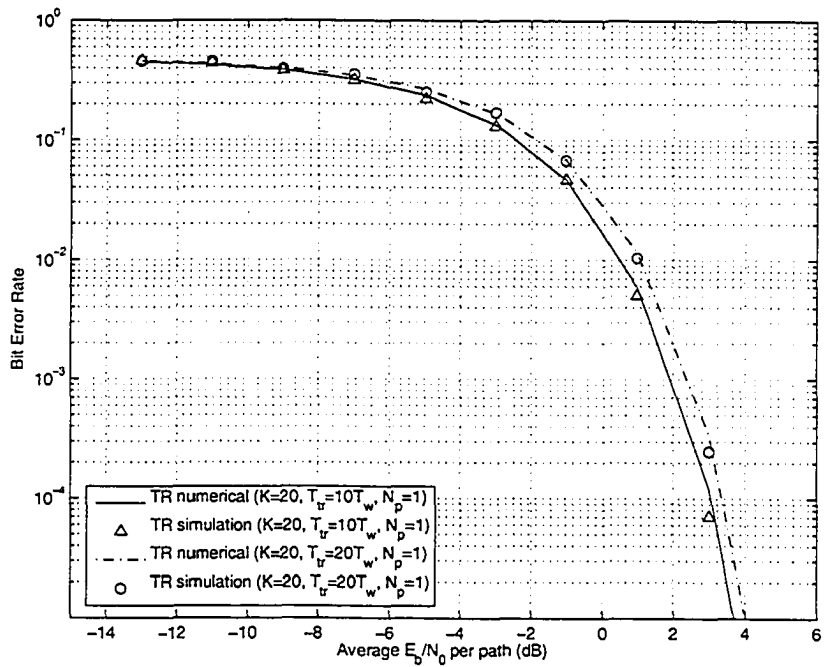


Figure 2.5: Performance of autocorrelation receiver in a 20 path channel

that the channel is static for the duration of N_p signal pairs, this technique will effectively reduce the noise variance in the received reference signal by N_p , while keeping the signal energy in the reference signal unchanged. With the addition of the noise averaging technique, the decision variable can now be expressed

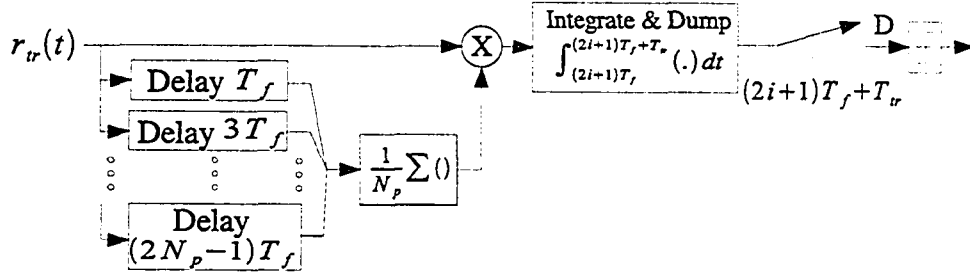


Figure 2.6: TR autocorrelation receiver with noise averaging block diagram

$$\begin{aligned}
 D &= \sum_{j=0}^{N_s-1} \int_{(2j+1)T_f}^{(2j+1)T_f+T_{tr}} r_i(t) \sum_{m=0}^{N_p-1} \frac{1}{N_p} r_i(t - 2mT_f - T_f) dt \\
 &= \sum_{j=0}^{N_s-1} \int_{(2j+1)T_f}^{(2j+1)T_f+T_{tr}} \left\{ \left[\sum_{k=1}^K [\alpha_k g_{rx}(t - 2jT_f - \tau_k) \right. \right. \\
 &\quad \left. \left. + \alpha_k b_i g_{rx}(t - (2j+1)T_f - \tau_k)] + n(t) \right] \right. \\
 &\quad \cdot \left[\sum_{m=0}^{N_p-1} \frac{1}{N_p} \sum_{k=1}^K [\alpha_k g_{rx}(t - 2mT_f - 2jT_f - T_f - \tau_k) \right. \\
 &\quad \left. \left. + \alpha_k b_i g_{rx}(t - 2mT_f - (2j+1)T_f - T_f - \tau_k)] + n(t - 2mT_f - T_f) \right] \right\} dt.
 \end{aligned} \tag{2.22}$$

Under the same channel assumption as in the previous subsection, (2.22) can be generalised as

$$\begin{aligned}
 D &= N_s b_i \int_0^{T_{tr}} \sum_{k=1}^K \alpha_k^2 \sum_{m=0}^{N_p-1} \frac{1}{N_p} g_{rx}(v - 2mT_f - \tau_k) g_{rx}(v - \tau_k) dv \\
 &\quad + \sum_{j=0}^{N_s-1} b_i \int_0^{T_{tr}} \sum_{k=1}^K \alpha_k g_{rx}(v - \tau_k) \frac{1}{N_p} \sum_{m=0}^{N_p-1} n(v + 2jT_f - 2mT_f) dv \\
 &\quad + \sum_{j=0}^{N_s-1} \int_0^{T_{tr}} \sum_{k=1}^K \alpha_k \sum_{m=0}^{N_p-1} \frac{1}{N_p} g_{rx}(v - 2mT_f - \tau_k) n(v + 2jT_f + T_f) dv \\
 &\quad + \sum_{j=0}^{N_s-1} \int_0^{T_{tr}} \frac{1}{N_p} \sum_{m=0}^{N_p-1} n(v + 2jT_f - 2mT_f) n(v + (2j+1)T_f) dv \\
 &= Y_1 + Y_2 + Y_3 + Y_4
 \end{aligned} \tag{2.23}$$

with Y_1 , Y_2 , Y_3 , and Y_4 simplified to,

$$Y_1 = b_i N_s R(0) |\alpha|^2 \quad (2.24)$$

$$Y_2 = b_i \sum_{j=0}^{N_s-1} \int_0^{T_{tr}} \sum_{k=1}^K \alpha_k g_{rx}(v - \tau_k) \frac{1}{N_p} \sum_{m=0}^{N_p-1} n(v + 2jT_f - 2mT_f) dv \quad (2.25)$$

$$Y_3 = \sum_{j=0}^{N_s-1} \int_0^{T_{tr}} \sum_{k=1}^K \alpha_k g_{rx}(v - \tau_k) n(v + 2jT_f + T_f) dv \quad (2.26)$$

$$Y_4 = \sum_{j=0}^{N_s-1} \int_0^{T_{tr}} \frac{1}{N_p} \sum_{m=0}^{N_p-1} n(v + 2jT_f - 2mT_f) n(v + (2j+1)T_f) dv. \quad (2.27)$$

Similar to the previous subsection, the term Y_2 and Y_3 can both be modeled as zero mean Gaussian variables with variances of $\frac{N_0}{2N_p} N_s R(0) |\alpha|^2$ and $\frac{N_0}{2} N_s R(0) |\alpha|^2$ respectively. Employing the approach for calculating the variance of X_4 in the previous subsection to calculate Y_4 yields

$$\begin{aligned} \sigma_{Y_4}^2 &\approx \frac{1}{N_p} \sum_{j=0}^{N_s-1} \int_0^{T_{tr}} \int_0^{T_{tr}} R_n^2(v_2 - v_1) dv_1 dv_2 \\ &= \frac{N_s}{N_p} \int_0^{T_{tr}} \int_0^{T_{tr}} R_n^2(v_2 - v_1) dv_1 dv_2 \end{aligned} \quad (2.28)$$

$$\approx N_s W \frac{N_0^2}{2N_p} T_{tr}. \quad (2.29)$$

The decision variable D of the autocorrelation receiver with noise averaging can also be approximated as a Gaussian R.V. with mean and variance given by

$$\mathbb{E}[D|b_i, \alpha, \tau] = b_i N_s R(0) |\alpha|^2 \quad (2.30)$$

$$\text{Var}[D|\alpha, \tau] = \frac{N_0}{2} N_s R(0) |\alpha|^2 + \frac{N_0}{2N_p} N_s R(0) |\alpha|^2 + \sigma_{Y_4}^2. \quad (2.31)$$

The conditional probability of error for the autocorrelation receiver with noise averaging is then given by

$$\begin{aligned} P(e|\alpha, \tau) &= P(D < 0 | b = 1, \alpha, \tau) \\ &= Q\left(\frac{N_s R(0) |\alpha|^2}{\sqrt{\frac{N_0}{2} N_s R(0) |\alpha|^2 + \frac{N_0}{2N_p} N_s R(0) |\alpha|^2 + \sigma_{Y_4}^2}}\right) \end{aligned} \quad (2.32)$$

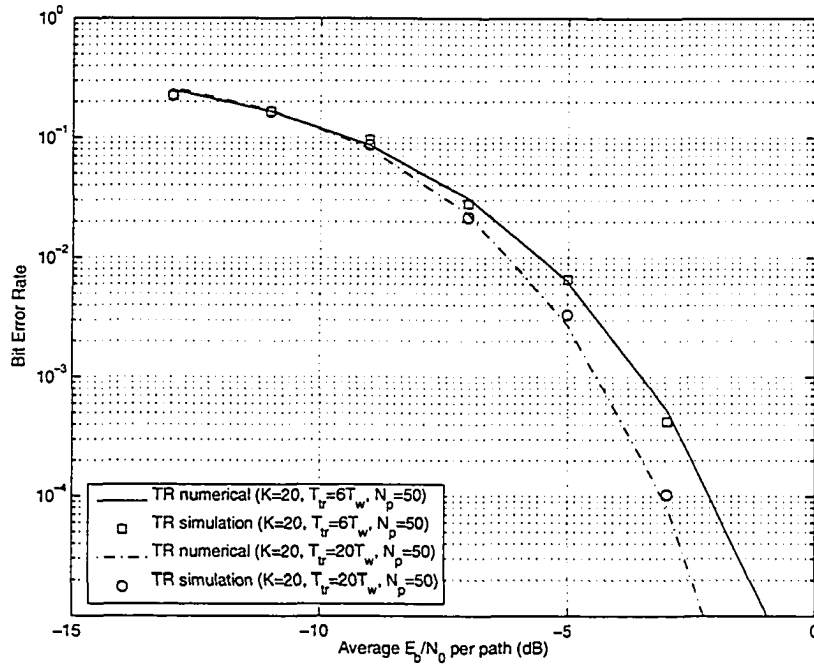


Figure 2.7: Performance of autocorrelation receiver with noise averaging in a 20 path channel

The analysis is evaluated with the same 20 paths channel as in the previous subsection. In Fig. 2.7, it is shown that the numerical analysis again agree with the simulation results. Also note that the performance of the system improved when compared to the system with no noise averaging in Fig. 2.5.

2.4 IEEE channel model

Realistic channel models are used for performance evaluation in this thesis. The channel models are obtained from the IEEE 802.15.3a high rate alternative physical layer (PHY) task group [30]. These UWB channel models are based on the Saleh-Valenzuela model [31], with multi-path components arriving in clusters. And the amplitudes have a log-normal distribution. The channel

models can be represented by the following discrete time impulse response

$$h(t) = X \sum_{l=0}^L \sum_{k=0}^K \alpha_{k,l} \delta(t - T_l - \tau_{k,l}) \quad (2.33)$$

where X represents the log-normal shadowing characterised by

$$20 \log_{10}(X_i) \sim \mathcal{N}(0, \sigma_x^2). \quad (2.34)$$

Also, T_l and $\tau_{k,l}$ are the delays of the l^{th} cluster and the k^{th} multipath of the l^{th} cluster, respectively. The distribution of T_l and $\tau_{k,l}$ are defined by the cluster and multipath arrival rate Λ and λ respectively as

$$p(T_l | T_{l-1}) = \Lambda \exp[-\Lambda(T_l - T_{l-1})], l > 0 \quad (2.35)$$

$$p(\tau_{k,l} | \tau_{(k-1),l}) = \lambda \exp[-\lambda(\tau_{k,l} - \tau_{(k-1),l})], k > 0 \quad (2.36)$$

The channel coefficient, $\alpha_{k,l}$, is defined as

$$\alpha_{k,l} = p_{k,l} \xi_l \beta_{k,l} \quad (2.37)$$

where $p_{k,l}$ equals ± 1 with equal probability representing the signal inversion due to reflection. And ξ_l represents the fading of l^{th} cluster and $\beta_{k,l}$ represents the fading of the k^{th} multipath in the l^{th} cluster, which have the following distribution

$$20 \log_{10}(\xi_l \beta_{k,l}) \sim \mathcal{N}(\mu_{k,l}, \sigma_1^2 + \sigma_2^2) \quad (2.38)$$

$$\mu_{k,l} = \frac{10 \ln(\Omega_0) - 10T_l/\Gamma - 10\tau_{k,l}/\gamma - (\sigma_1^2 + \sigma_2^2) \ln(10)}{\ln(10)} \quad (2.39)$$

where σ_1^2 and σ_2^2 are standard deviations of the log-normal fading term for the cluster and the multipath within the cluster respectively. The parameter Γ is the cluster decay factor and γ is the multipath decay factor.

The IEEE UWB channel contains four different channel models (CM1-4), each with different channel parameters and channel characteristics. CM1 represents a line of sight (LOS) channel. CM2 is a non-line of sight (NLOS) channel where the transmitter and the receiver are separated by less than 4

Parameters	CM 1	CM 2	CM 3	CM 4
Λ (1/nsec)	0.0233	0.4	0.0667	0.0667
λ (1/nsec)	2.5	0.5	2.1	2.1
Γ	7.1	5.5	14.0	24.0
γ	4.3	6.7	7.9	12
σ_1 (dB)	3.3941	3.3941	3.3941	3.3941
σ_2 (dB)	3.3941	3.3941	3.3941	3.3941
σ_z (dB)	3	3	3	3

Table 2.1: Model Parameters of IEEE channel models

Channel Statistics	CM 1	CM 2	CM 3	CM 4
Mean excess delay (nsec) (τ_m)	5.0	9.9	15.9	30.1
RMS delay (nsec) (τ_{rms})	5	8	15	25
Number of paths within 85% of the peak multipath arrival	20.8	33.9	64.7	123.3
Mean channel energy (dB)	-0.4	-0.5	0.0	0.3

Table 2.2: Channel Characteristics of IEEE channel models

meters. CM3 is also a NLOS channel with transmitter and receiver distance of 4 to 10 meters. CM4 is the representation of an extreme NLOS multi-path channel with a 25 nsec RMS delay spread. The detailed channel parameters are listed in Table 2.1. Sample channel response of an LOS channel (CM1) and an extreme NLOS channel (CM4) are presented in Fig. 2.8 and Fig. 2.9, respectively. One hundred channel realizations are generated for each channel model, and the key channel characteristics are shown in Table 2.2.

2.5 Simulation Results and Discussion

In the simulation, the TR modulated signal is transmitted through the different channel models proposed by the IEEE 802.15.3a working group as described in Section 2.4. These channel models provide realistic channels where fading and multipath interference are taken into the evaluation of the TR system. The performance of the scheme is first evaluated by varying the length of

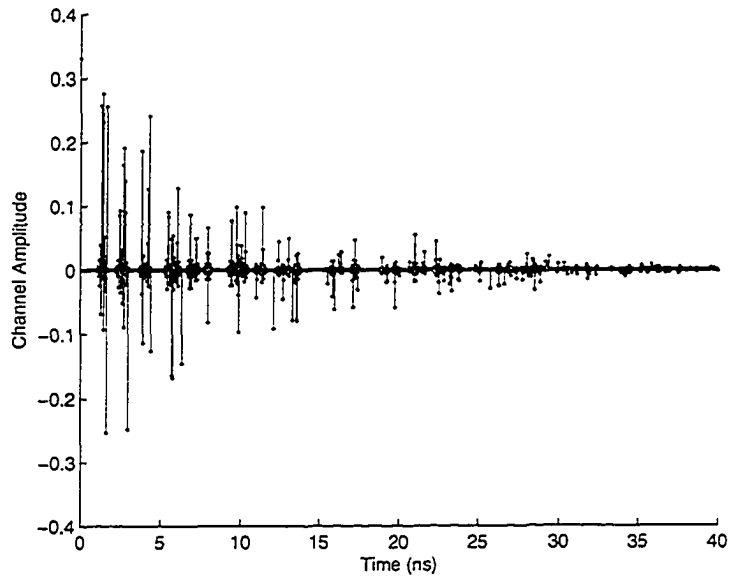


Figure 2.8: Sample channel realization of CM1

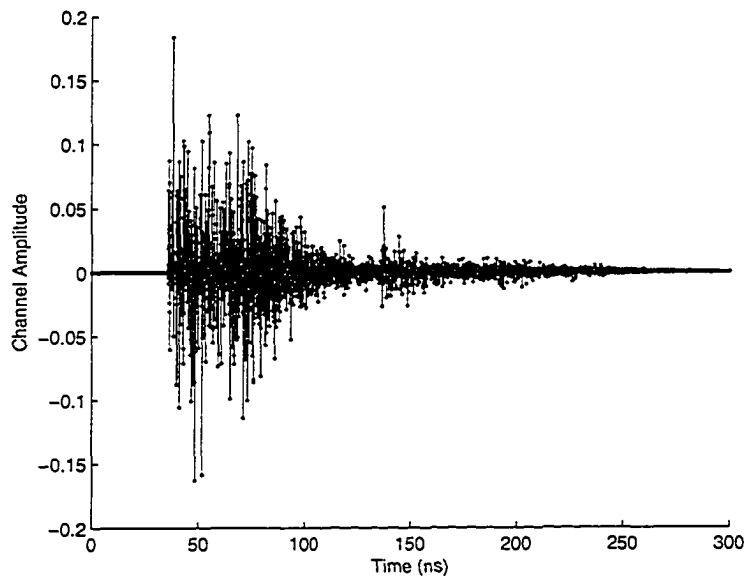


Figure 2.9: Sample channel realization of CM4

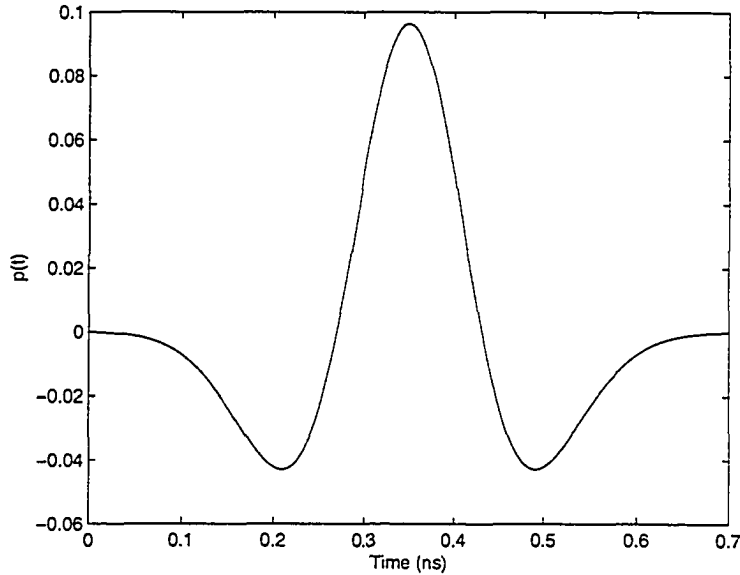


Figure 2.10: The pulse shape of the 2nd derivative Gaussian pulse $p(t)$

integration T_{tr} without the aid of noise averaging. Then the effect of T_{tr} on receiver with noise averaging is presented. Finally, effectiveness of noise averaging is evaluated by varying the number of reference pulses N_p used in the noise averaging technique.

2.5.1 Simulation Setup

The pulse used is based on a second derivative Gaussian pulse $p(t)$ given by [59]

$$p(t) = [1 - 4\pi((t - 0.35)/\tau_m)^2] \exp[-2\pi((t - 0.35)/\tau_m)^2] \quad (2.40)$$

where $\tau_m = 0.2877$ and the pulse have non-zero value only in time interval $[0, 0.7]$ ns as shown in Fig. 2.10. The Gaussian pulse has a zero DC component and a well defined frequency response as shown in Fig. 2.11. The Gaussian pulse is chosen over a rectangular pulse because it has less energy outside the allocated frequency band [19]. The transmitted UWB TR pulse is represented as

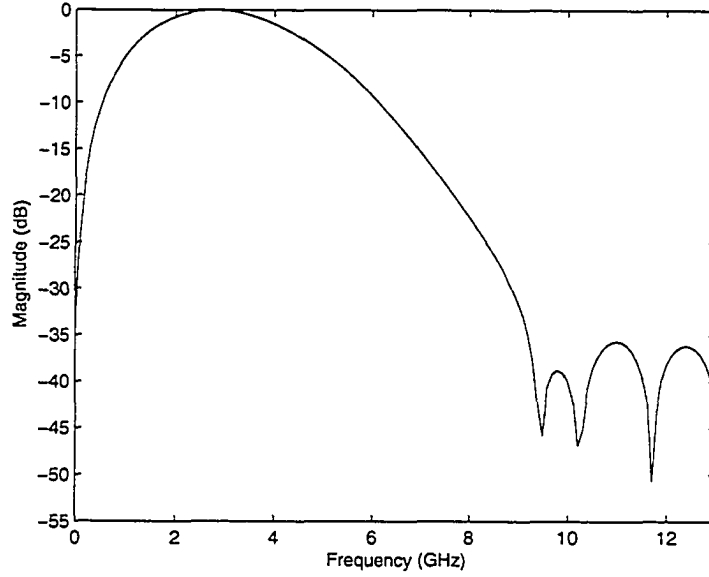


Figure 2.11: The frequency response of the 2nd derivative Gaussian pulse $p(t)$

$$g_{tr}(t) = p(t) \quad (2.41)$$

with $T_w = 0.7$ ns, and non-zero interval $[0, 0.7]$ ns. The signal $g_{tr}(t)$ is normalised to have energy $\frac{E_b}{2}$. The Monte Carlo simulation employs a sampling rate of 30 GHz and a lowpass filter with single side bandwidth $W = 7.2$ GHz. The lowpass filter is designed with a fixed Hamming window given by [60]

$$w[n] = 0.54 + 0.46 \cos\left(\frac{2\pi(n - M/2)}{M + 1}\right) \quad (2.42)$$

where $n \in [0, M]$ with $M = 50$ for the simulation. The bit error probability of each channel model is the average BER for the 100 channel realizations of each channel model. For each channel realization, simulation is set to terminate when either 1000 errors have been obtained or the maximum bit ceiling of 2×10^6 bits has been reached. The BERs are averaged over 100 channel realizations of each channel model to obtain the average BER. The channel models are assumed to be static. The start of the integration for the simulation is defined as the arrival of the first signal path.

2.5.2 The effect of T_{tr} on basic Autocorrelation Receiver

In rake receivers, the increasing number of fingers yields better performance [44]. Because increasing the amount of paths collected will increase the signal energy and thus increase the SNR and as a result yield a better BER. The amount of energy collected in a TR system is related to the integration length T_{tr} of the autocorrelator. The BER performance of a TR system using autocorrelation receivers with various integration length T_{tr} in UWB channels CM1-CM4 are shown in Figs. 2.12-2.15. As expected, the longer the integration period the lower the BER. However, this relationship does not always hold true. There is a point for every channel model where further increasing T_{tr} will result in worse performance. In Fig. 2.12, it is clearly shown that the lowest BER for CM1 is achieved when $T_{tr} = 7$ ns; when T_{tr} is increased to 28 ns the performance actually deteriorates. From Fig. 2.13, the lowest BER for CM2 is achieved when $T_{tr} = 28$ ns and BER increases as T_{tr} is increased beyond that point. The lowest BER performance for CM3 and CM4 is achieved with $T_{tr} = 42$ ns and $T_{tr} = 70$ ns as shown in Fig. 2.14 and Fig. 2.15, respectively. The reason is that after these T_{tr} , the increase of signal energy from collecting more channel paths does not outweigh the increase of noise power collected because as we move further away from mean access delay, the path strengths decrease. It is also shown in these figures that as the number of paths increases from CM1 to CM4, the increase in integration length T_{tr} has greater impact on the system performance. For example, the performance difference between $T_{tr} = 1.4$ ns and $T_{tr} = 14$ ns is less than 4 dB at BER = 10^{-1} for CM1 in Fig. 2.12, while the different is about 8 dB at BER = 10^{-1} for CM4 in Fig. 2.15. This is due to the energy of the channel being spread out to more paths in CM4, resulting in less energy per path.

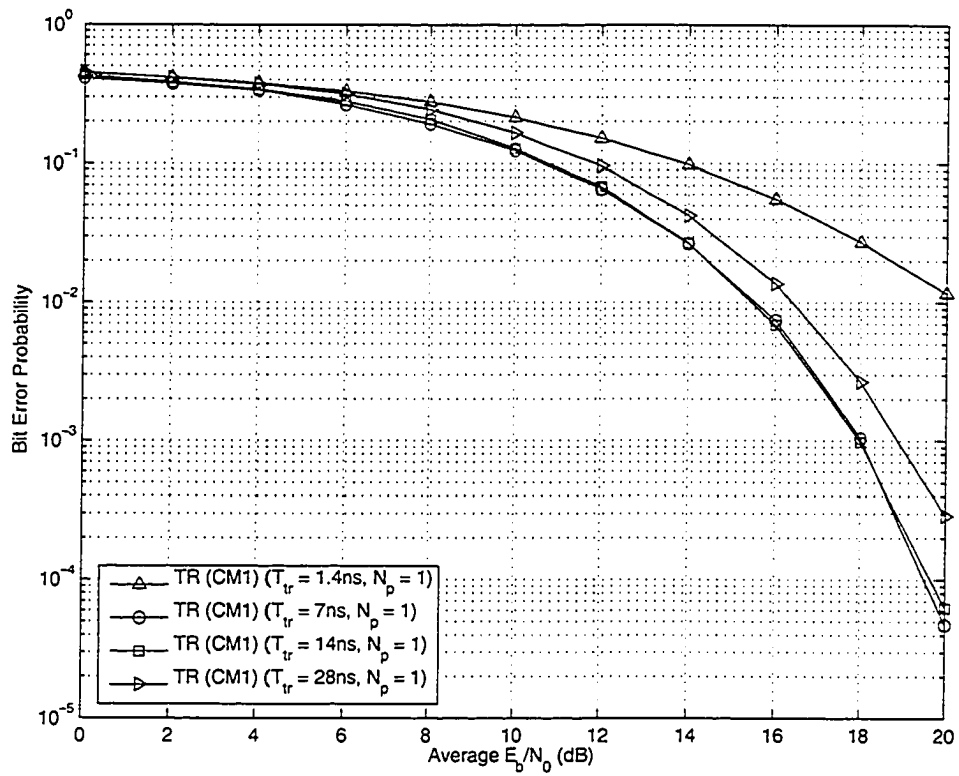


Figure 2.12: Effect of T_{tr} on TR systems with autocorrelation receiver in CM1

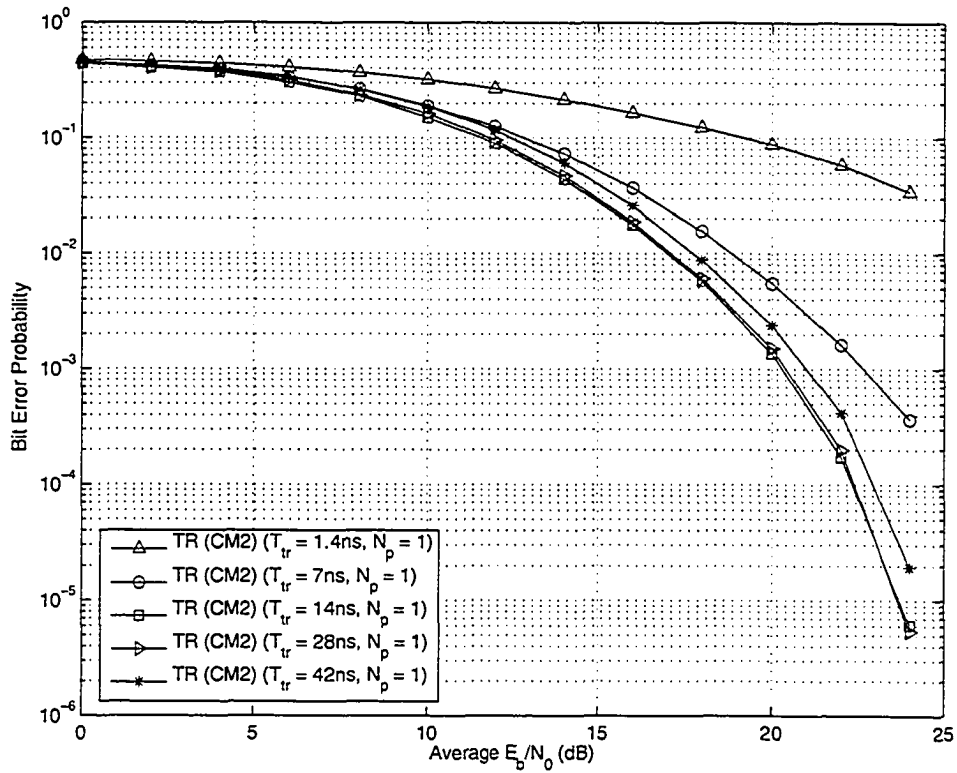


Figure 2.13: Effect of T_{tr} on TR systems with autocorrelation receiver in CM2

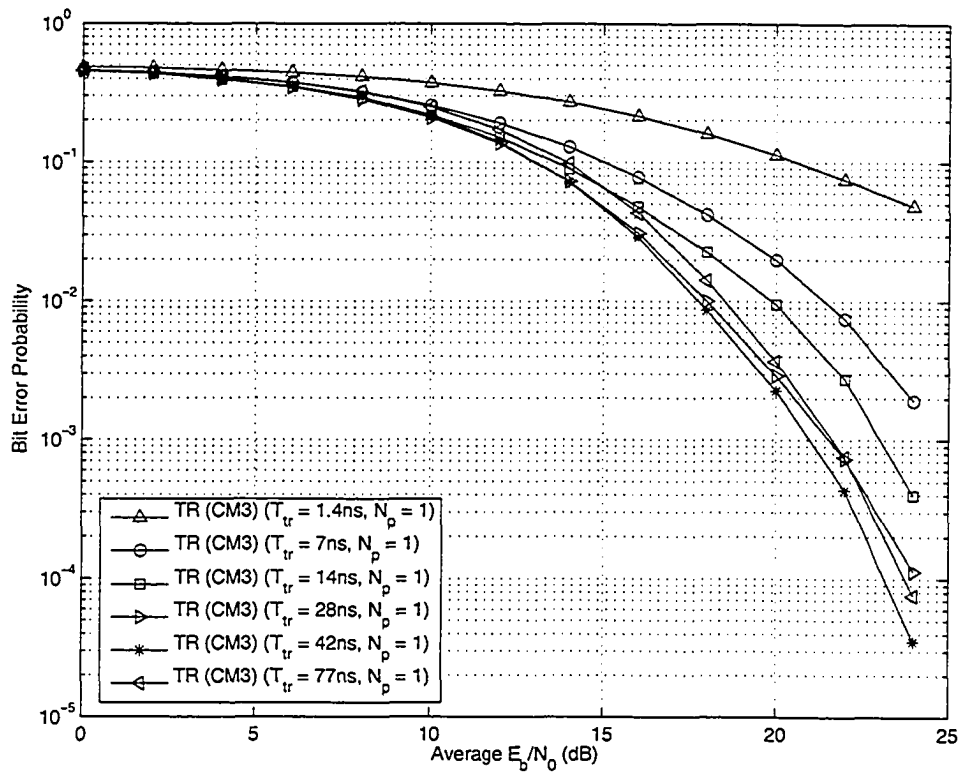


Figure 2.14: Effect of T_{tr} on TR systems with autocorrelation receiver in CM3

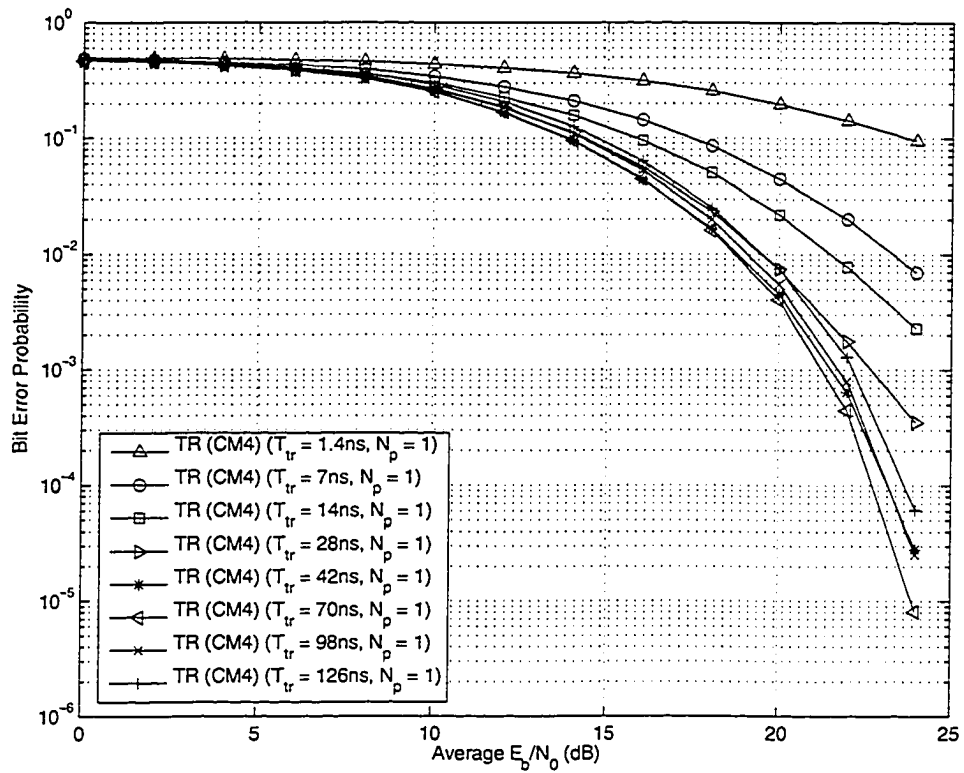


Figure 2.15: Effect of T_{tr} on TR systems with autocorrelation receiver in CM4

2.5.3 The effect of T_{tr} on noise averaging Autocorrelation Receiver

The performance difference from varying the T_{tr} in a TR system with noise averaging autocorrelation receiver ($N_p = 50$) was investigated for all four channel models. With noise averaging, the reference signals would have the noise averaged out and thus improve the SNR of the reference signals. Therefore as expected, systems with noise averaging (Figs. 2.16 - 2.19) significantly outperform systems without noise averaging (Figs. 2.12 - 2.15) regardless of the channel model. The effect of T_{tr} on the system performance for CM1-CM4 is similar to the regular autocorrelation receiver without noise averaging. As shown in Figs. 2.16 - 2.19, the system performance improves as T_{tr} increases, but like the autocorrelation receiver without noise averaging, the performance worsens as T_{tr} passes certain point for all the channel models. It was also observed that the performance of the TR system degrades as the number of paths increases from CM1 to CM4 for both receivers with noise averaging and without noise averaging. This showed that for the TR system in discussion, channels with less paths but greater energy per path performs better than channels with more paths but weaker energy per path.

2.5.4 The effect of N_p on noise averaging Autocorrelation Receiver

As a general concept, increasing the number of reference pulses N_p used for noise averaging will decrease the noise variance in the reference signal, and therefore improve the system performance. In Figs. 2.20 - 2.23, the performance improvement resulting from increased N_p is investigated for CM1 to CM4, respectively. Two reference curves are also included in all the figures for comparison. One reference curve shows the partial rake (PRAKE) receiver with perfect channel estimation at resolution of 0.7 ns interval. The PRAKE receivers have 40, 60, 110, 180 fingers for CM1, CM2, CM3, and CM4 respectively with each finger separated by 0.7 ns. These receivers thus collect the

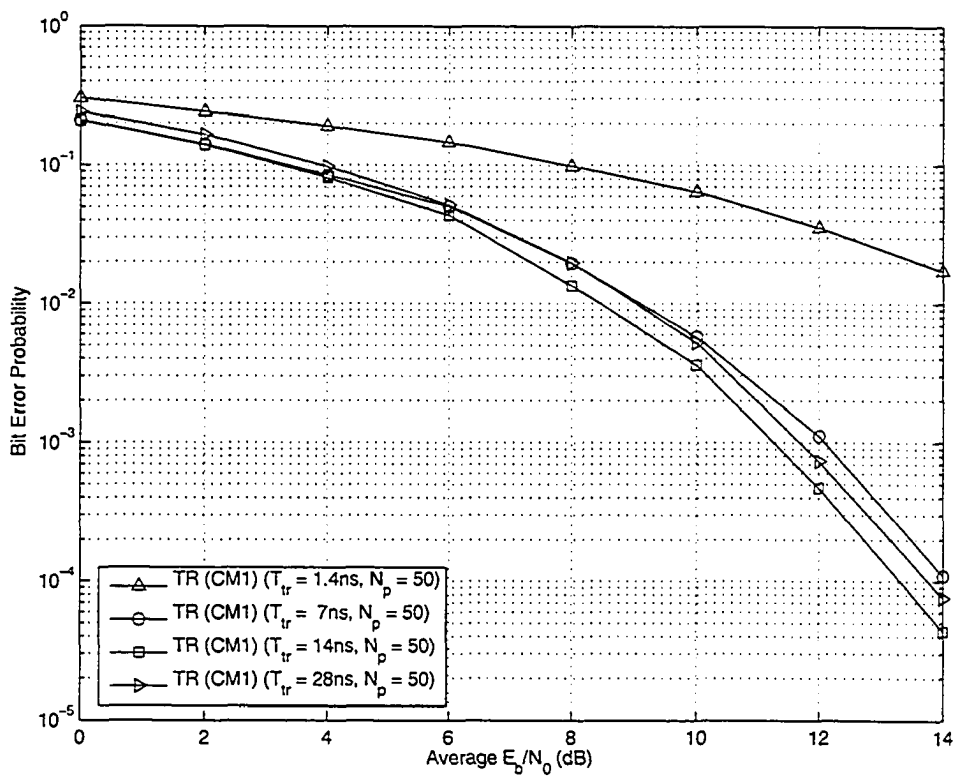


Figure 2.16: Effect of T_{tr} on TR systems with noise averaging autocorrelation receiver in CM1

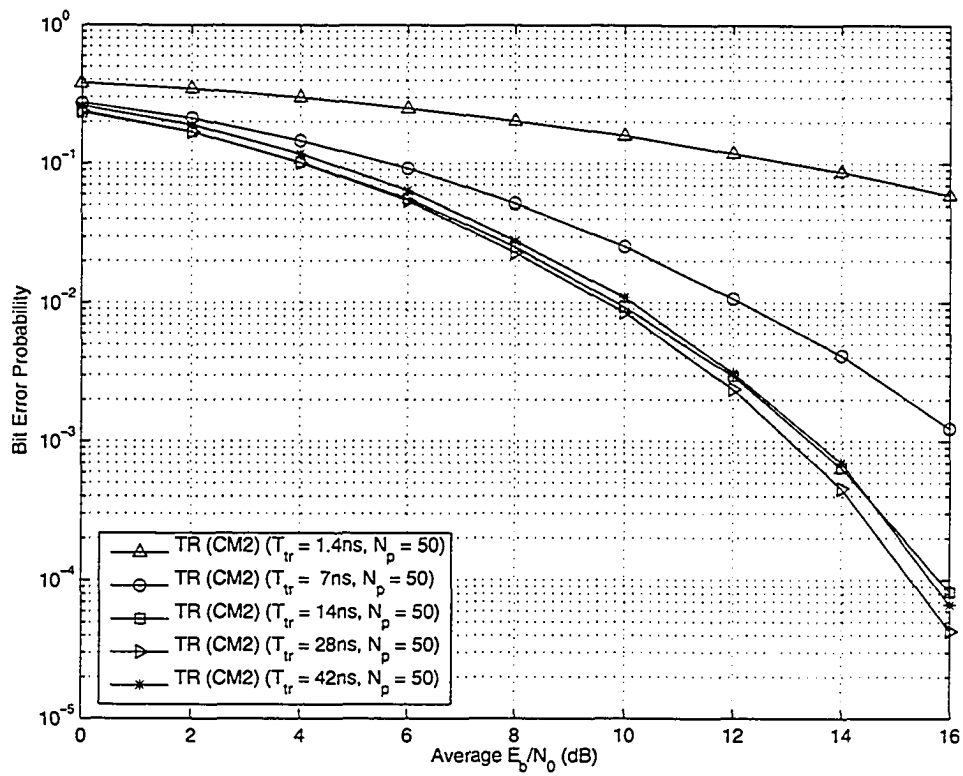


Figure 2.17: Effect of T_{tr} on TR systems with noise averaging autocorrelation receiver in CM2

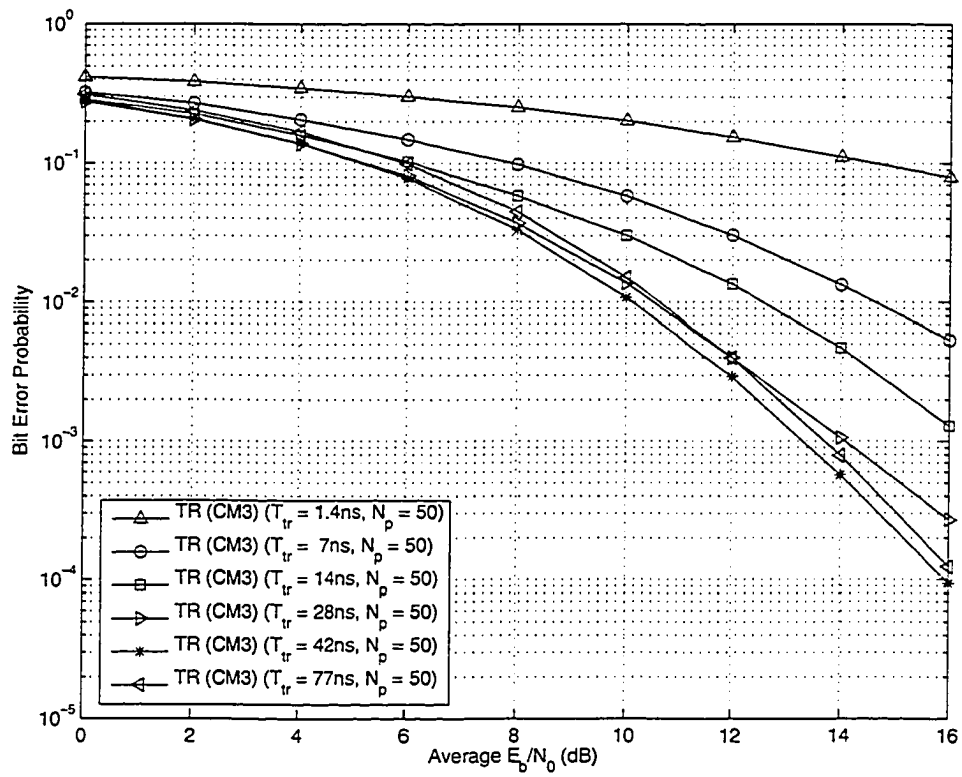


Figure 2.18: Effect of T_{tr} on TR systems with noise averaging autocorrelation receiver in CM3

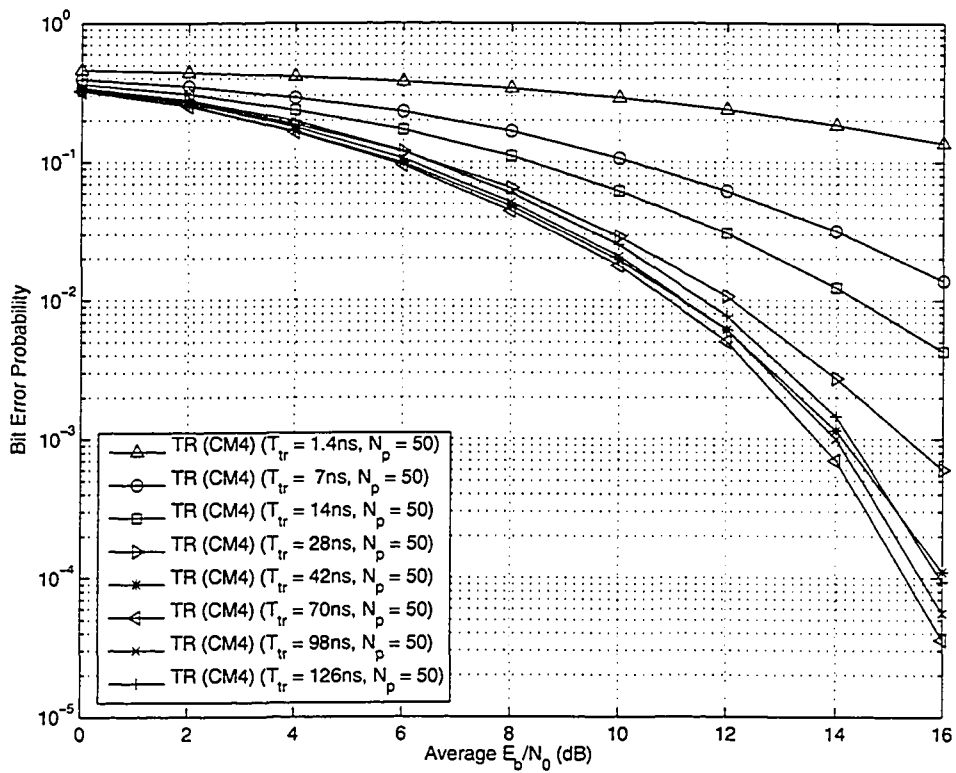


Figure 2.19: Effect of T_{tr} on TR systems with noise averaging autocorrelation receiver in CM4

first 28 ns, 42 ns, 77 ns, and 126 ns of signal energy after the first path arrival, which are the same as the maximum integration length of the TR autocorrelation receivers for CM1 to CM4 respectively. The pulse used for transmission and in the PRAKE match filter receiver is the same 2nd derivative Gaussian pulse defined in (2.40). The results of PRAKE receivers represent the performance of the suboptimal rake receiver. The other reference curve represents the “ideal” matched filter system with unlimited noise averaging ($N_p \rightarrow \infty$) of the reference signals and thus yielding noise free reference signals. This curve indicates the performance of the optimal TR receiver.

All the figures show that as N_p gets larger, the performance of the system indeed improves. It is evident that the biggest gain occurs when going from without averaging case $N_p = 1$ to averaging with $N_p = 10$. For all channel models, the rate of performance improvement from noise averaging slowed down as N_p increases. As seen in Figs. 2.20 - 2.23, at $\text{BER} = 10^{-3}$ the performance improvement from $N_p = 10$ to $N_p = 20$ in SNR is only about one third the performance improvement of $N_p = 1$ to $N_p = 10$ for CM1 to CM4. When changing from $N_p = 20$ to $N_p = 50$, an averaging of 30 more reference signals only results in performance gain equals to the gain obtained from $N_p = 10$ to $N_p = 20$. Figs. 2.20 - 2.23 also demonstrate that for all the channel models, the performance of TR system without noise averaging is worse than the suboptimal rake receiver performance. However, with noise averaging of $N_p = 20$ the TR system of CM1 to CM2 is able to outperform the PRAKE receivers at $\text{SNR} > 14$ dB. Figs. 2.22-2.23 show at $\text{SNR} > 15$ dB and $\text{SNR} > 17$ dB, the TR system with noise averaging of $N_p = 50$ is able to outperform the 110 and 180 finger PRAKE receiver in CM3 and CM4 respectively. When comparing the “ideal” TR system to the TR system with $N_p = 50$ noise averaging, we notice that as the number of paths increases from CM1 to CM4, the performance gap between them increases as well. This observation indicates that noise has greater affect on channels with large number of paths than channels with small number of paths.

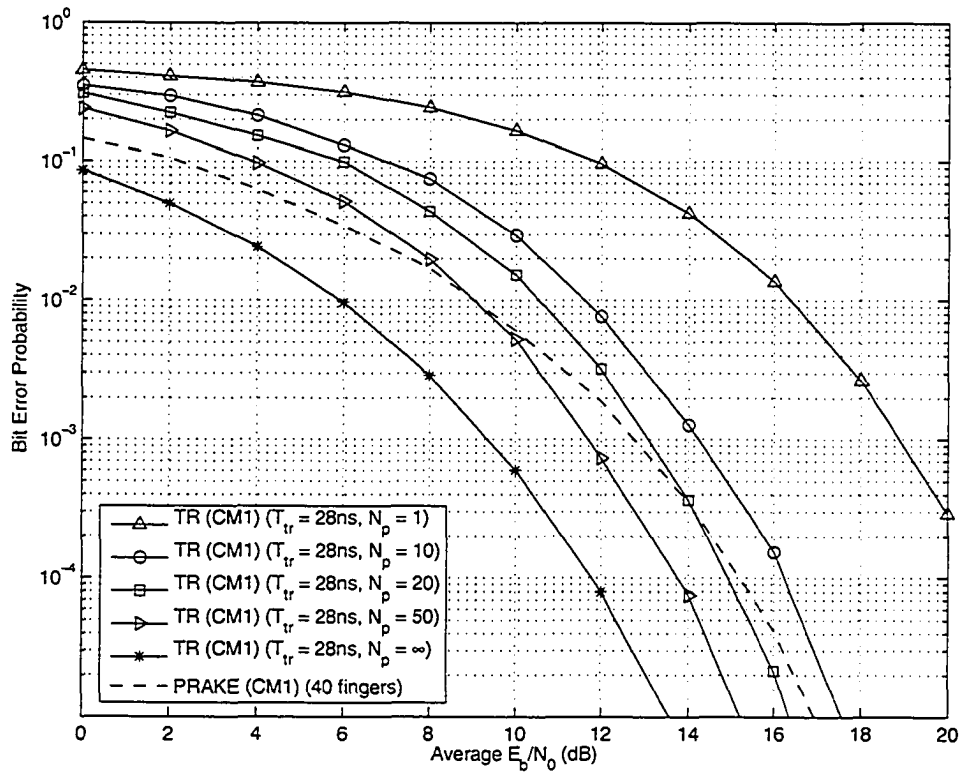


Figure 2.20: Effect of N_p on TR systems with noise averaging autocorrelation receiver in CM1

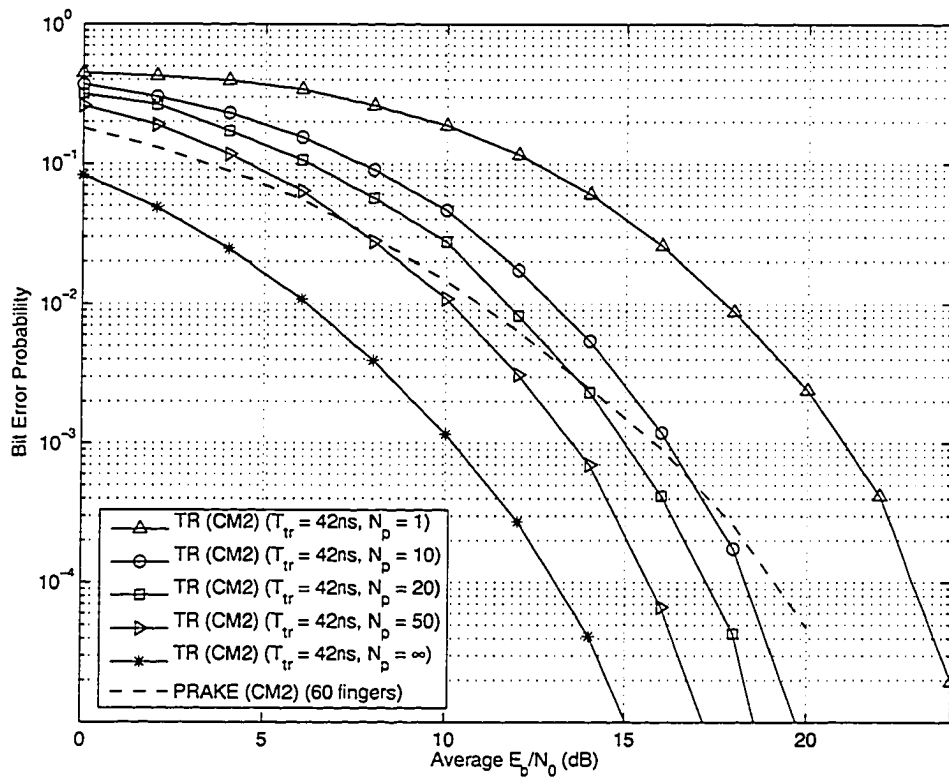


Figure 2.21: Effect of N_p on TR systems with noise averaging autocorrelation receiver in CM2

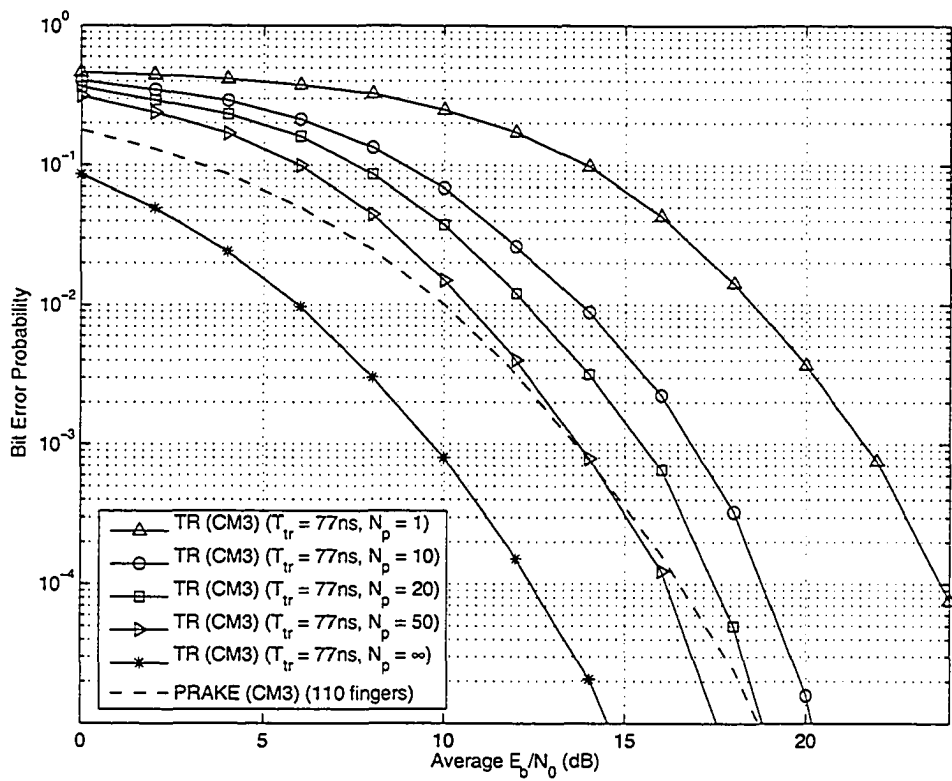


Figure 2.22: Effect of N_p on TR systems with noise averaging autocorrelation receiver in CM3

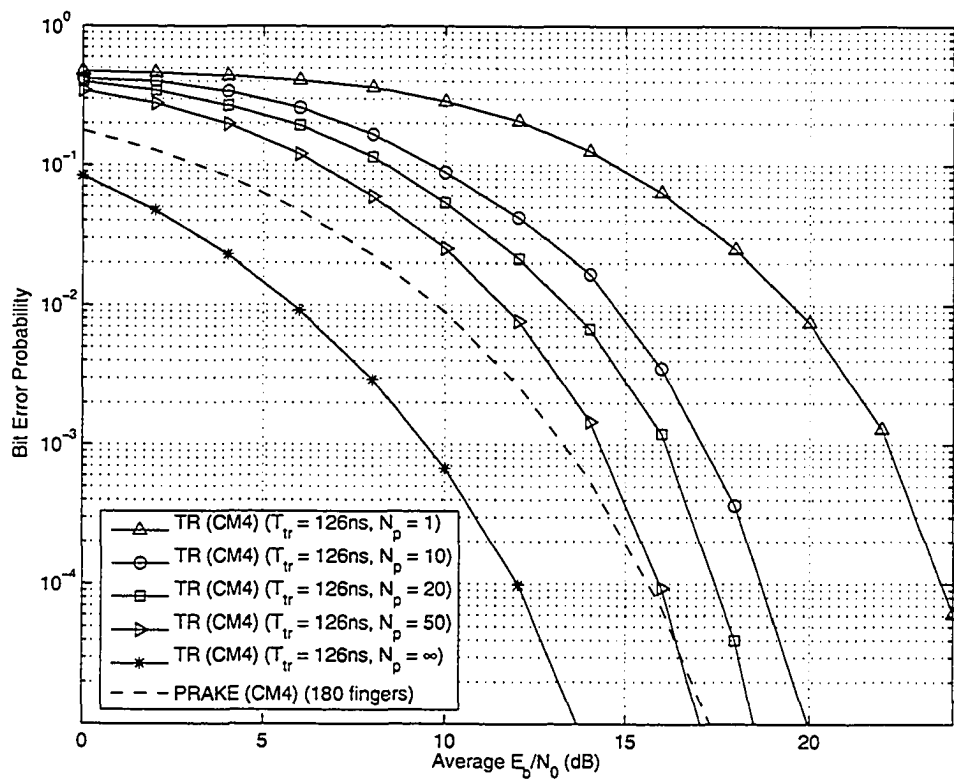


Figure 2.23: Effect of N_p on TR systems with noise averaging autocorrelation receiver in CM4

2.6 Conclusion

This chapter has demonstrated the application of the TR transmission scheme to the UWB channels, which has eliminated the requirement of the complicated channel estimator and relaxed the timing requirement. The TR system has been analysed numerically and by simulation. The IEEE standard channel models have been described and used to simulate real world system performance of the TR systems. It is concluded that the increase of the integration period T_{tr} up to a certain point will generally improve the system performance. The use of noise averaging technique has been proven to significantly enhance the performance of the system. It is also observed that noise degrades performance more on channels with large number of paths than channels with small number of paths.

Chapter 3

The DP - Dual Pulse system

3.1 Introduction

In the previous chapter, the application of the TR signal transmission scheme results in a simple autocorrelation receiver design, thus having a low system complexity. However, the TR system has rather low data rate since it takes two time frames to transmit a symbol. This has motivated the design of the new transmission and detection scheme. The new scheme uses a reference sub-pulse together with a modulated sub-pulse to constitute a dual pulse (DP) structure as the basic transmission unit. The first sub-pulse of the DP structure is either identical or inverse to the second sub-pulse. The basic transmission unit of the DP scheme can be considered as a single pulse and it takes only one time frame to transmit a symbol, thus it is more efficient than the TR scheme discussed in the previous chapter. Like systems based on the pilot symbol assisted scheme [50] and the differential scheme [61], this DP scheme can be considered as another type of generalisation of the TR method. The two sub-pulses of the DP scheme are expected to be affected by the channel in a similar manner, because two sub-pulses are transmitted one after the other and have the same pulse shape. For each resolvable multipath, the autocorrelation receiver uses the first half of the DP pulse (i.e., the reference sub-pulse) to demodulate the second half (i.e., the modulated sub-pulse). To effectively collect the signal energy of the multipaths, combining methods including generalised selection combining

(GSC), absolute threshold GSC (AT-GSC) and normalised threshold GSC (NT-GSC) are proposed for the DP scheme.

In this chapter, the DP scheme will be described in detail, including its receiver based on GSC, AT-GSC and NT-GSC combining. The performance of the DP systems will be analysed and compared with the TR system and the performance of GSC, AT-GSC, and NT-GSC combining methods for the DP system will be analysed. Another simple receiver for the DP scheme that performs the autocorrelation of the received signal and its half pulse duration delayed version over the effective channel length is also simulated and compared to the performance of GSC, AT-GSC, and NT-GSC schemes. To account for the possible multipath interference between the received reference signal and the data signal, the realistic IEEE UWB channel models introduced in Section 2.4 are employed in the simulations. The noise averaging technique is also applied in the DP system to reduce the noise variance and to eliminate the inter-path interference (IPI).

3.2 DP Transmitter System

In the newly proposed DP signalling scheme, the reference and data information are sent as one pulse $g_{dp}(t)$ of duration T_w . A DP pulse $g_{dp}(t)$ consists of two sub-pulses; the sub-pulse $p(t)$ having non-zero value in the first half interval $[0, T_w/2]$ represents the reference signal and the sub-pulse $s_2(t)$ in the second half interval $[T_w/2, T_w]$ represents the modulated data signal. The energy of the sub-pulse $p(t)$ is defined as $E_b/2$. The relationship between the sub-pulse $s_2(t)$ and the reference sub-pulse $p(t)$ depends on the particular modulation method used. For on-off keying (OOK) and pulse position modulated (PPM) signals, the basic unit of a UWB pulse is composed of two identical sub-pulses, i.e.,

$$s_2(t) = \begin{cases} p(t - \frac{T_w}{2}), & \frac{T_w}{2} \leq t \leq T_w \\ 0, & \text{elsewhere} \end{cases}$$

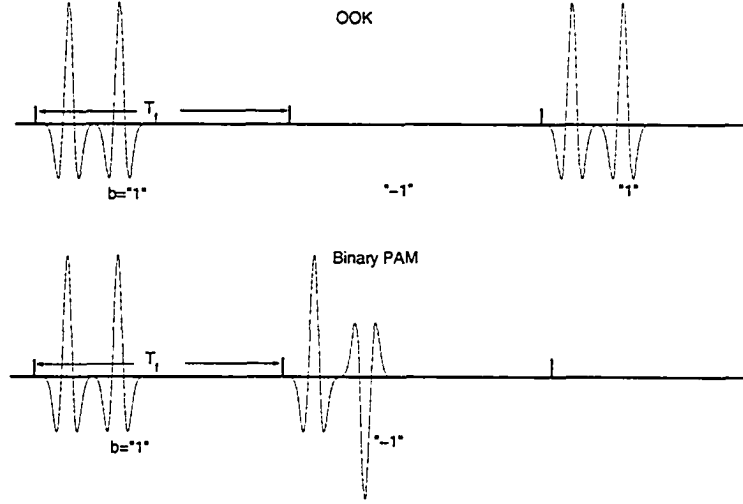


Figure 3.1: Illustration of OOK and binary PAM modulated DP signal $g_{dp}(t)$

and the UWB pulse $g_{dp}(t)$ given by

$$g_{dp}(t) = p(t) + p(t - \frac{T_w}{2}), 0 \leq t \leq T_w \quad (3.1)$$

The binary PAM modulated $s_2(t)$ can be represented as

$$s_2(t) = \begin{cases} b \cdot p(t - \frac{T_w}{2}), & \frac{T_w}{2} \leq t \leq T_w \\ 0, & \text{elsewhere} \end{cases}$$

and

$$g_{dp}(t) = p(t) + b \cdot p(t - \frac{T_w}{2}), 0 \leq t \leq T_w \quad (3.2)$$

where $b \in \{-1, 1\}$ is the data information bit. Since the energy of each sub-pulse is defined as $E_b/2$, the energy of the UWB pulse $g_{dp}(t)$ equals E_b . The dual pulse structure for OOK and binary PAM is illustrated in Fig. 3.1.

The transmitter for the binary PAM modulated DP signal pulse has a similar structure as the TR system and is illustrated in Fig. 3.2. Unlike the TR system in the previous chapter where it takes $2T_f$ to transmit a pulse pair, the dual sub-pulse structured pulses are designed to transmit every T_f

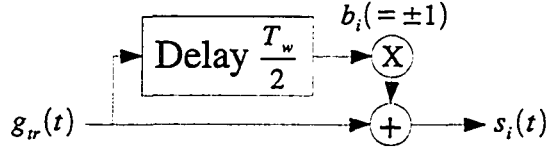


Figure 3.2: Binary PAM modulated DP system transmitter block diagram

interval, where T_f is defined as the transmission time frame. To improve the transmission reliability, the same dual pulse can be transmitted N_s times. A binary PAM modulated DP signal for transmission can be expressed as

$$s_{dp}(t) = \sum_{-\infty}^{\infty} p(t - iT_f) + b_{\lfloor i/N_s \rfloor} p(t - iT_f - \frac{T_w}{2}). \quad (3.3)$$

Since the DP structure is transmitted as one pulse, the two sub-pulses will experience the same channel distortion. The short pulse duration of the DP structure leads to the possible assumption of minimal interference between the two sub-pulses due to channel multipath. Therefore, the first sub-pulse of the received DP structure can be used as an interference free noisy reference for the detection of the modulated second sub-pulse of the received DP structure. This eliminates the need for explicit channel estimation. The received DP signal is expressed as

$$\begin{aligned} \bar{r}_{dp}(t) = & \sum_{i=-\infty}^{\infty} p(t - iT_f) * h(t) \\ & + b_{\lfloor i/N_s \rfloor} p(t - iT_f - \frac{T_w}{2}) * h(t) + \bar{n}(t) \end{aligned} \quad (3.4)$$

where $\bar{n}(t)$ is the zero mean additive white Gaussian noise with variance of $\frac{N_0}{2}$ and $h(t)$ is the multipath channel impulse response. The received DP signal is then passed through an ideal low-pass filter with a one-sided bandwidth of W Hz and unit magnitude, which is designed to limit the noise variance and allow the signal to pass through without distortion. With $h(t)$ defined in (2.4),

the received DP signal over one symbol duration after the filter is given by

$$r(t) = \sum_{i=0}^{N_s-1} \sum_{k=1}^K [\alpha_k p_{rx}(t - iT_f - \tau_k) + \alpha_k b p_{rx}(t - iT_f - \frac{T_w}{2} - \tau_k)] + n(t) \quad (3.5)$$

where $p_{rx}(t)$ is the received pulse shape corresponding to the transmitted $p(t)$ and $n(t)$ is the bandlimited noise. In next section, different receiver detection schemes designed for the DP system are presented and their performance analysed.

3.3 DP Receiver Performance

In this section, receiver designs with different levels of channel knowledge are presented. The first receiver design assumes the multipath channel delays τ_k 's are known, while other receiver designs assume the channel delays τ_k 's are unknown. The receiver design for the DP system can be generalised in two parts. The first part implements autocorrelation for each resolvable path in the received DP signals, while the second part combines the correlated outputs.

3.3.1 Known path delay τ_k 's

With the knowledge of the path delay τ_k , the receiver first correlates the filtered received signal and its $\frac{T_w}{2}$ delayed copy for every known path delay τ_k . A simple block diagram of the receiver structure is given in Fig. 3.3. The integrate-and-dump (I&D) device integrates the second half of the T_w duration input signal for each known multipath arrival instant and then is reset to zero at the end of the T_w interval. The receiver then sums up the first L ($\leq K$) results of the correlator D_k to form the decision variable D given by

$$\begin{aligned} D &= \sum_{j=0}^{N_s-1} \sum_{k=1}^L \int_{jT_f + \tau_k + \frac{T_w}{2}}^{jT_f + \tau_k + T_w} r(t)r(t - \frac{T_w}{2})dt \\ &= bN_s R(0) \sum_{k=1}^L |\alpha_k|^2 + \sum_{k=1}^L \alpha_k N_{1k} + \sum_{k=1}^L \alpha_k b N_{2k} + N \end{aligned} \quad (3.6)$$

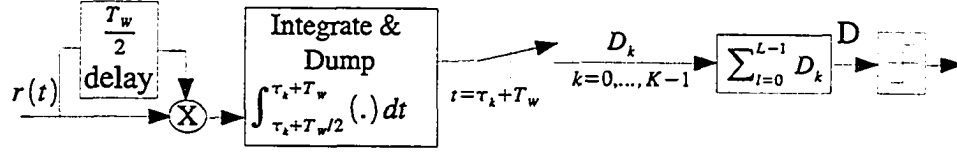


Figure 3.3: Block diagram for DP known τ receiver design

where

$$R(\tau) = \int_{-\infty}^{\infty} p_{rx}(t - \tau) p_{rx}(t) dt \quad (3.7)$$

$$N_{1k} = \sum_{j=0}^{N_s-1} \int_{jT_f + \tau_k + \frac{T_w}{2}}^{jT_f + \tau_k + T_w} n(t) p_{rx}(t - jT_f - \tau_k - \frac{T_w}{2}) dt \quad (3.8)$$

$$N_{2k} = \sum_{j=0}^{N_s-1} \int_{jT_f + \tau_k + \frac{T_w}{2}}^{jT_f + \tau_k + T_w} n(t - \frac{T_w}{2}) p_{rx}(t - jT_f - \tau_k - \frac{T_w}{2}) dt \quad (3.9)$$

$$N = \sum_{j=0}^{N_s-1} \sum_{k=1}^L \int_{jT_f + \tau_k + \frac{T_w}{2}}^{jT_f + \tau_k + T_w} n(t) n(t - \frac{T_w}{2}) dt. \quad (3.10)$$

For the analysis, the separation between channel delays τ_k and τ_{k-1} is assumed to be $\geq T_w$. Therefore, both N_{1k} 's and N_{2k} 's can be modeled as independently distributed zero mean Gaussian R.V.s with variance $\frac{N_0}{2} N_s R(0)$. From the central limit theorem, the noise to noise term N can be approximated as Gaussian distributed

$$\begin{aligned} \sigma_n^2 = \mathbb{E}[N^2] &= \sum_{j=0}^{N_s-1} \sum_{k=1}^L \int_{jT_f + \tau_k + \frac{T_w}{2}}^{jT_f + \tau_k + T_w} \int_{jT_f + \tau_k + \frac{T_w}{2}}^{jT_f + \tau_k + T_w} \mathbb{E}[n(t_1) n(t_1 - \frac{T_w}{2}) n(t_2) n(t_2 - \frac{T_w}{2})] dt_1 dt_2 \\ &= \sum_{j=0}^{N_s-1} \sum_{k=1}^L \int_{jT_f + \tau_k + \frac{T_w}{2}}^{jT_f + \tau_k + T_w} \int_{jT_f + \tau_k + \frac{T_w}{2}}^{jT_f + \tau_k + T_w} [R_n^2(\frac{T_w}{2}) + R_n^2(t_2 - t_1) \\ &\quad + R_n(t_2 - t_1 + \frac{T_w}{2}) R_n(t_2 - t_1 - \frac{T_w}{2})] dt_1 dt_2 \end{aligned} \quad (3.11)$$

where $R_n(\tau) = \mathbb{E}[n(t) n(t + \tau)] = N_0 W \text{sinc}(2W\tau)$ [58]. When $\tau \geq \frac{T_w}{2}$, $R(\tau)$ is assumed to be very small (i.e. ≈ 0). Therefore, (3.11) can be approximated

as

$$\begin{aligned}\sigma_n^2 &\approx \sum_{j=0}^{N_s-1} \sum_{k=1}^L \int_{jT_f+\tau_k+\frac{T_w}{2}}^{jT_f+\tau_k+T_w} \int_{jT_f+\tau_k+\frac{T_w}{2}}^{jT_f+\tau_k+T_w} R_n^2(t_2 - t_1) dt_1 dt_2 \\ &= N_s L \int_{\frac{T_w}{2}}^{T_w} \int_{\frac{T_w}{2}}^{T_w} R_n^2(t_2 - t_1) dt_1 dt_2\end{aligned}\quad (3.12)$$

where (3.12) can be further simplified to [49]

$$\sigma_n^2 \approx N_s L W \frac{T_w}{2} \frac{N_0^2}{2}.\quad (3.13)$$

With the above approximation, the noise to noise term N , is almost uncorrelated to, therefore independent of N_{1k} and N_{2k} .

Conditioned on b , $\boldsymbol{\alpha} = (\alpha_1, \dots, \alpha_L)$ and $\boldsymbol{\tau} = (\tau_1, \dots, \tau_L)$, the decision variable D can be represented as a Gaussian distribution

$$D = \mathcal{N}(bN_s R(0)|\boldsymbol{\alpha}|^2, \frac{N_0}{2} N_s R(0)|\boldsymbol{\alpha}|^2 (b^2 + 1) + \sigma_n^2).\quad (3.14)$$

The conditional probability of error for this transmission and detection scheme is given by

$$P(e|\boldsymbol{\alpha}, \boldsymbol{\tau}) = P(D < 0 | b = 1, \boldsymbol{\alpha}, \boldsymbol{\tau}) = Q\left(\frac{N_s R(0)|\boldsymbol{\alpha}|^2}{\sqrt{N_0 N_s R(0)|\boldsymbol{\alpha}|^2 + \sigma_n^2}}\right).\quad (3.15)$$

Comparison between numerical evaluation and simulation result of this transmission and detection scheme over a simple multipath channel is shown in Fig. 3.4 with $N_s = 1$. The 20 path test channel used is the same as Section 2.3.1. Fig. 3.4 shows that the analytical results are closely matched by the simulation results for both $L = 8$ and $L = 10$ cases. This confirms that the Gaussian approximation used for the analysis of this transmission and detection scheme is valid.

3.3.2 Known path delay τ_k 's with noise averaging

In the previous chapter, it has shown that the noise averaging technique when applied on the autocorrelation receiver will lower the noise variance and thus

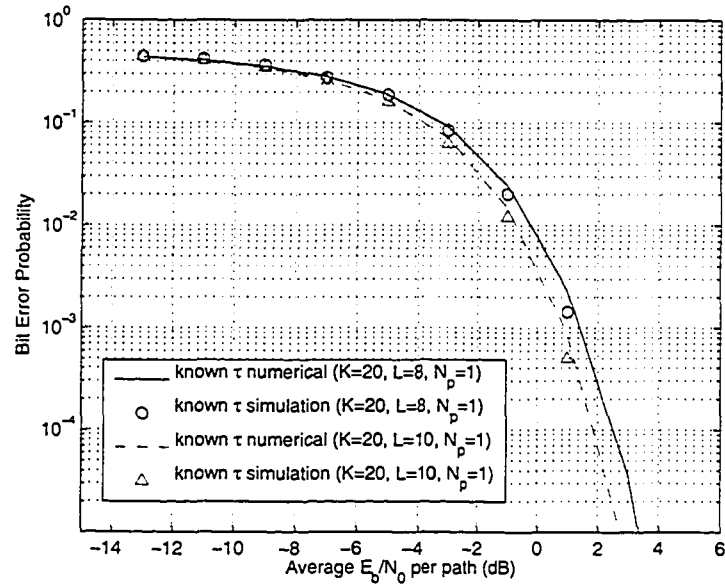


Figure 3.4: Numerical analysis and simulation comparison for known τ receiver

improve the performance of the TR system. The noise averaging technique is also applicable to the DP system much the same way as the TR system. And since the symbol duration of the DP system is only one time frame T_f instead of the two time frame for the TR system, the time span of delay blocks required for the noise averaging is reduced, thus reducing the latency caused by the noise averaging operation. Fig. 3.5 illustrates the DP receiver with known path delay τ_k 's and noise averaging. Note that the second part of the receiver structure is unchanged from that in the previous subsection Fig. 3.3, just with the noise averaging structure added at the beginning of the receiver. The noise averaging structure not only lowers the noise variance for the DP system, it also reduces the possible interference from the data sub-pulse onto the reference sub-pulse in a realistic channel with channel paths separated by less than T_w . This type of interference is referred to as IPI. Given a random data input with binary PAM modulation, the data sub-pulse will then cancel each other out when the received DP signal is summed up in the noise averaging

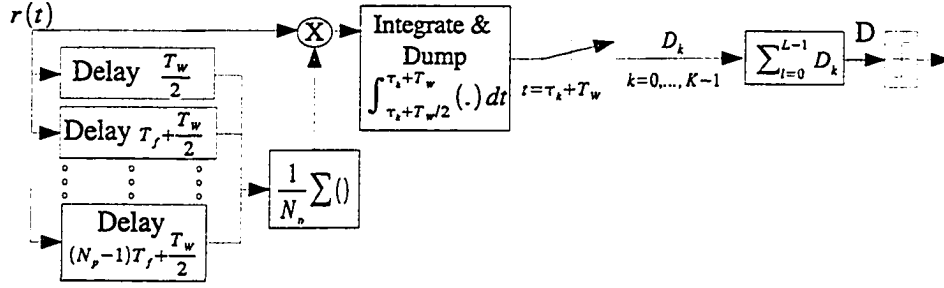


Figure 3.5: Block diagram for DP known τ receiver design

structure. With a large enough N_p , this will greatly suppress and/or eliminate the data signal following the reference sub-pulse. Thus a reference sub-pulse free from IPI is available to detect the modulated data sub-pulse. The decision variable when noise averaging is employed is given by

$$\begin{aligned}
 D &= \sum_{j=0}^{N_s-1} \sum_{k=1}^L \int_{jT_f + \tau_k + \frac{T_w}{2}}^{jT_f + \tau_k + T_w} r(t) \sum_{i=0}^{N_p-1} \frac{1}{N_p} r(t + iT_f - \frac{T_w}{2}) dt \\
 &= bN_s R(0) |\alpha|^2 + \sum_{k=1}^L \alpha_k N_{1k} + \sum_{k=1}^L \alpha_k b N_{2k} + N
 \end{aligned} \quad (3.16)$$

where

$$N_{1k} = \sum_{j=0}^{N_s-1} \int_{\frac{T_w}{2}}^{T_w} n(t + jT_f + \tau_k) p_{rx}(t - \frac{T_w}{2}) dt \quad (3.17)$$

$$\begin{aligned}
 N_{2k} &= \sum_{j=0}^{N_s-1} \int_{\frac{T_w}{2}}^{T_w} \frac{1}{N_p} \sum_{i=0}^{N_p-1} n(t + jT_f + \tau_k + iT_f - \frac{T_w}{2}) \\
 &\quad \times p_{rx}(t - \frac{T_w}{2}) dt
 \end{aligned} \quad (3.18)$$

$$\begin{aligned}
 N &= \sum_{j=0}^{N_s-1} \sum_{k=1}^L \int_{\frac{T_w}{2}}^{T_w} n(t + jT_f + \tau_k) \\
 &\quad \times \frac{1}{N_p} \sum_{i=0}^{N_p-1} n(t + jT_f + \tau_k + iT_f - \frac{T_w}{2}) dt.
 \end{aligned} \quad (3.19)$$

Like in the previous subsection, N_{1k} and N_{2k} are modeled as zero mean Gaussian R.V.s with variances $\frac{N_0}{2} N_s R(0)$ and $\frac{N_0}{2} \frac{N_s}{N_p} R(0)$, respectively. Similarly,

the noise to noise term can be approximated as a zero mean Gaussian R.V. with variance

$$\begin{aligned}\sigma_n^2 &\approx \frac{1}{N_p} \sum_{j=0}^{N_s-1} \sum_{k=1}^L \int_{jT_f+\tau_k+\frac{T_w}{2}}^{jT_f+\tau_k+T_w} \int_{jT_f+\tau_k+\frac{T_w}{2}}^{jT_f+\tau_k+T_w} R_n^2(t_2 - t_1) dt_1 dt_2 \\ &= \frac{N_s}{N_p} L \int_{\frac{T_w}{2}}^{T_w} \int_{\frac{T_w}{2}}^{T_w} R_n^2(t_2 - t_1) dt_1 dt_2\end{aligned}\quad (3.20)$$

$$\approx \frac{N_s L W T_w N_0^2}{4 N_p}.\quad (3.21)$$

Assuming all the noise terms (N_{1k} , N_{2k} and N) are independent, the conditional probability of error is given by

$$P(e|\alpha, \tau) = Q\left(\frac{N_s R(0) |\alpha|^2}{\sqrt{\frac{N_0}{2} N_s R(0) |\alpha|^2 + \frac{N_0}{2} \frac{N_s}{N_p} R(0) |\alpha|^2 + \sigma_n^2}}\right).\quad (3.22)$$

In Fig. 3.6, the probability of bit error is evaluated numerically from (3.22) with the 20 path channel and compared with simulation results. The figure shows that the performance of the simulation and numerical evaluation agree with each other, therefore proves that the assumptions for the analysis is valid. When compared with Fig. 3.4, it shows the noise averaging over 50 frames saves about 5 dB at BER = 10^{-3} .

3.3.3 Receiver design for unknown path delay τ_k 's

It is often desirable to know the channel path delay for better performance of the autocorrelation receiver. However, estimating the path delay is not an easy task and will increase the system complexity. In this section the receiver design presented will assume no knowledge of the path delay τ_k . For the analysis purpose the resolvable paths are assumed to arrive at integer multiples of T_w relative to the first path to avoid the IPI issue.

Without the knowledge of the path delay τ_k , modification will be applied to the I&D unit of the receiver shown in Fig. 3.3. The modified receiver is shown in Fig. 3.7, where the results from the I&D unit is shown as

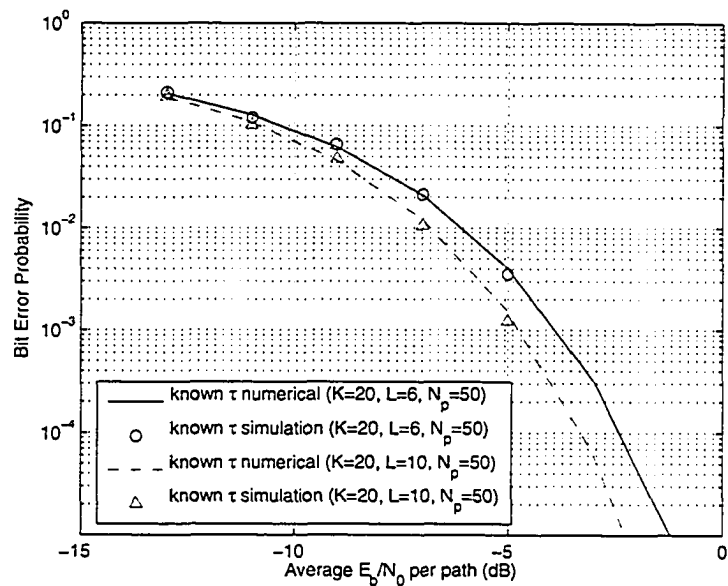


Figure 3.6: Numerical analysis and simulation comparison for noise averaging known τ receiver

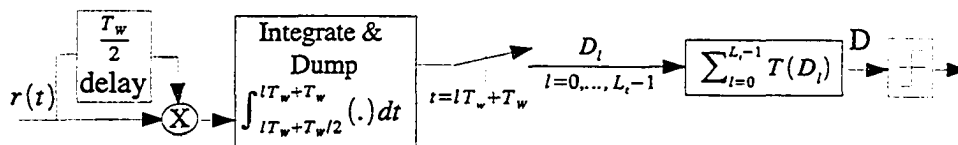


Figure 3.7: Block diagram for DP unknown τ receiver design

$$\begin{aligned}
D_l &= \sum_{j=0}^{N_s-1} \int_{jT_f+lT_w+\frac{T_w}{2}}^{jT_f+lT_w+T_w} r(t)r(t-\frac{T_w}{2})dt, \quad l = 0, \dots, L_t - 1 \\
&= \begin{cases} N_s|\alpha_k|^2 bR(0) + \alpha_k N_{1k} + \alpha_k N_{2k} + N_l, & lT_w = \tau_k \\ N_l, & lT_w \neq \tau_k \end{cases} \quad (3.23)
\end{aligned}$$

where $L_t = \frac{T_{mds}}{T_w}$ is the total number of possible paths and T_{mds} is the maximum delay spread of the channel. The noise N_{1k} , N_{2k} are defined in (3.8) and (3.9), and the noise to noise term N_l is given by

$$N_l = \sum_{j=0}^{N_s-1} \int_{jT_f+lT_w+\frac{T_w}{2}}^{jT_f+lT_w+T_w} n(t)n(t-jT_f-\frac{T_w}{2})dt. \quad (3.24)$$

With the same assumption as in the previous subsection, N_l can be approximated as a Gaussian R.V. with zero mean and variance defined by

$$\sigma_{N_l}^2 \approx N_s \int_{\frac{T_w}{2}}^{T_w} \int_{\frac{T_w}{2}}^{T_w} R_n^2(t_2 - t_1) dt_1 dt_2 \quad (3.25)$$

$$\approx \frac{N_0^2}{4} N_s W T_w. \quad (3.26)$$

Therefore, the decision variable D_l can be modeled by

$$\begin{aligned}
D_l &\sim \mathcal{N}(N_s|\alpha_k|^2 bR(0), N_0 N_s R(0) |\alpha_k|^2 + \frac{N_0^2}{4} N_s W T_w), \quad lT_w = \tau_k \\
D_l &\sim \mathcal{N}(0, \frac{N_0^2}{4} N_s W T_w), \quad lT_w \neq \tau_k.
\end{aligned} \quad (3.27)$$

The following three subsections will describe three different ways of combining the L_t independent D_l 's to form the decision variable D . Each different combining scheme will still use the same receiver structure as shown in Fig. 3.7 but with different definition of the test function $T(D_l)$.

3.3.3.1 Generalised Selection Combining (GSC)

This method selects L number of $\{D_l | l = 0, \dots, L_t - 1\}$ with the largest absolute values $|D_l|$'s. The test function is given by

$$T(D_l) = \begin{cases} D_l, & \text{if } |D_l| \geq |D^{(L)}| \\ 0, & \text{if } |D_l| < |D^{(L)}| \end{cases} \quad (3.28)$$

where $D^{(L)}$ represents the L -th largest absolute value among all D_l 's. The decision variable for GSC is then given by

$$D = \sum_{l=0}^{L_t-1} T(D_l). \quad (3.29)$$

The L_t -tuples form the probability space,

$$\mathcal{S}_D = \{(D_0, D_1, \dots, D_{L_t-1}) | D_l \in \mathbb{R}, l = 0, \dots, L_t - 1\}. \quad (3.30)$$

Following the probability space partition based approach in [62], the probability space \mathcal{S}_D can be partitioned into L_t subspaces $\mathcal{A}_i, i = 0, \dots, L_t - 1$ given by

$$\begin{aligned} \mathcal{A}_i &:= \{(D_0, D_1, \dots, D_{L_t-1}) | \exists \text{card}(I_i) = L - 1, \\ &\quad \text{s.t. } l \in I_i \Leftrightarrow |D_l| > |D_i| \text{ or } (|D_l| = |D_i|, l > i)\} \end{aligned} \quad (3.31)$$

where the set \mathcal{A}_i is a collection of all possible L_t -tuples (D_0, \dots, D_{L_t-1}) that has D_i as the L -th largest element in absolute value. $I_i \subset \{0, 1, \dots, L_t - 1\} - \{i\}$ is the index set, $\text{card}(I_i)$ denotes the cardinality of the set I_i , and *s.t.* is a short hand notation for "such that". This implies that the index set I_i contains $L - 1$ elements chosen from the set $\{0, 1, \dots, L_t - 1\} - \{i\}$. The elements in I_i are the indices of the $L - 1$ variables (i.e., D_l 's) having absolute values greater than D_i . There are $\binom{L_t-1}{L-1}$ possible combinations for I_i .

Take $L_t = 4$ and $L = 3$ as an example, which is essentially selecting 3 D_l 's with the largest absolute values out of the total 4 D_l 's, i.e., D_0, D_1, D_2, D_3 . In this case, the sets \mathcal{A}_i 's are given in details as following.

$\mathcal{A}_0 := \{(D_0, D_1, D_2, D_3)\}$ is a collection of 4-tuples where

$$\begin{aligned} &\left. \begin{array}{l} |D_1| \geq |D_2| \geq |D_0| > |D_3| \\ |D_2| > |D_1| \geq |D_0| > |D_3| \end{array} \right\} I_0^1 = \{1, 2\} \\ &\left. \begin{array}{l} |D_1| \geq |D_3| \geq |D_0| > |D_2| \\ |D_3| > |D_1| \geq |D_0| > |D_2| \end{array} \right\} I_0^2 = \{1, 3\} \\ &\left. \begin{array}{l} |D_2| \geq |D_3| \geq |D_0| > |D_1| \\ |D_3| > |D_2| \geq |D_0| > |D_1| \end{array} \right\} I_0^3 = \{2, 3\} \end{aligned}$$

$A_1 := \{(D_0, D_1, D_2, D_3)\}$ is a collection of 4-tuples where

$$\left. \begin{array}{l} |D_0| > |D_2| \geq |D_1| > |D_3| \\ |D_2| \geq |D_0| > |D_1| > |D_3| \end{array} \right\} I_1^1 = \{0, 2\}$$

$$\left. \begin{array}{l} |D_0| > |D_3| \geq |D_1| > |D_2| \\ |D_3| \geq |D_0| > |D_1| > |D_2| \end{array} \right\} I_1^2 = \{0, 3\}$$

$$\left. \begin{array}{l} |D_2| \geq |D_3| \geq |D_1| \geq |D_0| \\ |D_3| > |D_2| \geq |D_1| \geq |D_0| \end{array} \right\} I_1^3 = \{2, 3\}$$

$A_2 := \{(D_0, D_1, D_2, D_3)\}$ is a collection of 4-tuples where

$$\left. \begin{array}{l} |D_0| \geq |D_1| > |D_2| > |D_3| \\ |D_1| > |D_0| > |D_2| > |D_3| \end{array} \right\} I_2^1 = \{0, 1\}$$

$$\left. \begin{array}{l} |D_0| > |D_3| \geq |D_2| \geq |D_1| \\ |D_3| \geq |D_0| > |D_2| \geq |D_1| \end{array} \right\} I_2^2 = \{0, 3\}$$

$$\left. \begin{array}{l} |D_1| > |D_3| \geq |D_2| \geq |D_0| \\ |D_3| \geq |D_1| > |D_2| \geq |D_0| \end{array} \right\} I_2^3 = \{1, 3\}$$

$A_3 := \{(D_0, D_1, D_2, D_3)\}$ is a collection of 4-tuples where

$$\left. \begin{array}{l} |D_0| \geq |D_1| > |D_3| \geq |D_2| \\ |D_1| > |D_0| > |D_3| \geq |D_2| \end{array} \right\} I_3^1 = \{0, 1\}$$

$$\left. \begin{array}{l} |D_0| \geq |D_2| > |D_3| \geq |D_1| \\ |D_2| > |D_0| > |D_3| \geq |D_1| \end{array} \right\} I_3^2 = \{0, 2\}$$

$$\left. \begin{array}{l} |D_1| \geq |D_2| > |D_3| \geq |D_0| \\ |D_2| > |D_1| > |D_3| \geq |D_0| \end{array} \right\} I_3^3 = \{1, 2\}$$

Obviously in this example, for any i there are always 3 possible I_i 's, i.e., I_i^1 , I_i^2 , and I_i^3 .

With the probability space S_D partitioned into subspaces $\{\mathcal{A}_i\}$, the moment generating function (MGF) of the noncoherent GSC decision variable D

can be expressed as

$$\begin{aligned}
\Phi_{GSC}(s) &= \mathbb{E}[e^{sD}] = \mathbb{E}_{S_D} \left[\exp \left(s \sum_{l=0}^{L_t-1} T(D_l) \right) \right] \\
&= \sum_{i=0}^{L_t-1} \mathbb{E}_{\mathcal{A}_i} \left[\exp \left(s \sum_{l=0}^{L_t-1} T(D_l) \right) \right] \\
&= \sum_{i=0}^{L_t-1} \mathbb{E}_{\mathcal{A}_i} \left[\prod_{l=0}^{L_t-1} [e^{sT(D_l)}] \right]. \tag{3.32}
\end{aligned}$$

Therefore, the expectation over the entire probability space S_D can be obtained as the sum of the expectation over each subspace \mathcal{A}_i . It further leads to [63]

$$\begin{aligned}
\Phi_{GSC}(s) &= \sum_{i=0}^{L_t-1} \int_{-\infty}^{\infty} \left\{ \sum_{\substack{\text{all } I_i \\ \text{card}\{I_i\}=L-1}} \underbrace{\int_{|D_i|}^{\infty} \cdots \int_{|D_i|}^{\infty}}_{L-1} \underbrace{\int_{-|D_i|}^{|D_i|} \cdots \int_{-|D_i|}^{|D_i|}}_{L_t-L} \right. \\
&\quad \prod_{l=0}^{L_t-1} [e^{sT(D_l)} f_l(D_l)] dD_{l_1} \cdots dD_{l_{(L-1)}} dD_{l'_1} \cdots dD_{l'_{(L_t-L)}} \\
&\quad + \underbrace{\int_{-\infty}^{-|D_i|} \cdots \int_{-\infty}^{-|D_i|}}_{L-1} \underbrace{\int_{-|D_i|}^{|D_i|} \cdots \int_{-|D_i|}^{|D_i|}}_{L_t-L} \\
&\quad \left. \prod_{l=0}^{L_t-1} [e^{sT(D_l)} f_l(D_l)] dD_{l_1} \cdots dD_{l_{(L-1)}} dD_{l'_1} \cdots dD_{l'_{(L_t-L)}} \right\} dD_i \tag{3.33}
\end{aligned}$$

where $f_l(x)$ is the probability density function (PDF) of D_l . Moreover, $l_j \in I_i$ for $j = 1, \dots, L-1$ and $l'_j \notin I_i$ for $j = 1, \dots, L_t-L$. Since $L-1$ D_{l_j} 's all have absolute values greater than or equal to that of D_i , the integration interval of these variables then should be $[\infty, -|D_i|]$ and $[|D_i|, \infty]$, while the integration interval for $D_{l'_j}$'s should be $[-|D_i|, |D_i|]$. This is essentially what is contained in (3.33). Given the definition of $T(D_l)$ in (3.28), eq. (3.33) can be further simplified to

$$\Phi_{GSC}(s) = \sum_{i=0}^{L_t-1} \int_{-\infty}^{\infty} f_i(D_i) e^{sD_i} \sum_{\text{all } I_i} \prod_{l \in I_i} \Psi_l(s, D_i) \prod_{\substack{l' \notin I_i \\ l' \neq i}} [F_{l'}(|D_i|) - F_{l'}(-|D_i|)] dD_i \tag{3.34}$$

where $F_l(y)$ is the cumulative distribution function (CDF) of D_l . The function $\Psi_l(s, x)$, $l = 0, \dots, L_t - 1$ is the incomplete MGF of the first kind of D_l and defined as

$$\Psi_l(s, x) = \int_{-\infty}^{-|x|} f_l(y)e^{sy}dy + \int_{|x|}^{\infty} f_l(y)e^{sy}dy. \quad (3.35)$$

For $D_l \sim \mathcal{N}(\mu_l, \sigma_l^2)$ with μ_l and σ_l^2 defined in (3.27), the incomplete MGF of the first kind of D_l is derived as

$$\Psi_l(s, x) = \frac{1}{2}e^{s\mu_l + \frac{\sigma_l^2}{2}s^2} \left[\operatorname{erfc} \left(\frac{|x| + (\mu_l + \sigma_l^2 s)}{\sqrt{2}\sigma_l} \right) + \operatorname{erfc} \left(\frac{|x| - (\mu_l + \sigma_l^2 s)}{\sqrt{2}\sigma_l} \right) \right] \quad (3.36)$$

and the CDF $F_l(\cdot)$ of D_l is given by

$$\begin{aligned} F_l(|x|) &= \frac{1}{2} \operatorname{erfc} \left(\frac{\mu_l - |x|}{\sqrt{2}\sigma_l} \right) \\ F_l(-|x|) &= \frac{1}{2} \operatorname{erfc} \left(\frac{\mu_l + |x|}{\sqrt{2}\sigma_l} \right). \end{aligned} \quad (3.37)$$

The probability of error for DP GSC scheme can be evaluated using the Laplace inversion formula [64]

$$P(e|\alpha, \tau) = P(D < 0|b = +1, \alpha, \tau) = \frac{1}{2\pi j} \int_{c-j\infty}^{c+j\infty} \frac{\Phi_{GSC}(s)}{s} ds \quad (3.38)$$

where $c > 0$ is set as the saddle point of the integrand. To efficiently evaluate the above integral, trapezoidal rule [64] is applied, i.e.,

$$P(e|\alpha, \tau) = \frac{\Delta y}{\pi} \left[\frac{1}{2} \Re\{c^{-1}\Phi_{GSC}(c)\} + \sum_{m=1}^M \Re\{(c + jm\Delta y)^{-1}\Phi_{GSC}(c + jm\Delta y)\} \right] \quad (3.39)$$

where Δy is the step size and M is the parameter related to the truncation error. Usually M is chosen sufficiently large so that $\Re\{(c + jm\Delta y)^{-1}\Phi_{GSC}(c + jm\Delta y)\}$ has negligible values for $m > M$. The evaluation of complementary error functions with complex argument is required to evaluate the MGF in (3.39). The calculation detail for complex complementary error function is presented in [65].

To prove the correctness of the analysis result of the DP GSC scheme, the numerical evaluated analytical results are compared with the simulated

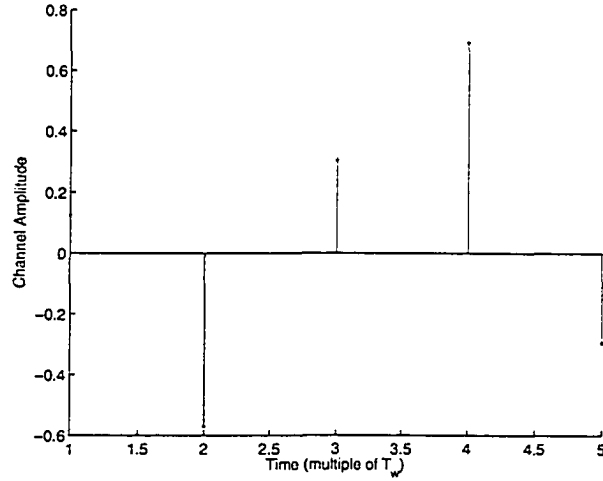


Figure 3.8: The impulse response of a simple 5 path test channel

results with D_l 's generated as independent and non-identically distributed (i.n.d.) Gaussian R.V.'s by the mean and variance defined in (3.27). The channel model used for this comparison is a unit gain 5 path test channel with path arrivals at integer multiples of T_w . The channel is illustrated in Fig. 3.8. In Fig. 3.9, the comparison of DP GSC scheme with $L = 2$ and $L = 4$ cases both shows that analytical and simulation results agree with each other.

3.3.3.2 Absolute Threshold GSC (AT-GSC)

An alternative method to the GSC scheme is absolute threshold general selection combining (AT-GSC). With this scheme, each autocorrelation output D_l is compared to a fixed threshold $D_{th} (> 0)$. This scheme will then select and combine all the D_l 's with absolute values greater than D_{th} . The AT-GSC test function is defined as

$$y_l = T(D_l) = \begin{cases} D_l, & \text{if } |D_l| \geq D_{th} \\ 0, & \text{if } |D_l| < D_{th} \end{cases}, \quad (3.40)$$

and the decision variable D is given by

$$D = \sum_{l=0}^{L_t-1} y_l. \quad (3.41)$$

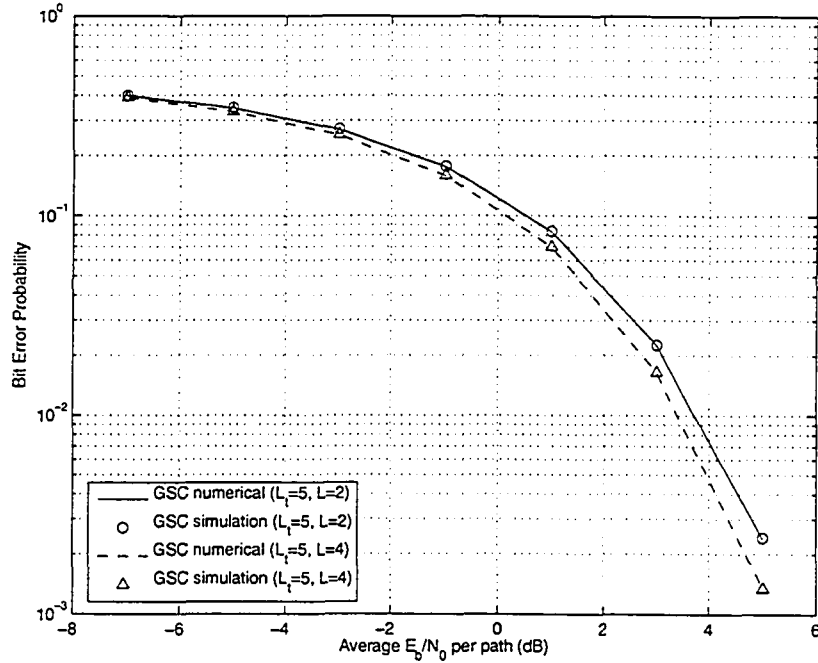


Figure 3.9: Numerical analysis and simulation comparison for DP GSC scheme

Similar to [66], the PDF of y_l can be expressed as a combination of PDF and CDF of D_l by

$$f_{y_l}(y_l) = \begin{cases} f_l(y_l), & |y_l| \geq D_{th} \\ 0, & 0 < |y_l| < D_{th} \\ [F_l(D_{th}) - F_l(-D_{th})]\delta(y_l), & y_l = 0 \end{cases} \quad (3.42)$$

where $\delta(\cdot)$ is the Dirac delta function. The MGF of y_l is represented by

$$\begin{aligned} \Phi_{y_l}(s) &= \int_{-\infty}^{\infty} f_{y_l}(y_l) e^{sy_l} dy_l \\ &= [F_l(D_{th}) - F_l(-D_{th})] + \int_{-\infty}^{-D_{th}} f_l(y_l) e^{sy_l} dy_l + \int_{D_{th}}^{\infty} f_l(y_l) e^{sy_l} dy_l \\ &= [F_l(D_{th}) - F_l(-D_{th})] + \Psi_l(s, D_{th}), \end{aligned} \quad (3.43)$$

where the function $\Psi_l(s, x)$ is defined in the previous subsection. Since D_l 's are independent but not necessarily identically distributed, same would be true for y_l 's. The MGF of D is hence given by

$$\Phi_{AT-GSC}(s) = \prod_{l=0}^{L_t-1} \Phi_{y_l}(s) = \prod_{l=0}^{L_t-1} [F_l(D_{th}) - F_l(-D_{th}) + \Psi_l(s, D_{th})]. \quad (3.44)$$

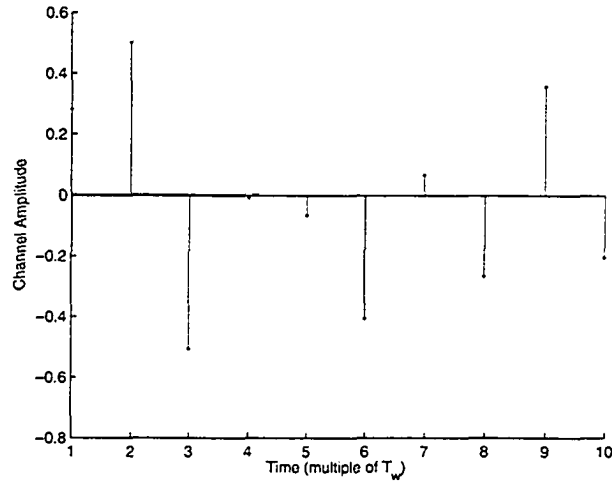


Figure 3.10: The channel response of a simple 10 path test channel

Replace $\Phi_{GSC}(s)$ in (3.39) with $\Phi_{AT-GSC}(s)$ given by (3.44) will give the conditional probability of error formulation for the proposed DP AT-GSC scheme. The numerically evaluated analytical result is plotted against the simulation result for DP AT-GSC scheme in Fig. 3.11. The plotted results are based on a 10 path test channel with channel response shown in Fig. 3.10. Fig. 3.11 demonstrates that there is no noticeable differences between the simulation result and the numerical result, thus validating the analysis.

3.3.3.3 Normalised Threshold (NT-GSC)

While the AT-GSC receiver of last subsection used a preset absolute decision threshold D_{th} , the NT-GSC receiver forms the decision threshold by taking a fixed fraction η_{th} of $D_{max} = \max |D_l|$ (i.e., $D_{th} = \eta_{th} D_{max}$). The NT-GSC test function therefore is defined as

$$T(D_l) = \begin{cases} D_l, & \text{if } |D_l| \geq \eta_{th} D_{max} \\ 0, & \text{if } |D_l| < \eta_{th} D_{max} \end{cases} \quad (3.45)$$

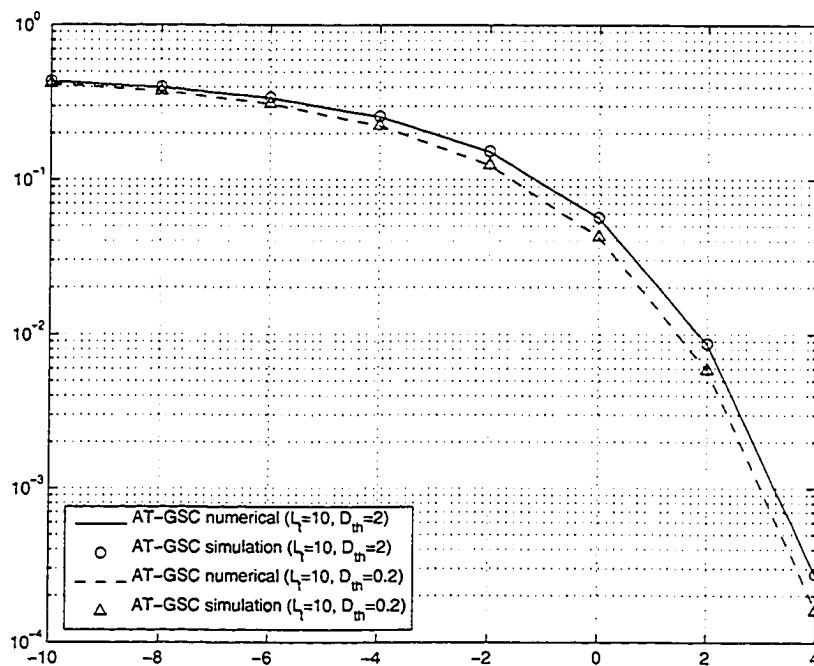


Figure 3.11: Numerical analysis and simulation comparison for DP AT-GSC scheme

With the decision variable D defined as $D = \sum_{l=0}^{L_t-1} T(D_l)$, the MGF of NT-GSC is given by

$$\Phi_{NT-GSC}(s) = \mathbb{E}_{\mathcal{S}_D} \left[\exp \left(s \sum_{l=0}^{L_t-1} T(D_l) \right) \right] \quad (3.46)$$

where $\mathcal{S}_D = \{(D_0, \dots, D_{L_t-1})\}$ is the probability space formed by L_t -tuples. Following the probability space partition based method presented in [62], \mathcal{S}_D is partitioned into subspaces \mathcal{B}_i 's given by

$$\mathcal{B}_i := \{(D_0, D_1, \dots, D_{L_t-1}) \mid |D_i| < |D_l|, \forall l \neq i \text{ or } (|D_l| = |D_i|, l < i)\}. \quad (3.47)$$

In subspace \mathcal{B}_i , D_i has the largest absolute value, $\bigcup_{i=0}^{L_t-1} \mathcal{B}_i = \mathcal{S}_D$ and $\mathcal{B}_i \cap \mathcal{B}_j = \emptyset$, $i \neq j$. Therefore, the MGF of D from (3.46) can be rewritten as

$$\begin{aligned} \Phi_{NT-GSC}(s) &= \sum_{i=0}^{L_t-1} \mathbb{E}_{\mathcal{B}_i} \left[\exp \left(s \sum_{l=0}^{L_t-1} T(D_l) \right) \right] \\ &= \sum_{i=0}^{L_t-1} \int_{-\infty}^{\infty} f_i(D_i) e^{sT(D_i)} \prod_{\substack{l=0 \\ l \neq i}}^{L_t-1} \left[\int_{-|D_i|}^{|D_i|} f_l(D_l) e^{sT(D_l)} dD_l \right] dD_i. \end{aligned} \quad (3.48)$$

Since $D_{max} = |D_i|$, the threshold is then $D_{th} = \eta_{th}|D_i|$. Therefore, applying the definition of the test function $T(D_l)$ from (3.45), (3.48) is now given by

$$\begin{aligned} \Phi_{NT-GSC}(s) &= \sum_{i=0}^{L_t-1} \int_{-\infty}^{\infty} f_i(D_i) e^{sD_i} \prod_{\substack{l=0 \\ l \neq i}}^{L_t-1} \left[\int_{-|D_i|}^{-\eta_{th}|D_i|} f_l(D_l) e^{sD_l} dD_l \right. \\ &\quad \left. + \int_{\eta_{th}|D_i|}^{|D_i|} f_l(D_l) e^{sD_l} dD_l + \int_{-\eta_{th}|D_i|}^{\eta_{th}|D_i|} f_l(D_l) e^{s \cdot 0} dD_l \right] dD_i \\ &= \sum_{i=0}^{L_t-1} \int_{-\infty}^{\infty} f_i(D_i) e^{sD_i} \\ &\quad \times \prod_{\substack{l=0 \\ l \neq i}}^{L_t-1} \left[\tilde{\Psi}_l(s, \eta_{th}D_i, D_i) + F_l(\eta_{th}|D_i|) - F_l(-\eta_{th}|D_i|) \right] dD_i \end{aligned} \quad (3.49)$$

where $\tilde{\Psi}_l(s, x, y)$ is named the incomplete MGF of the second kind and defined as

$$\begin{aligned}
\tilde{\Psi}_l(s, x, y) &= \int_{-|y|}^{-|x|} f_l(D_l) e^{sD_l} dD_l + \int_{|x|}^{|y|} f_l(D_l) e^{sD_l} dD_l \\
&= \int_{-\infty}^{-|x|} f_l(D_l) e^{sD_l} dD_l - \int_{-\infty}^{-|y|} f_l(D_l) e^{sD_l} dD_l \\
&\quad + \int_{|x|}^{\infty} f_l(D_l) e^{sD_l} dD_l - \int_{|y|}^{\infty} f_l(D_l) e^{sD_l} dD_l \\
&= \Psi_l(s, x) - \Psi_l(s, y).
\end{aligned} \tag{3.50}$$

Where Ψ_l is defined in (3.36). For $D_l \sim \mathcal{N}(\mu_l, \sigma_l^2)$, eq. (3.50) is derived as

$$\begin{aligned}
\tilde{\Psi}_l(s, x, y) &= \frac{1}{2} e^{s\mu_l + \frac{\sigma_l^2}{2} s^2} \left[\operatorname{erfc} \left(\frac{|x| + (\mu_l + \sigma_l^2 s)}{\sqrt{2}\sigma_l} \right) - \operatorname{erfc} \left(\frac{|y| + (\mu_l + \sigma_l^2 s)}{\sqrt{2}\sigma_l} \right) \right. \\
&\quad \left. + \operatorname{erfc} \left(\frac{|x| - (\mu_l + \sigma_l^2 s)}{\sqrt{2}\sigma_l} \right) - \operatorname{erfc} \left(\frac{|y| - (\mu_l + \sigma_l^2 s)}{\sqrt{2}\sigma_l} \right) \right].
\end{aligned} \tag{3.51}$$

Same as the GSC and AT-GSC system, the conditional probability of error for DP NT-GSC scheme can be evaluated by replacing $\Phi_{GSC}(s)$ in (3.39) with $\Phi_{NT-GSC}(s)$ given by (3.49). Fig. 3.12 plots a comparison between the DP NT-GSC numerical analysis result and simulation result based on D_l as Gaussian R.V. with mean and variance defined (3.27). The same 10 path test channel shown in Fig. 3.10 is used for the evaluation. Fig. 3.12 shows that in both cases when $\eta_{th} = 0.5$ and $\eta_{th} = 0.2$ the simulation matches the analysis results closely, thus validating the analysis.

3.3.4 Noise averaging applied on unknown path delay τ_k 's

The application of noise averaging to lower the noise variance in the unknown path delay receiver design is similar to the known path delay case. The resulting receiver will have the noise averaging structure in Fig. 3.5 added before the autocorrelator and the rest of structure will be the same as Fig. 3.7. Since the noise averaging structure is employed before the autocorrelation module, it does not affect the test functions, and therefore the analyse of the previous

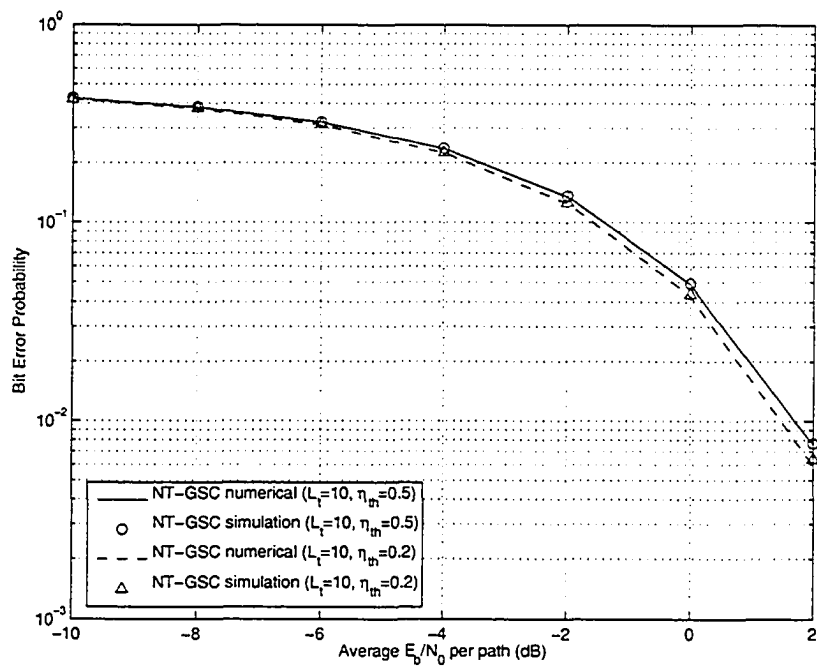


Figure 3.12: Numerical analysis and simulation comparison for DP NT-GSC scheme

three different selection schemes still apply. However, with the lower noise variance, the autocorrelator output D_l is substituted by

$$\begin{aligned}
D_l &\sim \mathcal{N}(N_s|\alpha_k|^2 bR(0), \frac{N_0}{2} N_s R(0)|\alpha_k|^2 (1 + \frac{1}{N_p}) + \frac{N_0^2}{4N_p} N_s W T_w), & lT_w = \tau_k \\
D_l &\sim \mathcal{N}(0, \frac{N_0^2}{4N_p} N_s W T_w), & lT_w \neq \tau_k. \\
D_l &\sim \mathcal{N}(N_s|\alpha_k|^2 bR(0), \frac{N_0}{2} N_s R(0)|\alpha_k|^2 (1 + \frac{1}{N_p}) + \frac{N_0^2}{4N_p} N_s W T_w), & lT_w = \tau_k \quad \text{\textit{GSC}} \\
D_l &\sim \mathcal{N}(0, \frac{N_0^2}{4N_p} N_s W T_w), & lT_w \neq \tau_k. & \text{\textit{an a}} \\
\end{aligned} \tag{3.52}$$

receivers are calculated by

$$D_l = \sum_{j=0}^{N_s-1} \int_{jT_f + \frac{T_w}{2}}^{jT_f + \frac{T_w}{2} + T_w} r(t)r(t - \frac{T_w}{2})dt, \quad l = 0, \dots, L_t - 1 \tag{3.53}$$

where $L_t = 2T_{mfs}/T_w$. This modification will increase the multipath energy collected by the receiver in a time frame. This is the D_l used in the simulation of the next section.

3.4 Simulation Results and Discussion

In this section, the performance of the DP system with noncoherent GSC, AT-GSC and NT-GSC receiver designs are studied by simulation for the channel models (CM1-CM4) described in Section 2.4. Also included in the simulation is a DP-Int autocorrelation receiver given by

$$D = \sum_{j=0}^{N_s-1} \int_{jT_f + \frac{T_w}{2}}^{jT_f + \frac{T_w}{2} + T_{dp-int}} r(t)r(t - \frac{T_w}{2})dt \tag{3.54}$$

where T_{dp-int} is the integration interval for this DP-Int receiver. Apparently, it is very similar to the conventional TR receiver and has the same complexity. It requires sampling rate of $1/T_f$, lower than the $2/T_w$ rate in the ‘‘GSC’’ type receivers. Extensive simulation tests are carried out to examine the effect of different design parameters, that is, the number of combined branches L in GSC, the absolute threshold D_{th} in AT-GSC, the normalised threshold η_{th} in NT-GSC and the integration length T_{dp-int} in the DP-Int receiver. Both

noise averaging and no noise averaging cases are studied for each parameter. Finally, the performances of GSC, AT-GSC, NT-GSC, and DP-Int receivers are compared with the TR system performance obtained from the previous chapter.

3.4.1 Simulation setup

As described in Section 3.2, the transmitted pulse $g_{dp}(t)$ of the DP system is created from joining an unmodulated sub-pulse with a modulated sub-pulse. For the simulation, binary PAM modulation is employed and the sub-pulse is based on a second derivative Gaussian pulse given by (2.40). The sub-pulse has non-zero value in the interval $[0, 0.7]$ ns, therefore the pulse duration T_w of $g_{dp}(t)$ is 1.4 ns with $g_{dp}(t)$ defined in (3.2). The TR system plotted for comparison will have pulse duration of 0.7 ns (i.e. using the same 2nd derivative Gaussian pulse). Each sub-pulse $p(t)$ is normalised to have energy $\frac{E_b}{2}$, which is to ensure the energy per data transmitted is the same as TR system of previous section. The Monte Carlo simulation has a sampling rate of 30 GHz and the same lowpass filter with a fixed Hamming window as the TR system of Section 2.5. For each channel realization, termination of the simulation is based on collecting 1000 errors or when 2×10^6 bits have been simulated. The bit error probability of each channel model is then obtained by averaging the BERs of the 100 channel realizations of the channel model.

3.4.2 The effect of L on the basic GSC Receiver

In the TR system of the previous section, it shows that as the length of integration T_{tr} increases, the performance of the TR system increases, much like the effect of increasing the number of fingers in a partial rake receiver. In the DP system with GSC receiver, increasing the number of D_l 's collected, L , to form decision variable D will also increase the performance of the system. However, since the autocorrelator results D_l 's are sorted from the absolute highest to the absolute lowest value, the stronger paths are designed to be collected first,

allowing good performance with a relatively low L .

The BER performance of a DP system employing GSC receivers with various L number of collected autocorrelation results for CM1-CM4 are shown in Figs. 3.13-3.16. In Fig. 3.13, it shows that the performance of collecting just the 10 largest correlator results (i.e. $L = 10$) is almost the same as collecting all the available results (i.e. $L = 40$) for CM1. As the total number of paths increases for different channels, the effect of increasing L in performance improvement is more pronounced. In Fig. 3.15 and Fig. 3.16 for CM3 and CM4 respectively, it can be clearly observed that when L increases from 10 to 20 there is a noticeable performance increase of less than 1 dB at $\text{BER} = 10^{-3}$. The performance gain results from increasing L beyond 20 is not significant even at high signal to noise ratio (SNR). These figures prove that only a small number of autocorrelator results L is required to achieve good result, and thus GSC is an efficient combining method for the DP autocorrelator.

3.4.3 The effect of L on the GSC Receiver with noise averaging

The performance difference from varying L in the DP-GSC system with noise averaging ($N_p = 50$) is investigated for CM1-CM4. As with the TR scheme of the previous chapter, DP-GSC receivers with noise averaging (Figs. 3.17-3.20) provide significant performance improvements over GSC receivers without noise averaging (Fig. 3.13-3.16) in CM1-CM4. Fig. 3.17 shows that the performance improvement from increasing L is not noticeable for CM1. For CM2 (Fig. 3.18), only at higher SNR can the improvement due to the increase of L be observed, but the improvement is minimal. Even in CM3 and CM4 (Figs. 3.19 and 3.20), the only observable performance improvement of less than 1 dB occurs at $\text{BER} = 10^{-3}$ when L increases from 10 to 20. When L passes 20, the improvement is marginal. Similar to the results obtained from the GSC receivers without noise averaging, these results further indicate increasing L substantially does not worsen performance but has limited effect

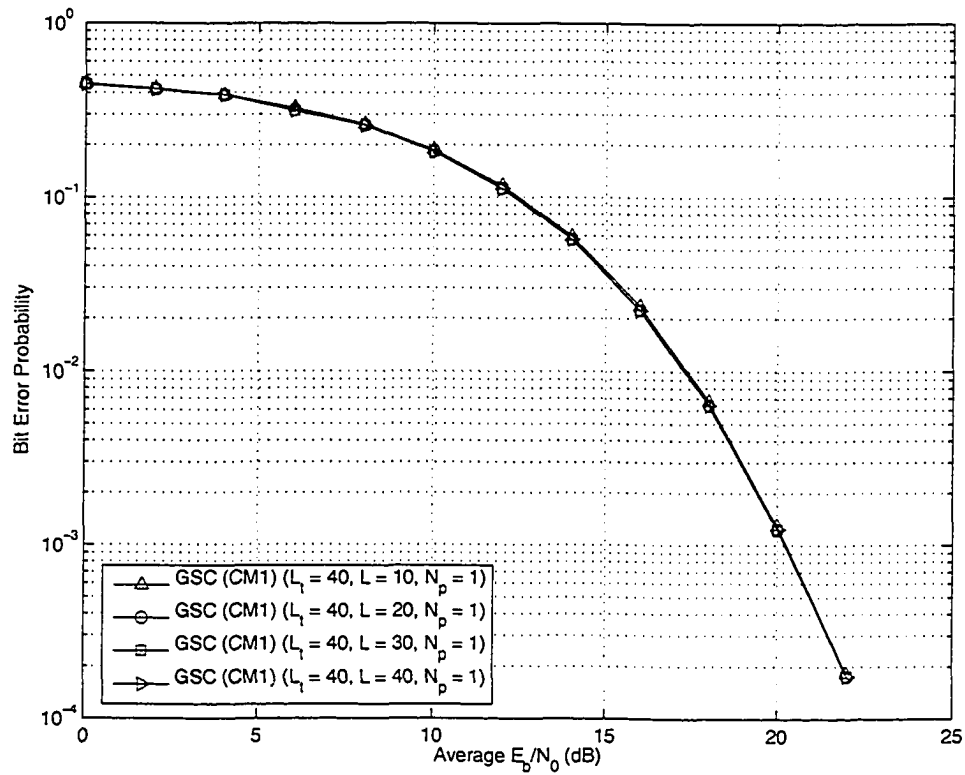


Figure 3.13: Effect of L on DP-GSC systems in CM1

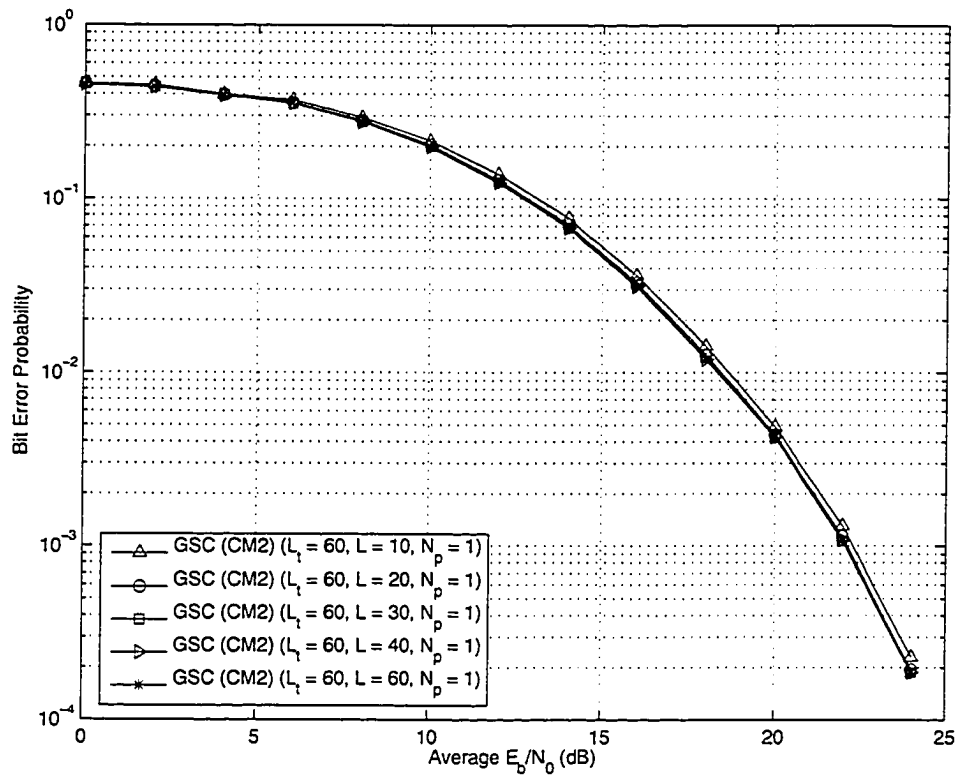


Figure 3.14: Effect of L on DP-GSC systems in CM2

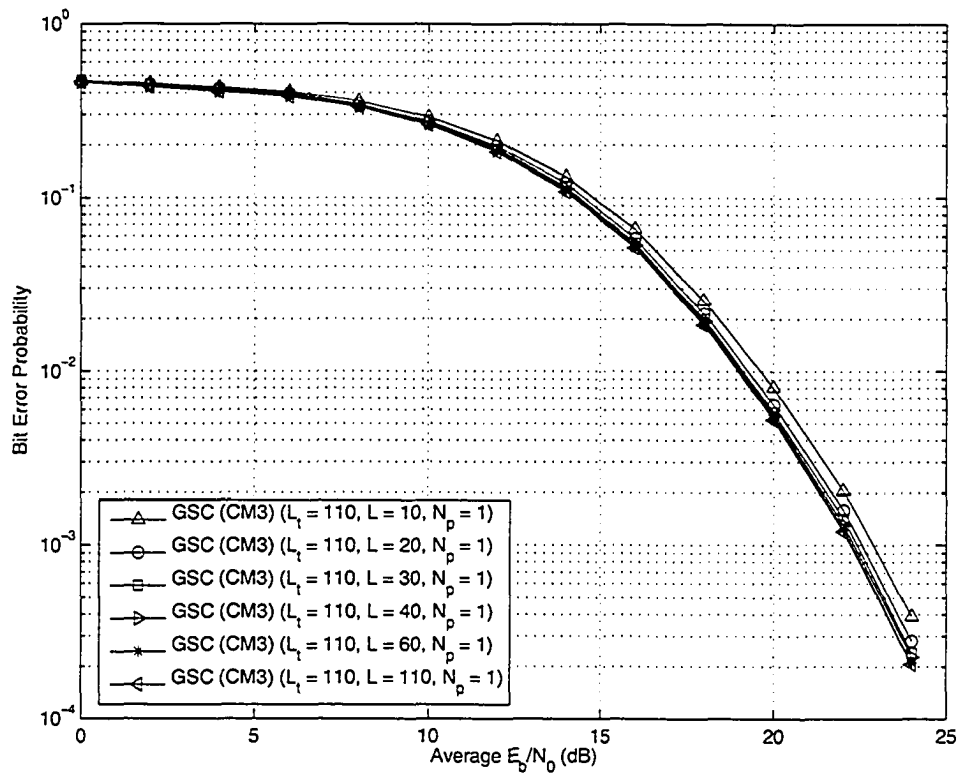


Figure 3.15: Effect of L on DP-GSC systems in CM3

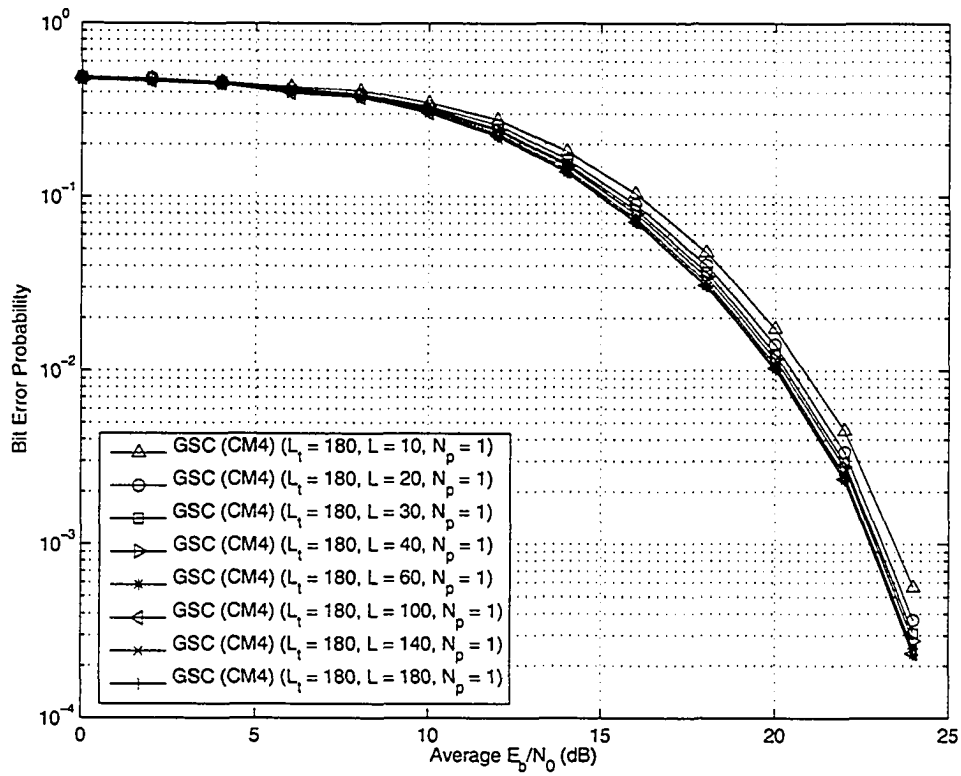


Figure 3.16: Effect of L on DP-GSC systems in CM4

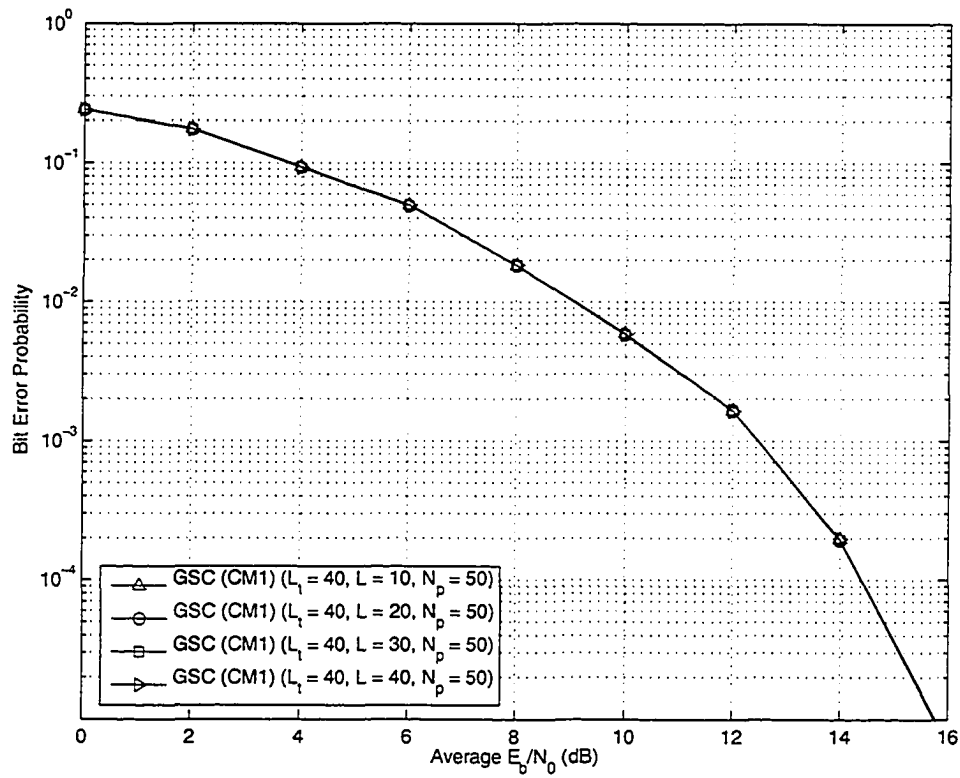


Figure 3.17: Effect of L on DP-GSC systems with noise averaging in CM1

on improving the performance.

3.4.4 The effect of N_p on GSC Receiver with noise averaging

The previous chapter showed that increasing N_p will decrease the noise variance, thus improving performance of the system. In the DP system the use of noise averaging not only reduces the noise variance, it also suppresses the possible interference between the received reference sub-pulse and the data sub-pulse as mentioned in Section 3.3.2. The performance improvement resulted from increasing N_p for CM1-CM4 is investigated in Figs. 3.21-3.24, respectively. Similar to the TR system, the performance improvement for CM1-CM4 from the noise averaging is greatest when N_p increases from 1 to

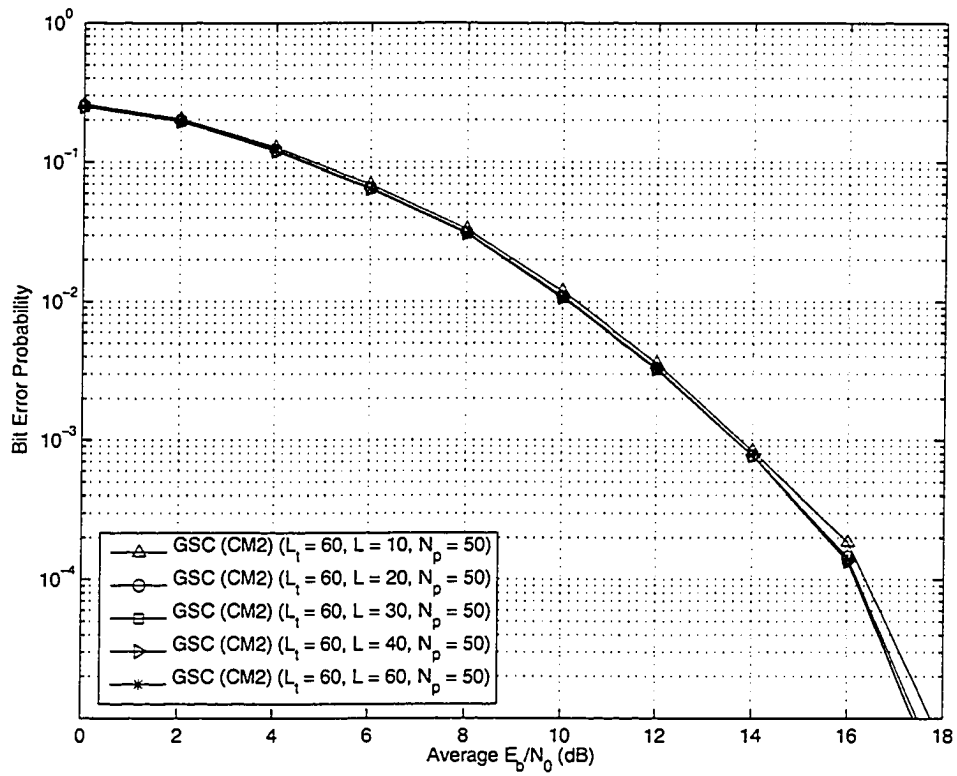


Figure 3.18: Effect of L on DP-GSC systems with noise averaging in CM2

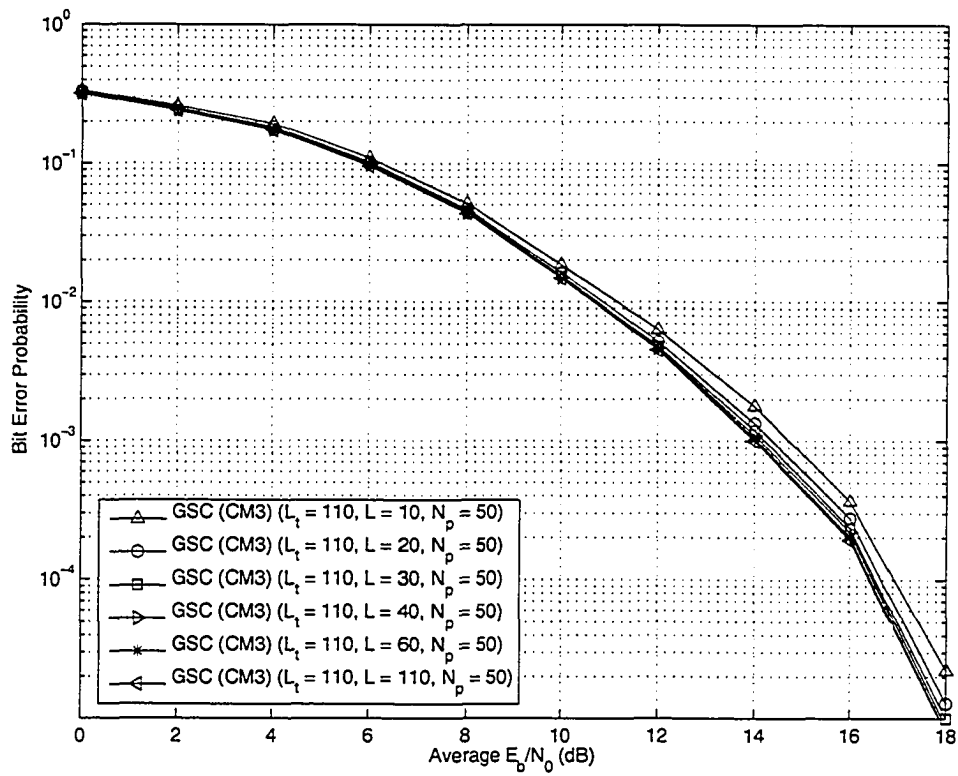


Figure 3.19: Effect of L on DP-GSC systems with noise averaging in CM3

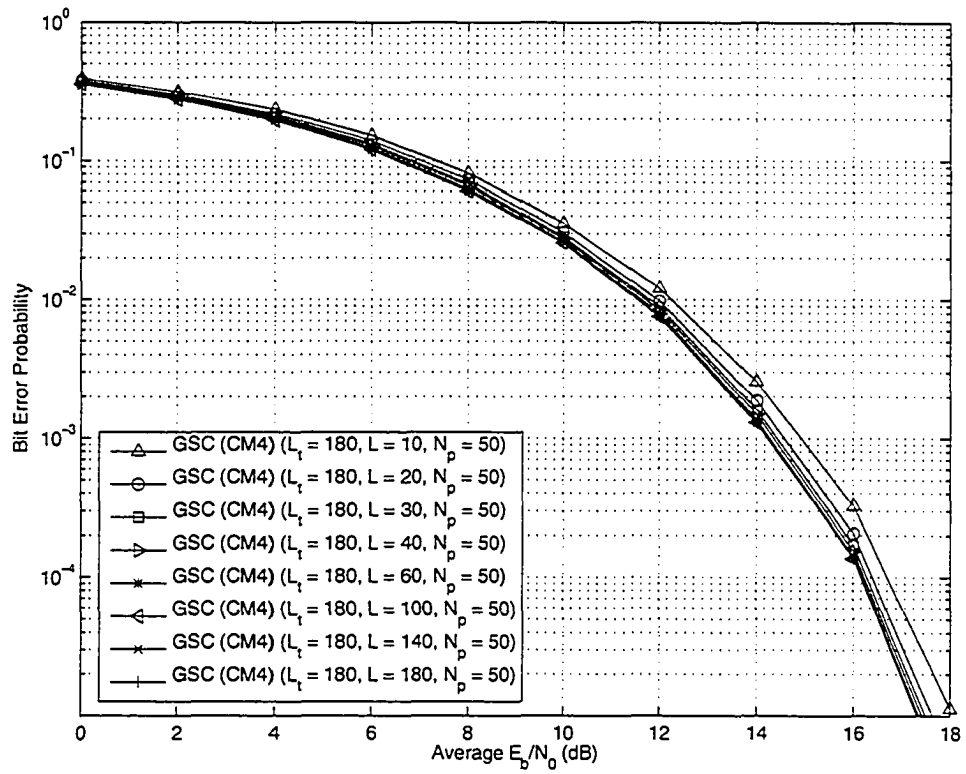


Figure 3.20: Effect of L on DP-GSC systems with noise averaging in CM4

10, with over 5 dB power savings achieved at $\text{BER} = 10^{-3}$. As shown in Figs. 3.21-3.24, the performance improvement from $N_p = 10$ to $N_p = 20$ and from $N_p = 30$ to $N_p = 50$ is only a fraction of the improvement from $N_p = 1$ to $N_p = 10$ for all the channel models. When compared with the “ideal” TR system with $N_p = \infty$, the performance of the GSC receiver with $N_p = 50$ is separated by roughly 1.5 to 2 dB. The “ideal” TR system as used in Section 2.5.4 is essentially a perfect coherent detector that provides the best achievable performance as benchmark in an ultra-wideband channel. While the PRAKE receiver represents the performance of the suboptimal rake receiver as described in Section 2.5.4. The GSC systems in channels with less multipaths (CM1, CM2) achieve performances slightly closer to the “ideal” TR system than channels with more multipaths (CM3, CM4). When compared to the PRAKE receiver, the non-coherent GSC receiver with $N_p = 20$ outperforms the PRAKE receiver at $\text{SNR} > 16$ dB for CM1 and CM2 as shown in Figs. 3.21-3.22. For CM3 and CM4 shown in Figs. 3.23-3.24, the non-coherent GSC receiver with $N_p = 50$ is able to achieve performance close to the PRAKE receiver at high SNR.

3.4.5 The effect of D_{th} on the basic AT-GSC Receiver

The decision threshold D_{th} of the AT-GSC receiver has a sizable impact on the performance of the DP AT-GSC system. Figs. 3.25-3.28 for CM1 to CM4 respectively, show the performance improves as the threshold D_{th} is lowered. This allows the receiver to collect more energy. All the plots show that the performance of the AT-GSC scheme improves most when moved from $D_{th} = 5$ to $D_{th} = 3$. It also reveals that in systems without noise averaging, when $D_{th} < 1.5$ the performance of the system does not improve at all, a sign that the threshold has hit the noise floor and it is the optimal performance of the AT-GSC system without noise averaging for the given channel model. When comparing Fig. 3.25 with Fig. 3.28, it reveals that the setting of the D_{th} is also affected by the number of channel paths. The performance improvement

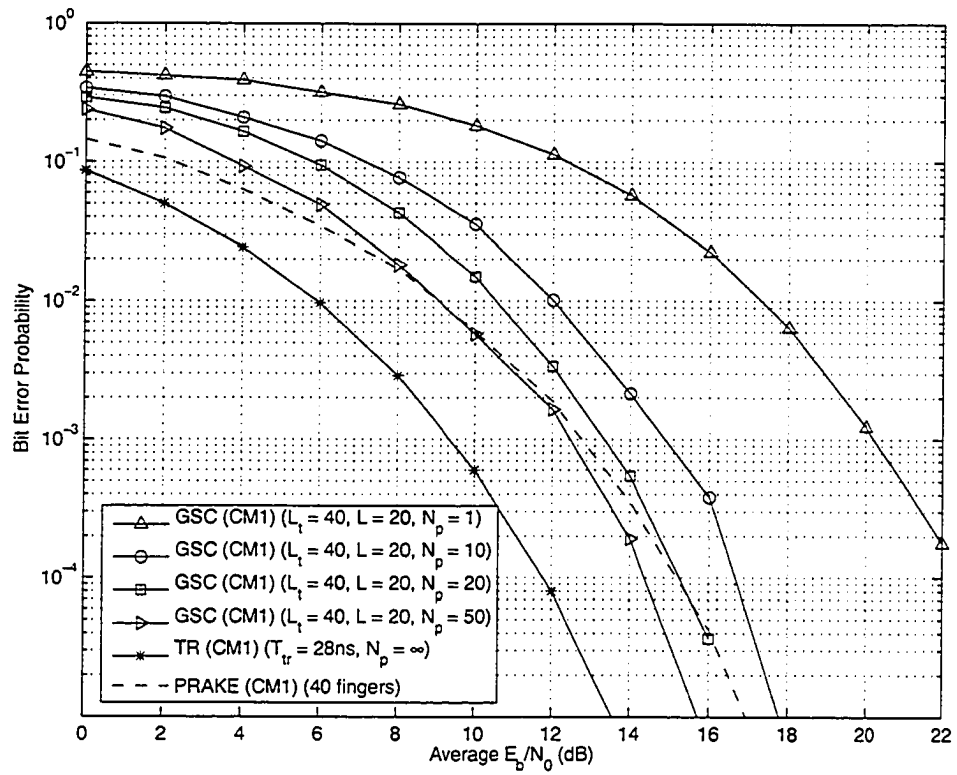


Figure 3.21: Effect of N_p on DP-GSC systems with noise averaging in CM1

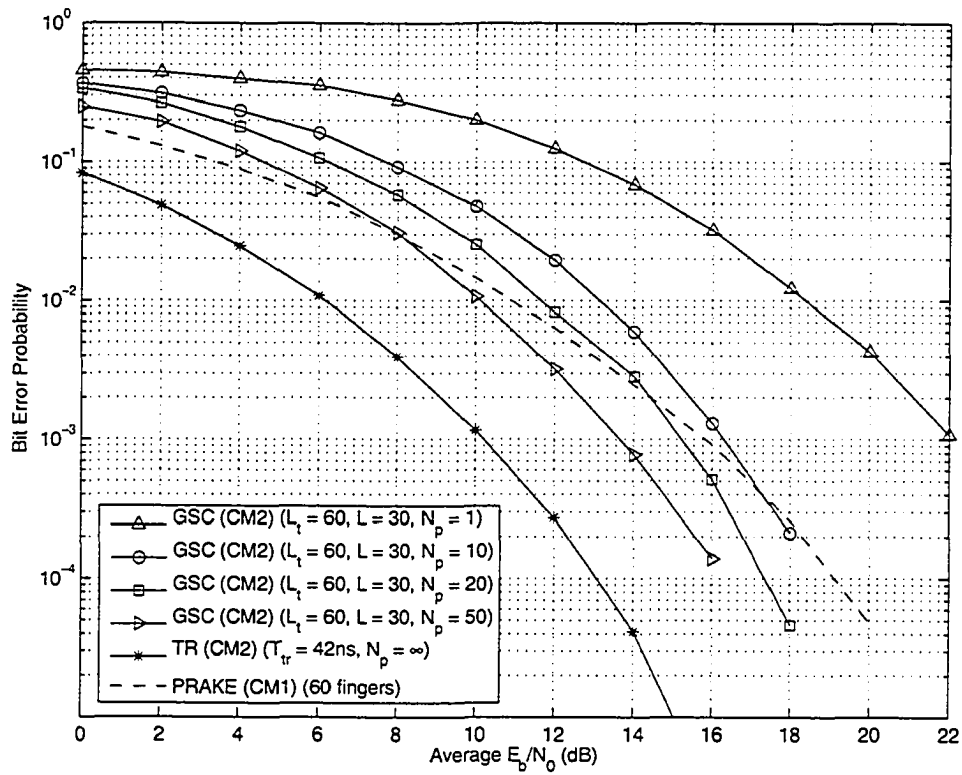


Figure 3.22: Effect of N_p on DP-GSC systems with noise averaging in CM2

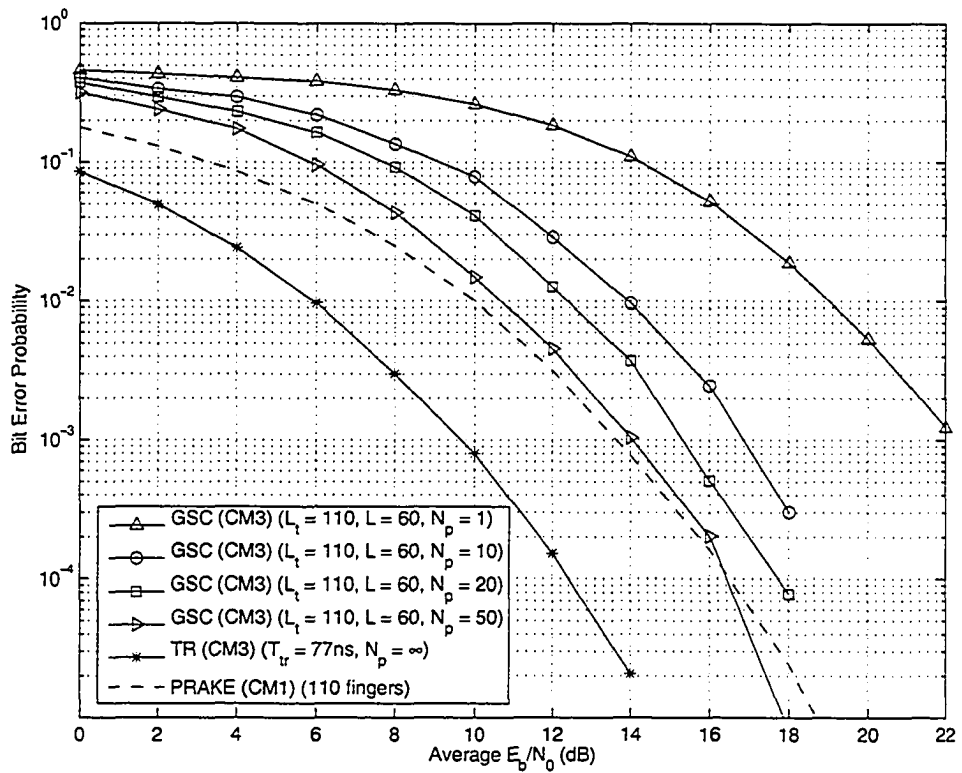


Figure 3.23: Effect of N_p on DP-GSC systems with noise averaging in CM3

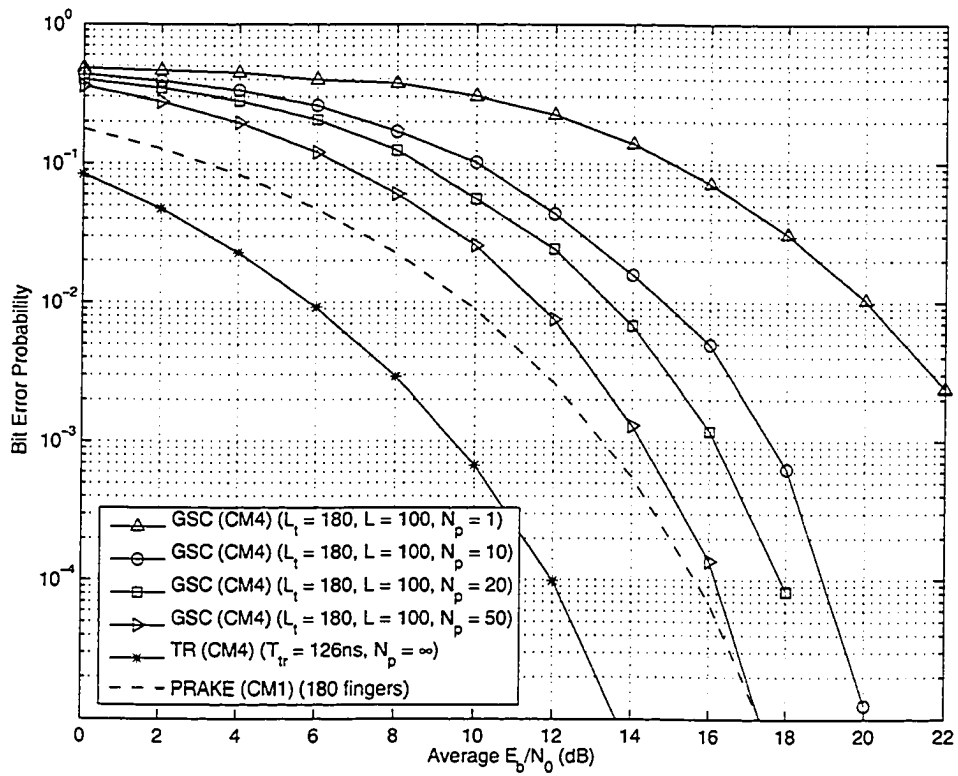


Figure 3.24: Effect of N_p on DP-GSC systems with noise averaging in CM4

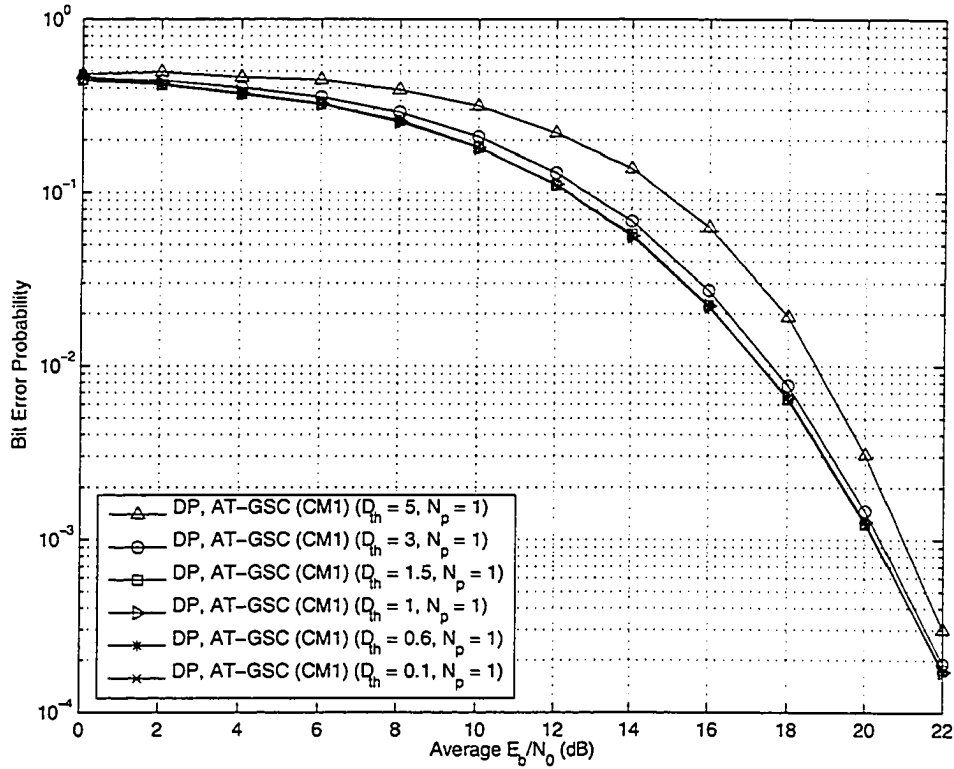


Figure 3.25: Effect of D_{th} on DP AT-GSC systems in CM1

from changing $D_{th} = 3$ to $D_{th} = 1.5$ in channels with few number of paths (i.e. Fig. 3.25 of CM1) is not as significant as in channels with large number of paths (i.e. Fig. 3.28 of CM4). These indicate that to get better performance in channels with large number of paths, D_{th} needs to be set lower. This is due to the channel energy being spread into more paths and thus lower power of each path, which results in lower autocorrelation values and requires a lower D_{th} setting to collect more multipath energy.

3.4.6 The effect of D_{th} on the AT-GSC Receiver with noise averaging

The following subsection investigates the performance of the DP system with noise averaging AT-GSC receiver while varying the decision threshold D_{th} .

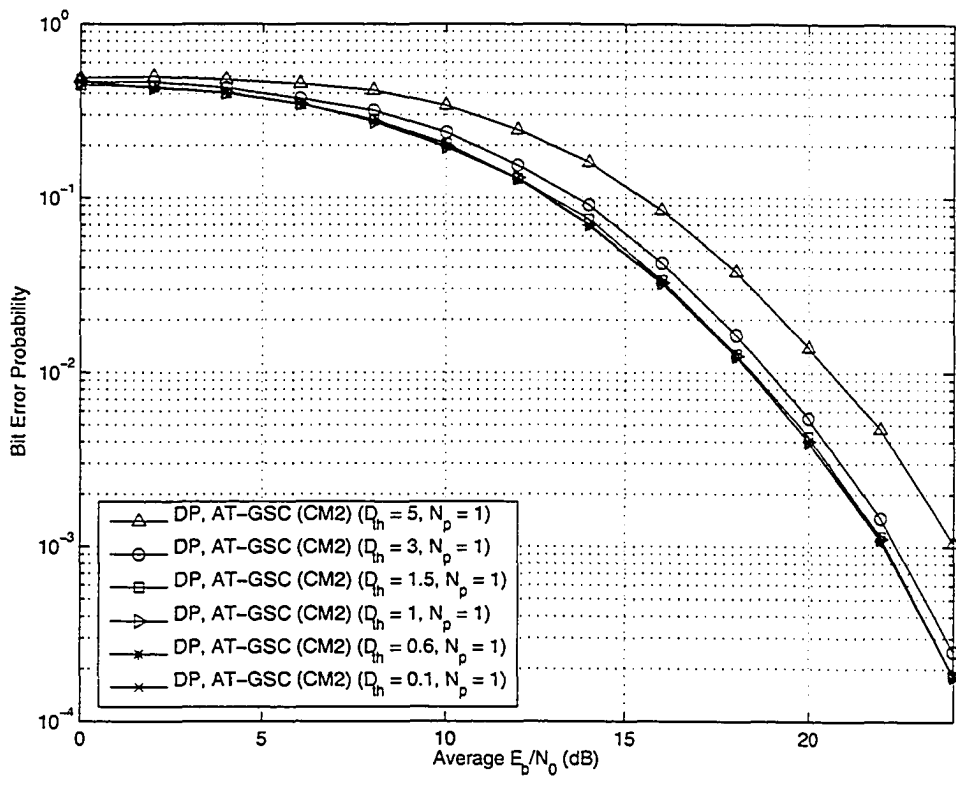


Figure 3.26: Effect of D_{th} on DP AT-GSC systems in CM2

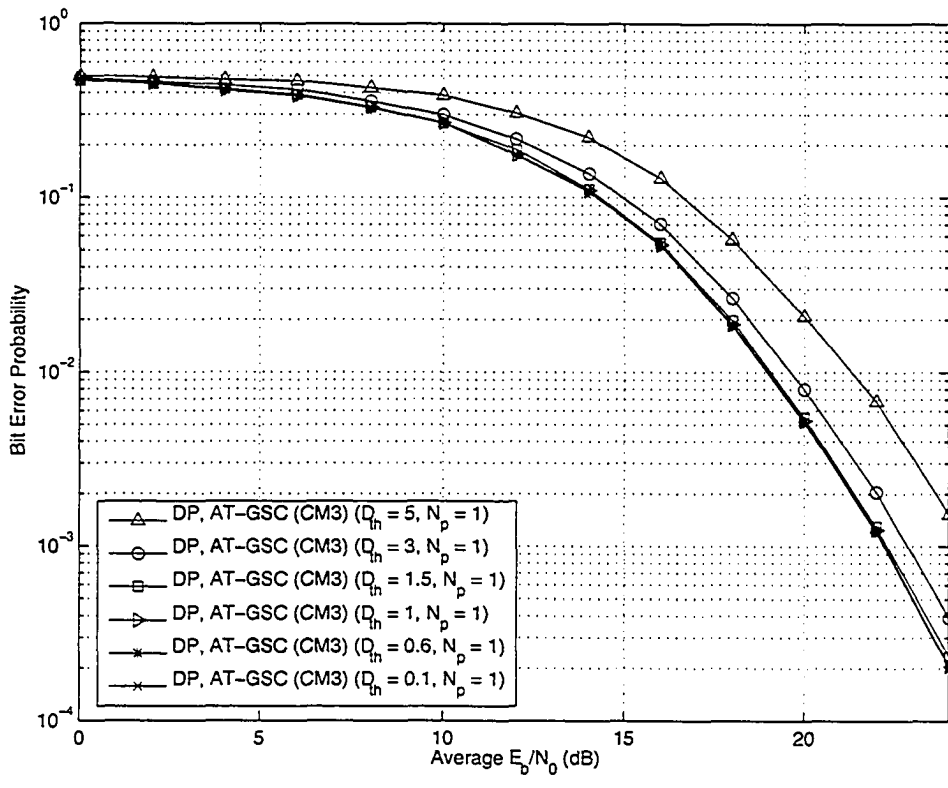


Figure 3.27: Effect of D_{th} on DP AT-GSC systems in CM3

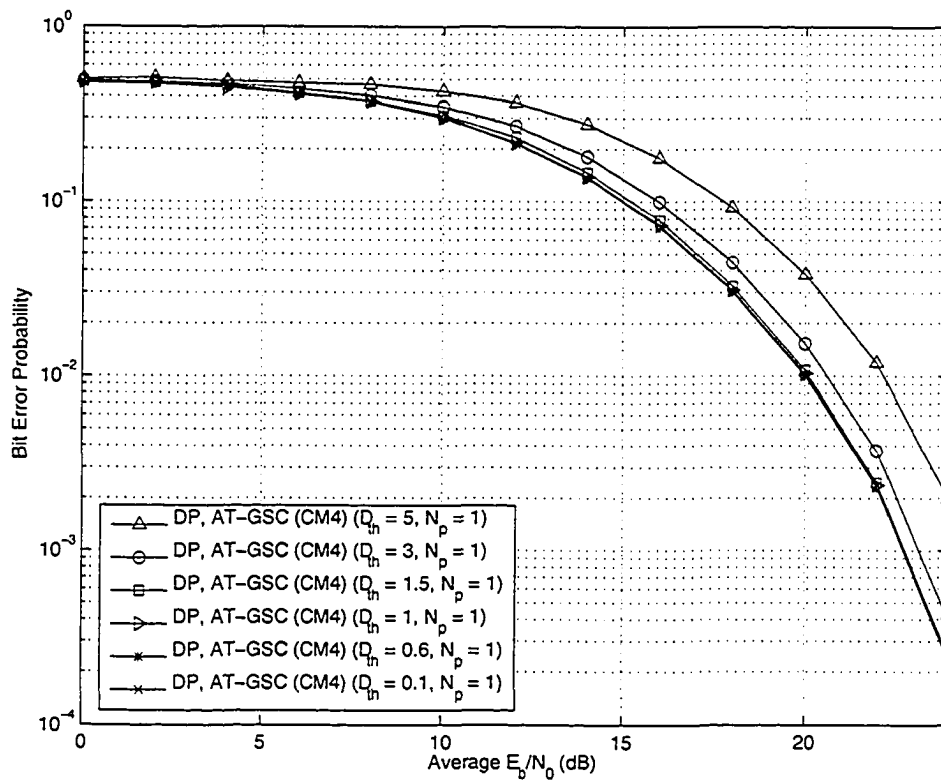


Figure 3.28: Effect of D_{th} on DP AT-GSC systems in CM4

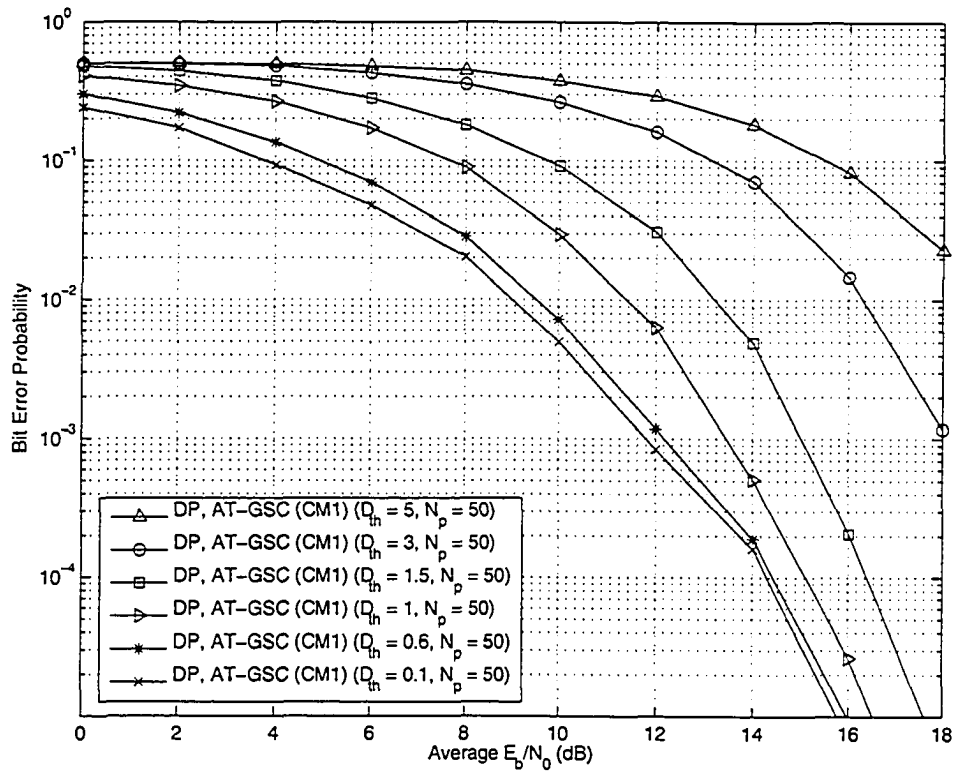


Figure 3.29: Effect of D_{th} on DP AT-GSC systems with noise averaging in CM1

Figs. 3.29-3.32 demonstrate that the effect of D_{th} is even more significant in the noise averaging AT-GSC receiver than the AT-GSC system without noise averaging in Section 3.4.5. For CM1, Fig. 3.29 shows the performance of the system improves significantly (≈ 10 dB) as D_{th} is lowered from 5 to 0.1. The improvement is even more significant (≈ 14 dB) in channels with large number of paths such as Fig. 3.31 and Fig. 3.32 for CM3 and CM4 respectively. Fig. 3.29 shows that the performance curve of $D_{th} = 1$ gets closer to the performance curve of $D_{th} = 0.1$ as SNR increases, as expected.

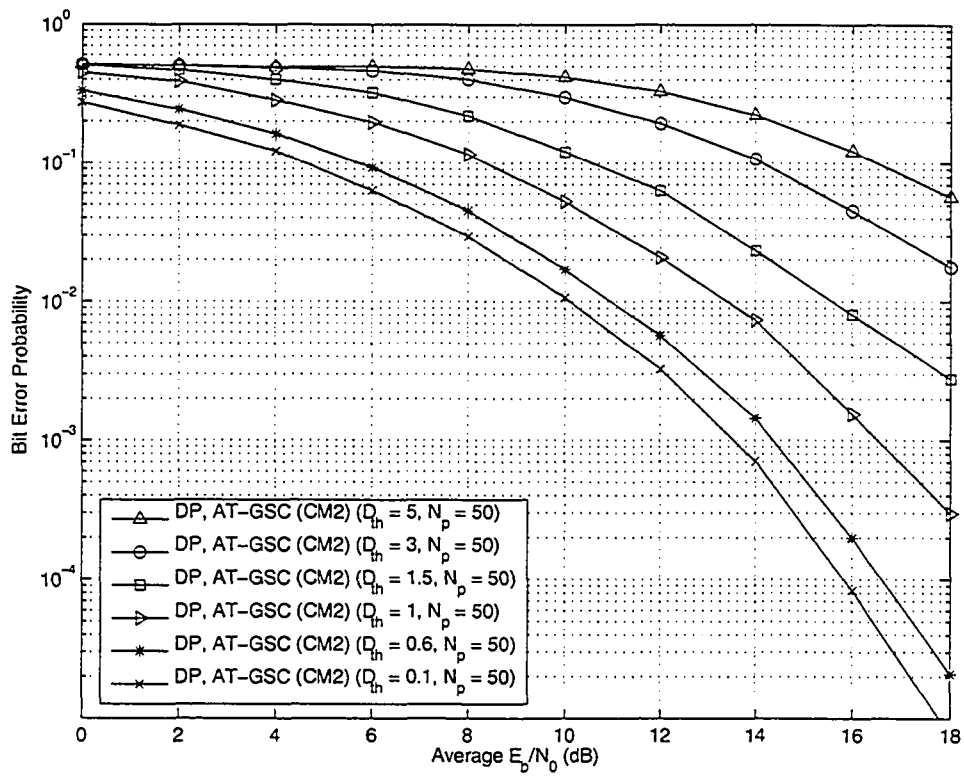


Figure 3.30: Effect of D_{th} on DP AT-GSC systems with noise averaging in CM2

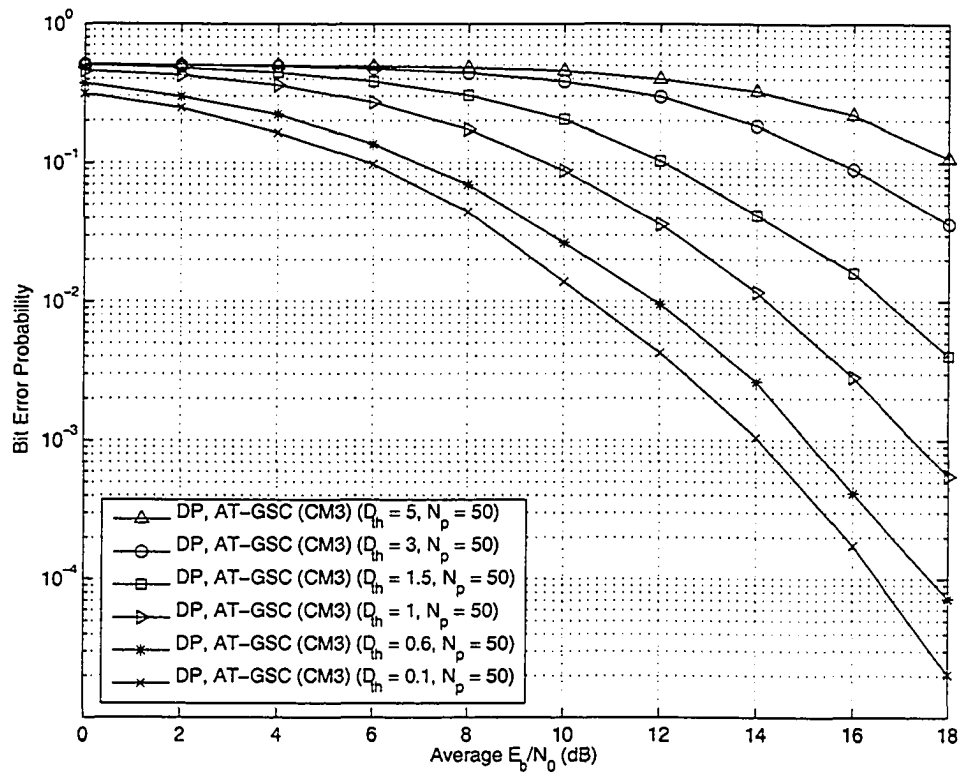


Figure 3.31: Effect of D_{th} on DP AT-GSC systems with noise averaging in CM3

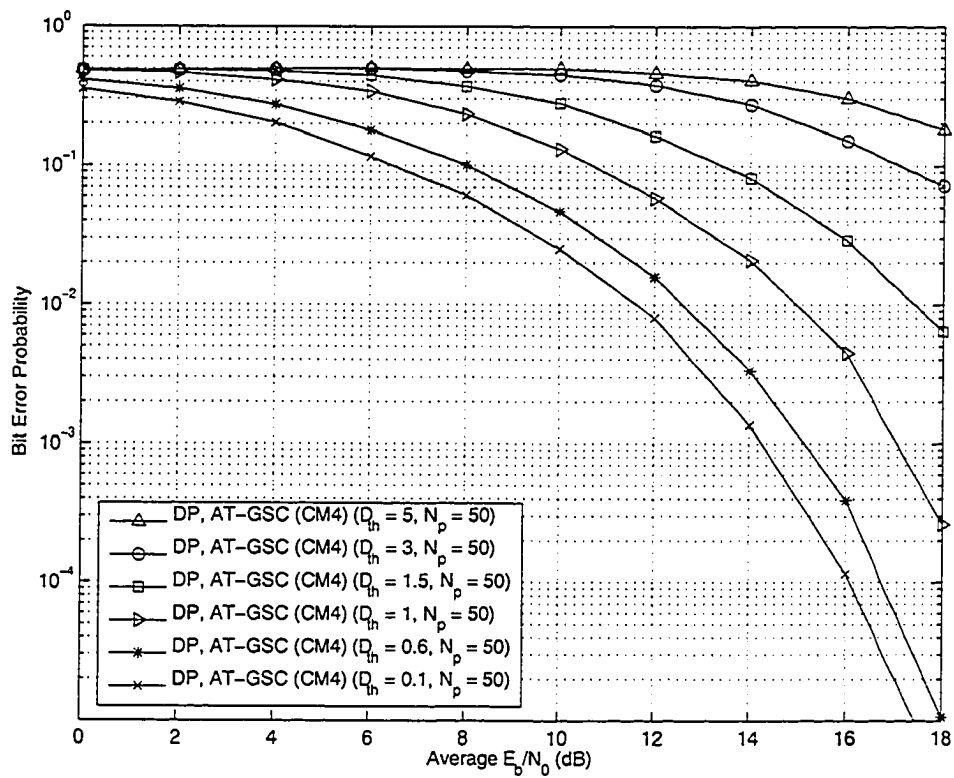


Figure 3.32: Effect of D_{th} on DP AT-GSC systems with noise averaging in CM4

3.4.7 The effect of N_p on the AT-GSC Receiver with noise averaging

Like the TR system and the DP-GSC system presented earlier, noise averaging improves the performance of the DP AT-GSC system in much the same way. In Figs. 3.33-3.36, the effect of N_p on the performance of the AT-GSC receiver is investigated for CM1 to CM4. The results are also compared with the PRAKE suboptimal system and the “ideal” TR system. Figs. 3.33-3.34 show that the DP AT-GSC system with minimum noise averaging ($N_p = 20$) outperforms the PRAKE receiver when SNR is greater than 17 dB and 14 dB respectively for CM1 and CM2. However, in Fig. 3.35 and Fig. 3.36 for CM3 and CM4, it shows that the performance of the DP AT-GSC system does not outperform PRAKE, but the DP AT-GSC system with $N_p = 50$ get performance that approaches the PRAKE receiver. When compared with the “ideal” TR system at $\text{BER} = 10^{-4}$, AT-GSC systems with $N_p = 50$ requires additional ~ 3 dB for CM1 and CM2 and ~ 4 dB for CM3 and CM4.

3.4.8 The effect of η_{th} on the basic NT-GSC Receiver

In Figs. 3.37-3.40, the effect of normalised threshold η_{th} of the NT-GSC receiver on the performance in CM1 to CM4 is studied. As expected, reducing η_{th} will improve the system performance gradually as more energy is collected in the receiver. However, the performance improvement drops off as η_{th} gets even smaller. In the case of CM1, Fig. 3.37 shows that the performance improvement levels off at $\eta_{th} = 0.5$. In Fig. 3.40, the performance improvement levels off at $\eta_{th} = 0.2$ for CM4.

3.4.9 The effect of η_{th} on the NT-GSC Receiver with noise averaging

As shown in Figs. 3.41-3.44, the decrease of normalised threshold η_{th} results in more noticeable performance gain on the NT-GSC receiver with noise averaging at higher SNR values than at low SNR's. This is because as SNR

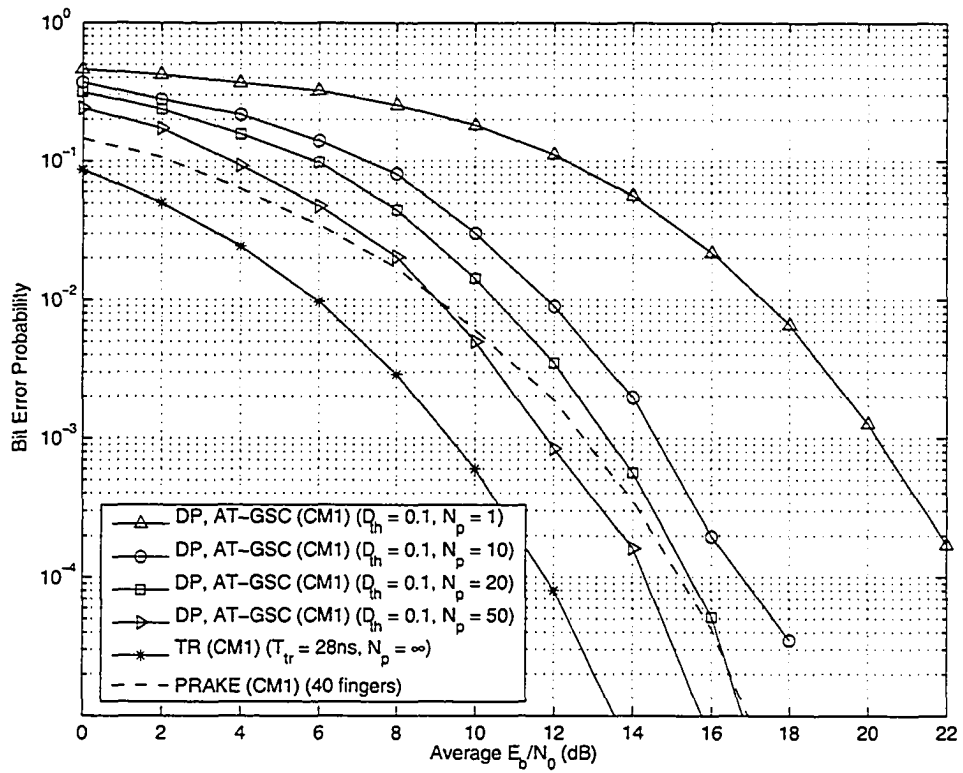


Figure 3.33: Effect of N_p on DP AT-GSC systems with noise averaging in CM1

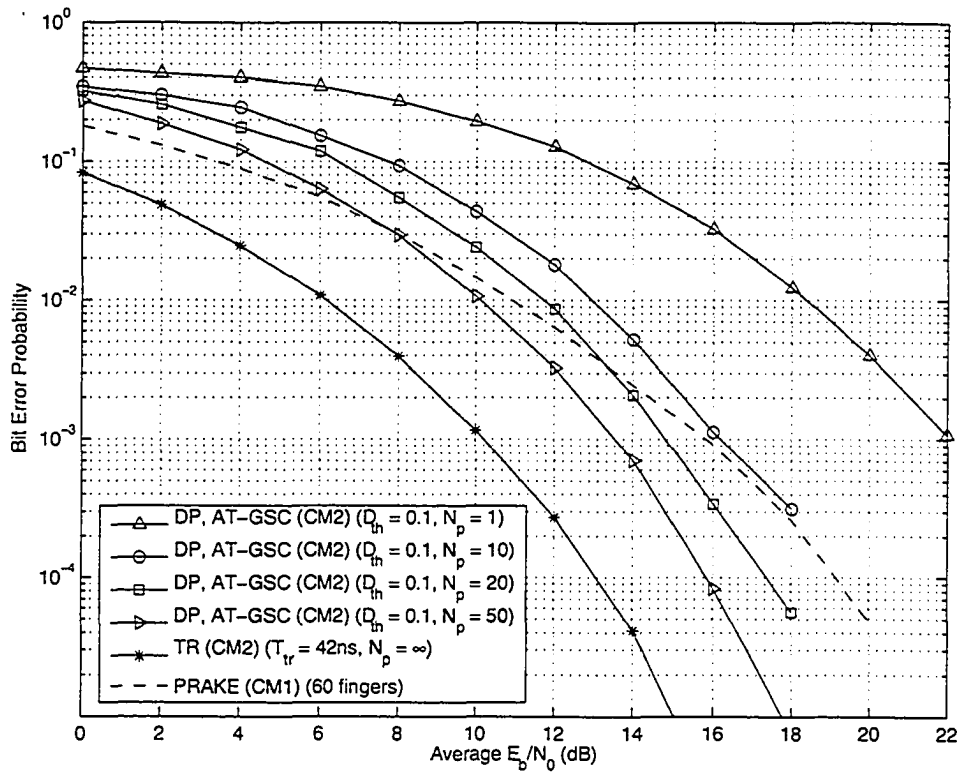


Figure 3.34: Effect of N_p on DP AT-GSC systems with noise averaging in CM2

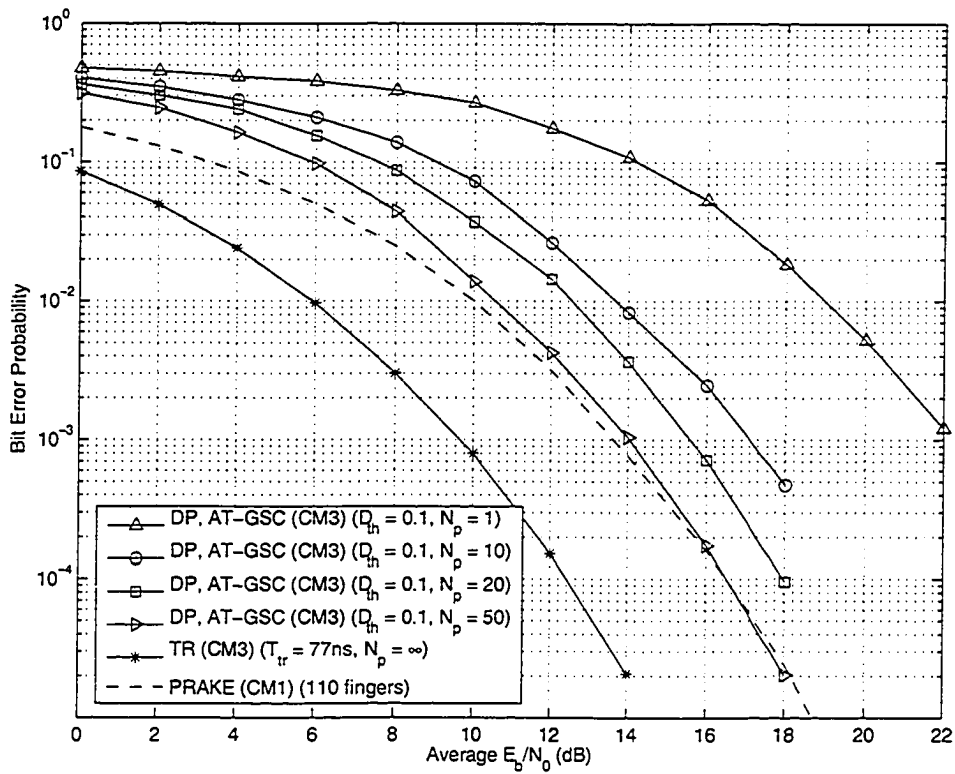


Figure 3.35: Effect of N_p on DP AT-GSC systems with noise averaging in CM3

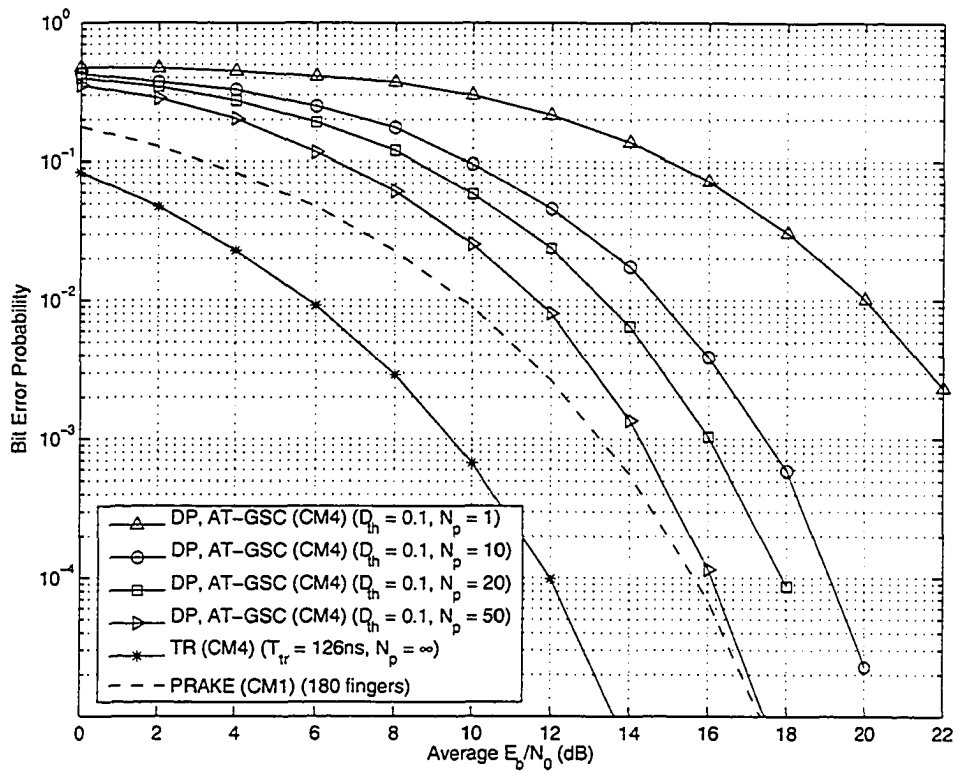


Figure 3.36: Effect of N_p on DP AT-GSC systems with noise averaging in CM4

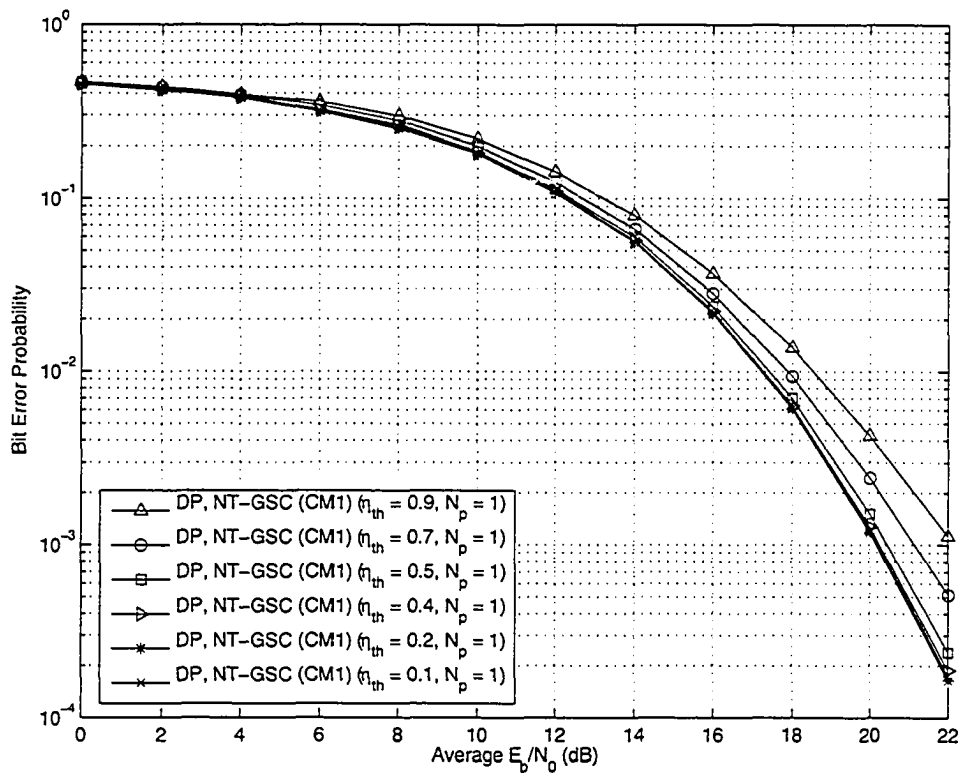


Figure 3.37: Effect of η_{th} on DP NT-GSC systems in CM1

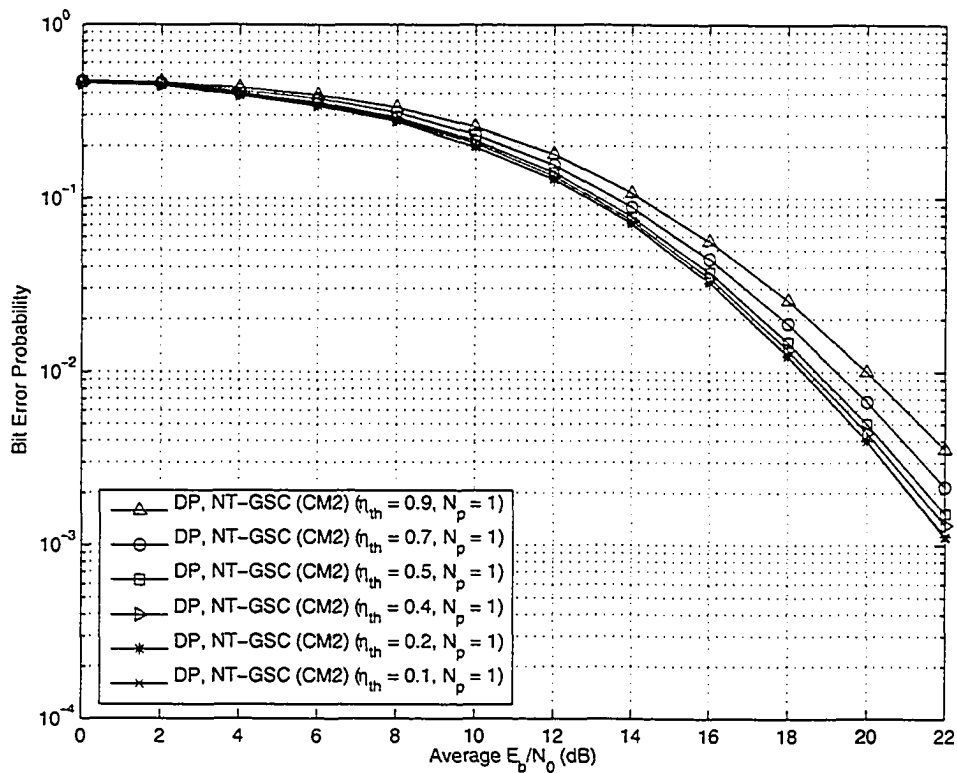


Figure 3.38: Effect of η_{th} on DP NT-GSC systems in CM2

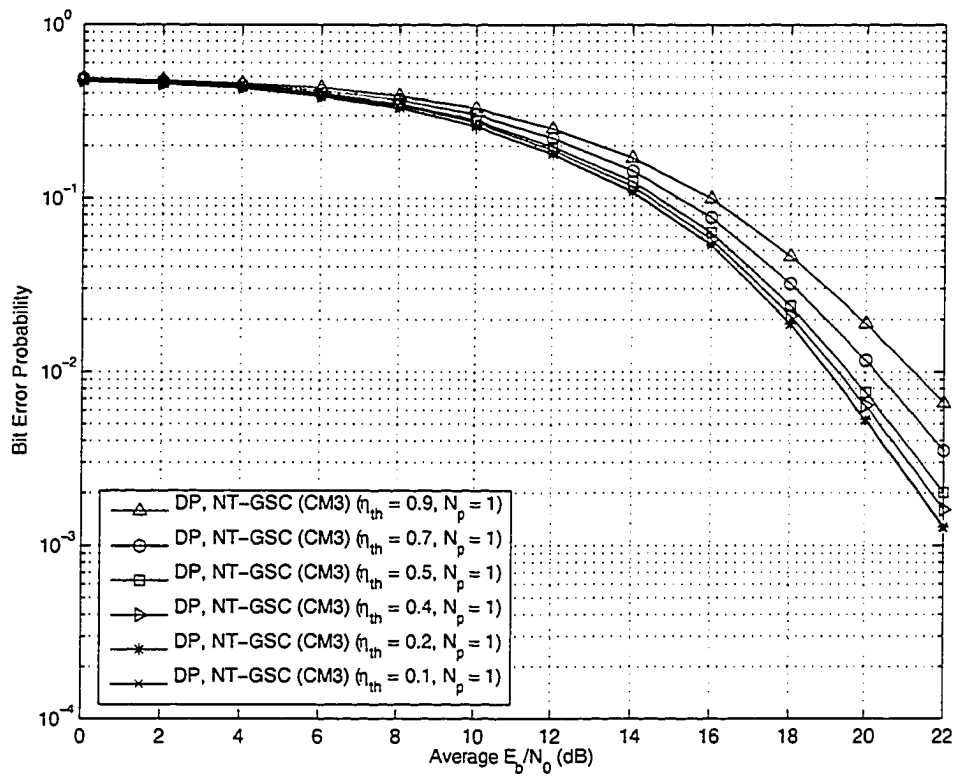


Figure 3.39: Effect of η_{th} on DP NT-GSC systems in CM3

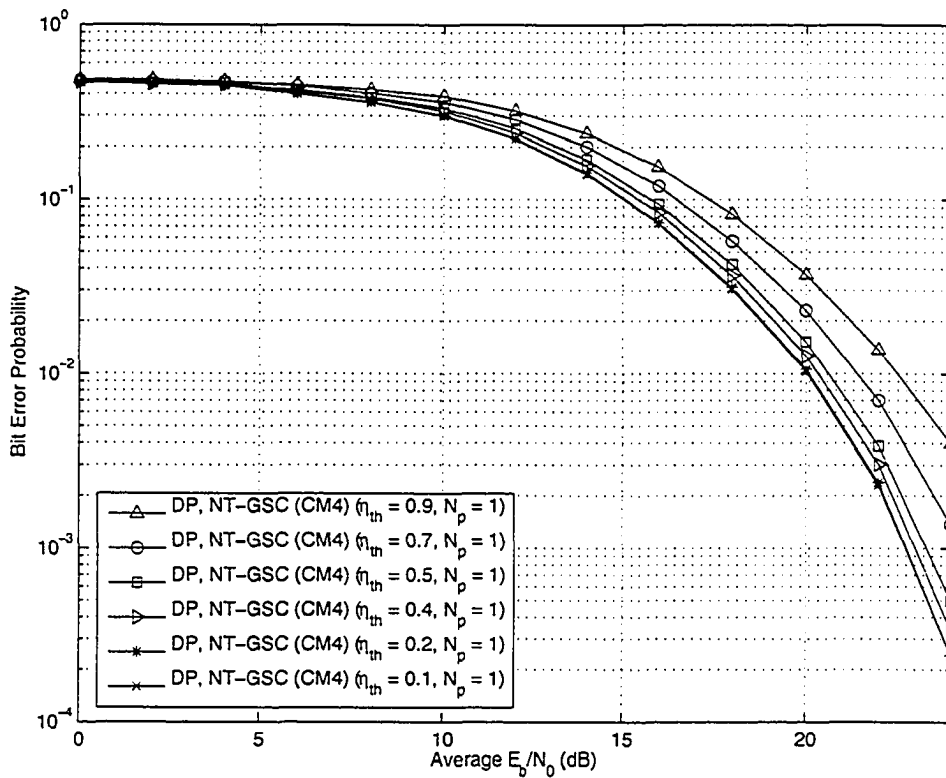


Figure 3.40: Effect of η_{th} on DP NT-GSC systems in CM4

increases, the weaker paths are less affected by noise and including it in the decision variable D by lowering η_{th} will enhance the signal to noise ratio and thus result in better performance. These figures also suggest that lowering the η_{th} will lead to greater performance improvements on channels with large number of paths than channels with fewer paths. For instance, Fig. 3.41 shows the performance improvement from $\eta_{th} = 0.9$ to $\eta_{th} = 0.2$ is ~ 2 dB at $\text{BER} = 10^{-3}$ for CM1, and this performance difference enlarges as it goes from CM1 to CM4. Fig. 3.44 shows the performance gain from $\eta_{th} = 0.9$ to $\eta_{th} = 0.2$ is more than 3 dB at $\text{BER} = 10^{-3}$ for CM4. Figs. 3.37-3.44 show that while setting the η_{th} lower will not guarantee an improvement in the performance of the DP NT-GSC system, however lowering η_{th} does not show any negative effect on the performance of the system either.

3.4.10 The effect of N_p on the NT-GSC Receiver with noise averaging

The noise averaging technique when applied on the NT-GSC receiver provides similar benefits as the previous mentioned systems. As shown in Figs. 3.45-3.48, the performance of NT-GSC receiver is greatly enhanced for CM1-CM4 with the application of noise averaging. The NT-GSC receiver is able to eventually outperform the PRAKE receiver in the high SNR range for CM1 and CM2 with $N_p = 20$. For CM3 and CM4 shown in Fig.3.47 and Fig.3.48, it requires the NT-GSC receiver with $N_p = 50$ to get performance close to the PRAKE receiver in the SNR range shown. When compared with the “ideal” TR system, the system performance at $N_p = 50$ yields about 3 to 4 dB degradation at $\text{BER} = 10^{-4}$ with the gap widening as one moves from channels of less paths (CM1,CM2) to channels of more paths (CM3,CM4).

3.4.11 The effect of T_{dp-int} on the basic DP-Int Receiver

The DP-Int receiver is really an autocorrelation receiver much like the one presented for the TR system in Section 2.3.1. However, the delay T_d now

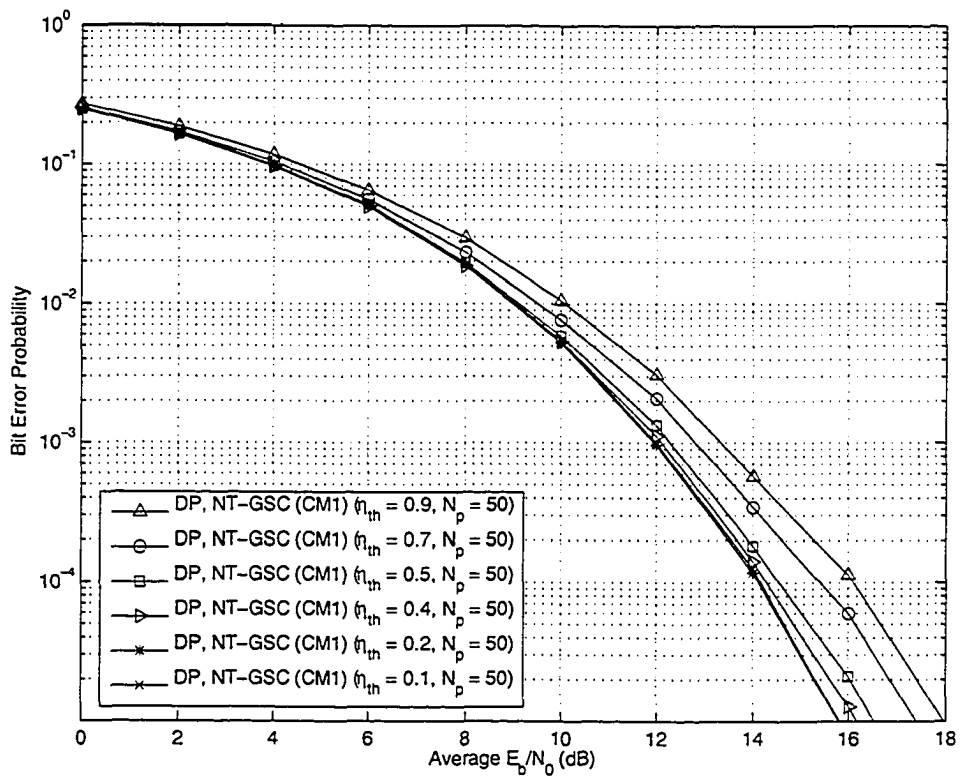


Figure 3.41: Effect of η_{th} on DP NT-GSC systems with noise averaging in CM1

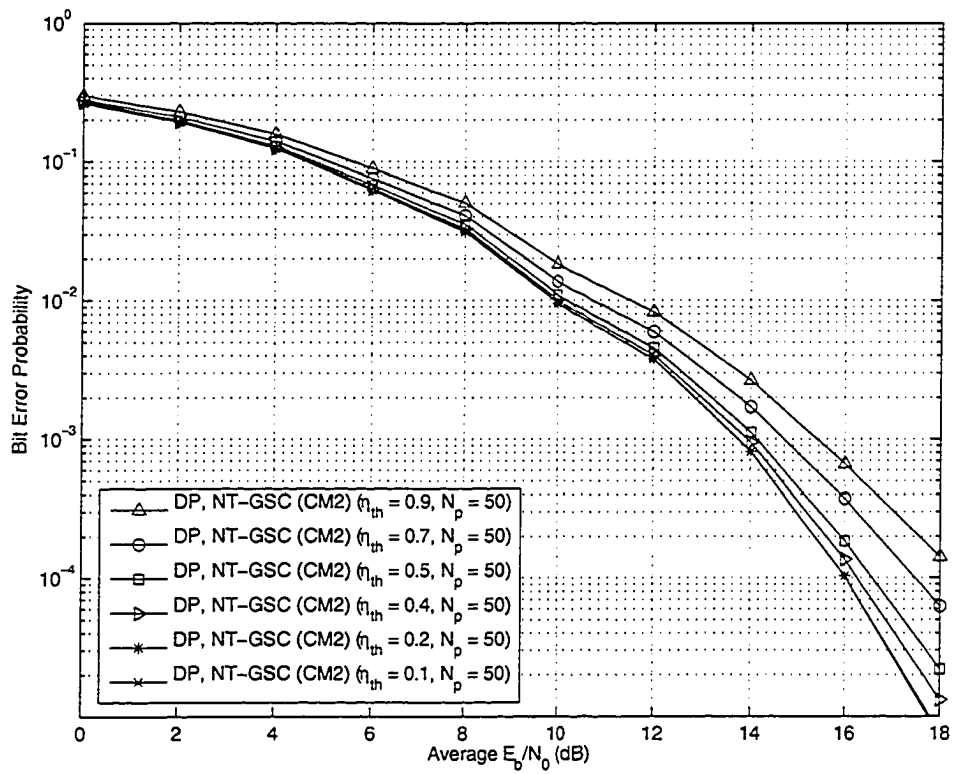


Figure 3.42: Effect of η_{th} on DP NT-GSC systems with noise averaging in CM2

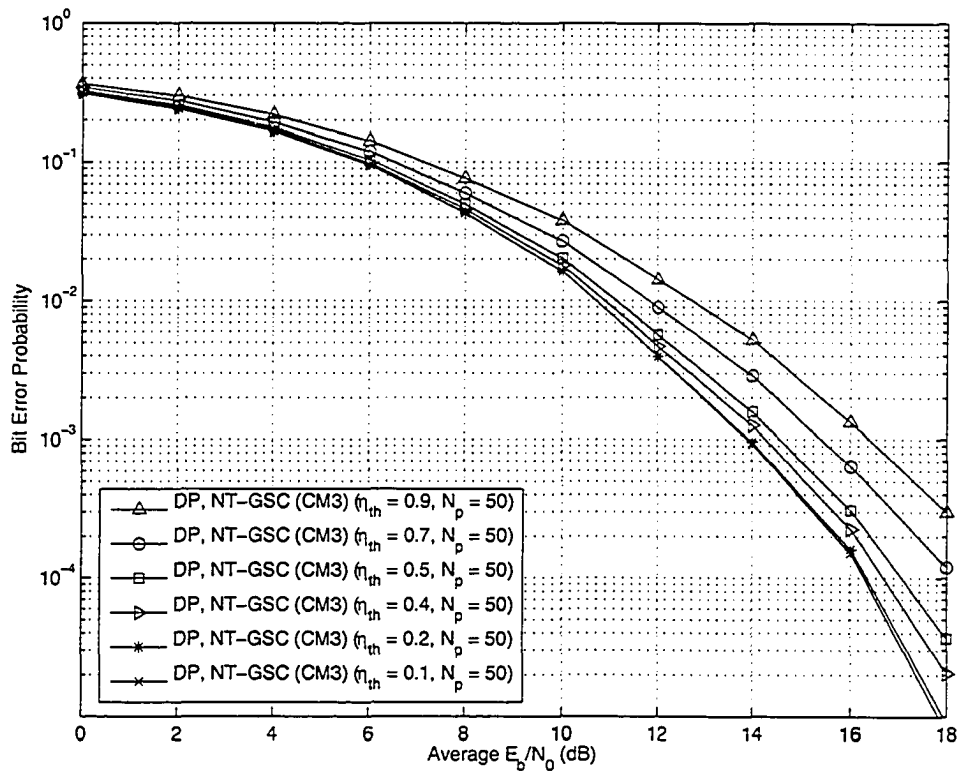


Figure 3.43: Effect of η_{th} on DP NT-GSC systems with noise averaging in CM3

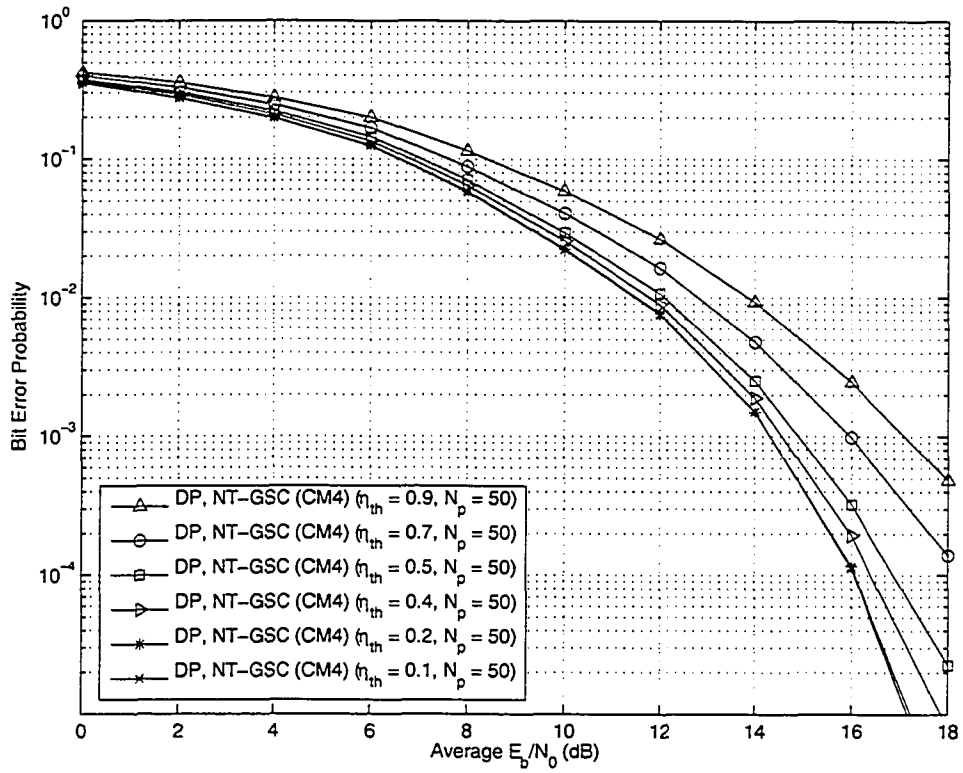


Figure 3.44: Effect of η_{th} on DP NT-GSC systems with noise averaging in CM4

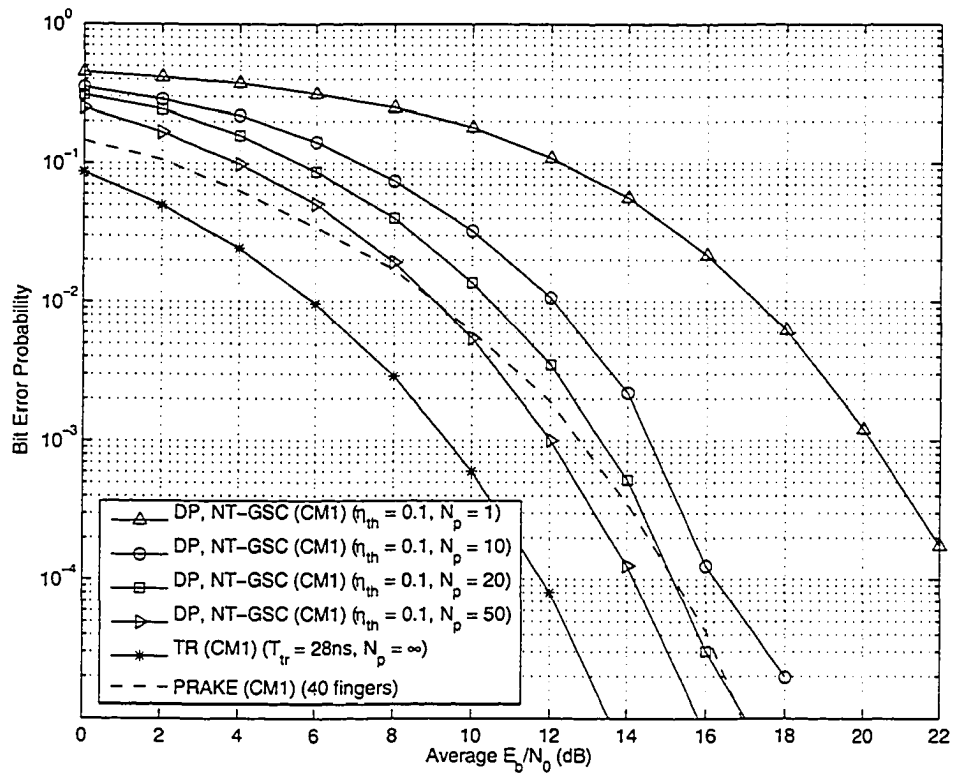


Figure 3.45: Effect of N_p on DP NT-GSC systems with noise averaging in CM1

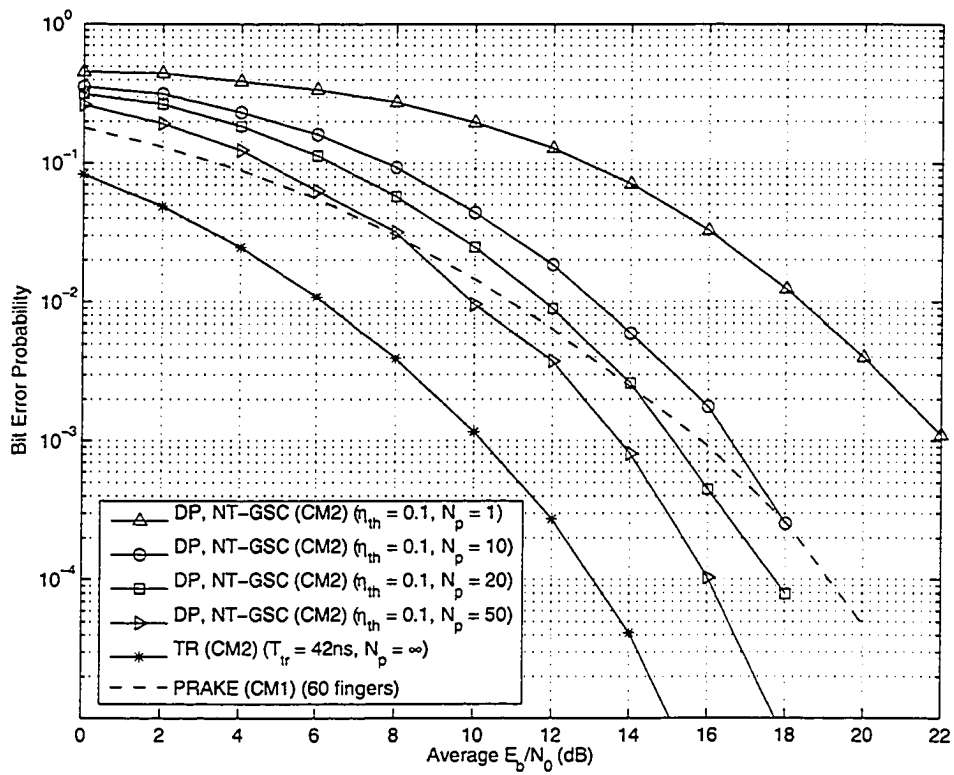


Figure 3.46: Effect of N_p on DP NT-GSC systems with noise averaging in CM2

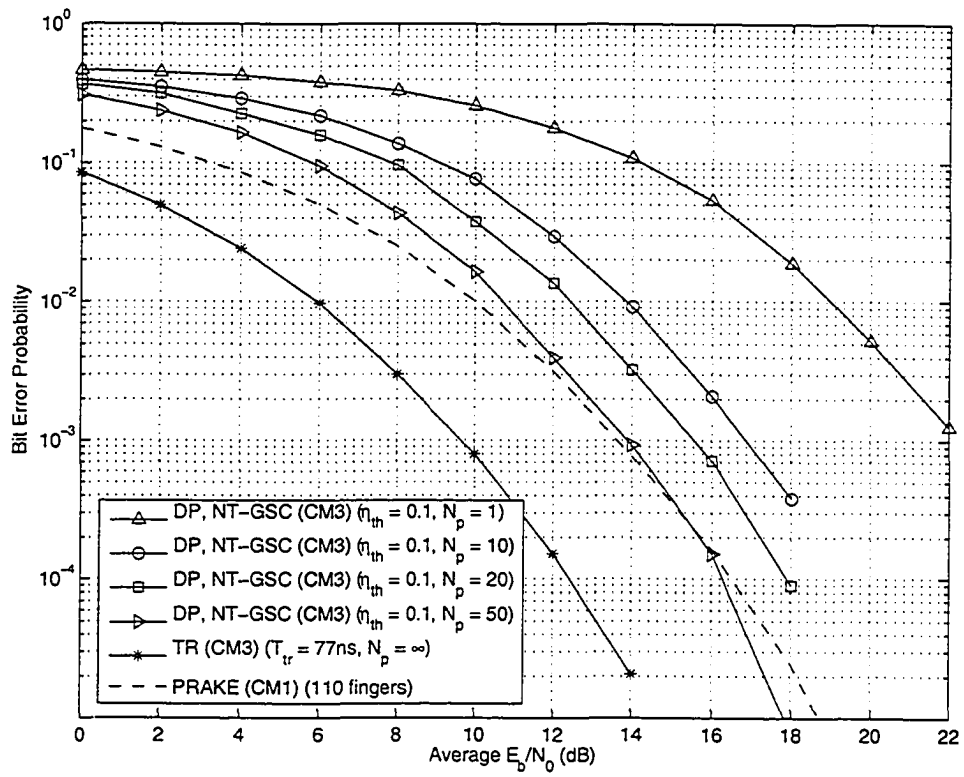


Figure 3.47: Effect of N_p on DP NT-GSC systems with noise averaging in CM3

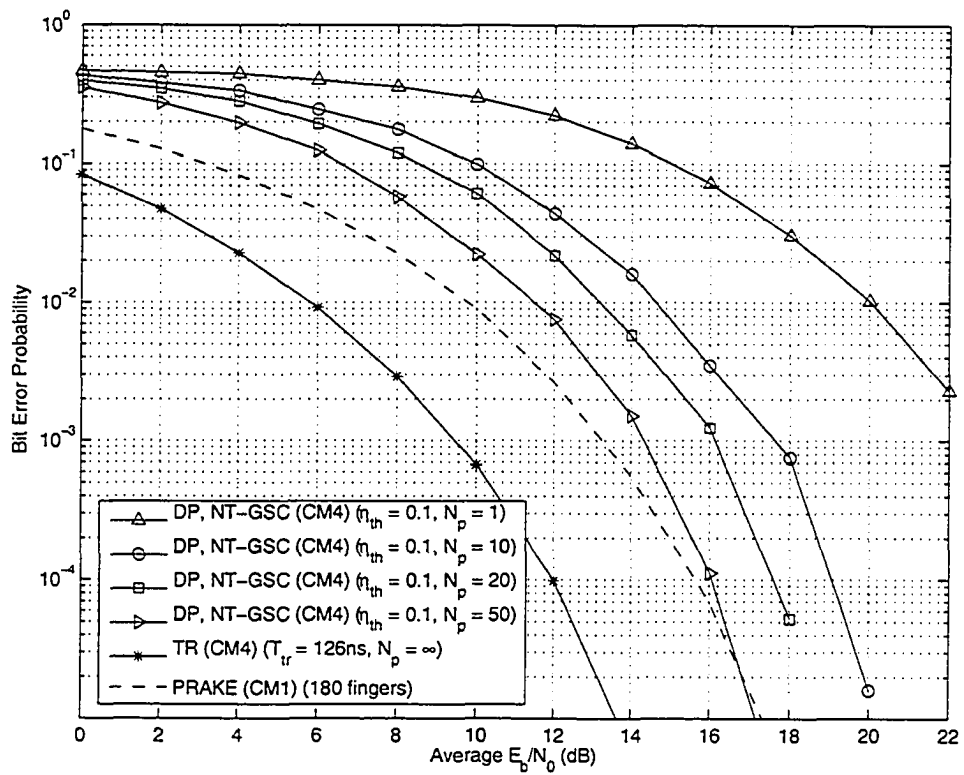


Figure 3.48: Effect of N_p on DP NT-GSC systems with noise averaging in CM4

equals to $\frac{T_u}{2}$ to reflect the delay between reference sub-pulse and data sub-pulse of the DP signalling scheme. The integrate-and-dump unit will integrate from every iT_f to $iT_f + T_{dp-int}$ with sampling at the end of $iT_f + T_{dp-int}$ to form the decision variable D .

The effect of the integration length T_{dp-int} of the DP-Int receiver on the performance is presented in Figs. 3.49-3.52 for CM1 to CM4 respectively. The figures show that the effect of T_{dp-int} on the DP-Int receiver is very similar to effect of T_{tr} on the TR system in Section 2.5.2. As T_{dp-int} increases, the performance of the system increases. However, much like the TR system, the performance starts to deteriorate after some point for all the channel models. In Fig. 3.49 it is noted that the performance of the system for CM1 peaks when $T_{dp-int} = 14$ ns and as T_{dp-int} increases further, the performance drops. Figs. 3.50-3.52 show T_{dp-int} is optimal at 21 ns, 42 ns, and 70 ns for CM2, CM3, and CM4 respectively. The performance degradation as T_{dp-int} past the optimal value is likely caused by the much weaker paths after T_{dp-int} which adversely affect the detection signal to noise ratio.

3.4.12 The effect of T_{dp-int} on the DP-Int Receiver with noise averaging

The DP-Int receiver with noise averaging contains the autocorrelator as defined in the previous subsection as well as the noise averaging structure of the DP-GSC receivers in Section 3.3.2 replacing the signal delay block of the autocorrelator structure.

The effect of T_{dp-int} on the performance of the DP-Int receiver with noise averaging is very similar to the basic DP-Int receiver. Figs. 3.53-3.56 show the optimal value of T_{dp-int} lies between the minimum and maximum integration length chosen for most of the SNR values. One observation is that the worsening of performance from increasing the T_{dp-int} past the optimal value is less severe as SNR increases. In fact, at 18 dB, Fig. 3.55 shows that T_{dp-int} taking the maximum integration length of 77 ns actually gives the best performance.

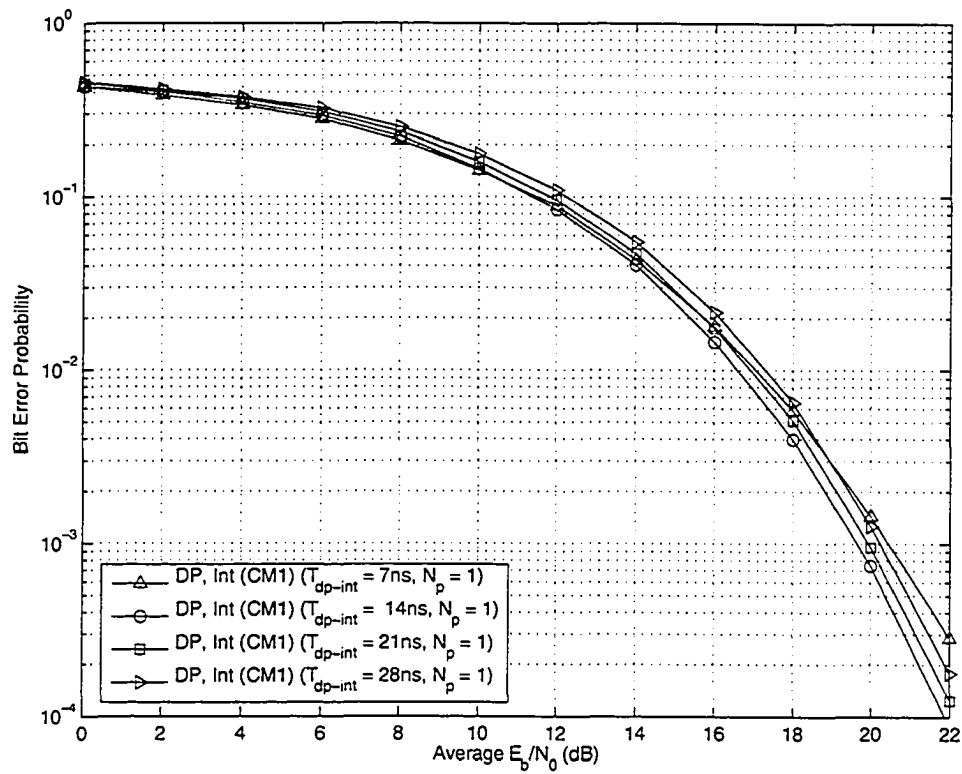


Figure 3.49: Effect of T_{dp-int} on DP-Int systems in CM1

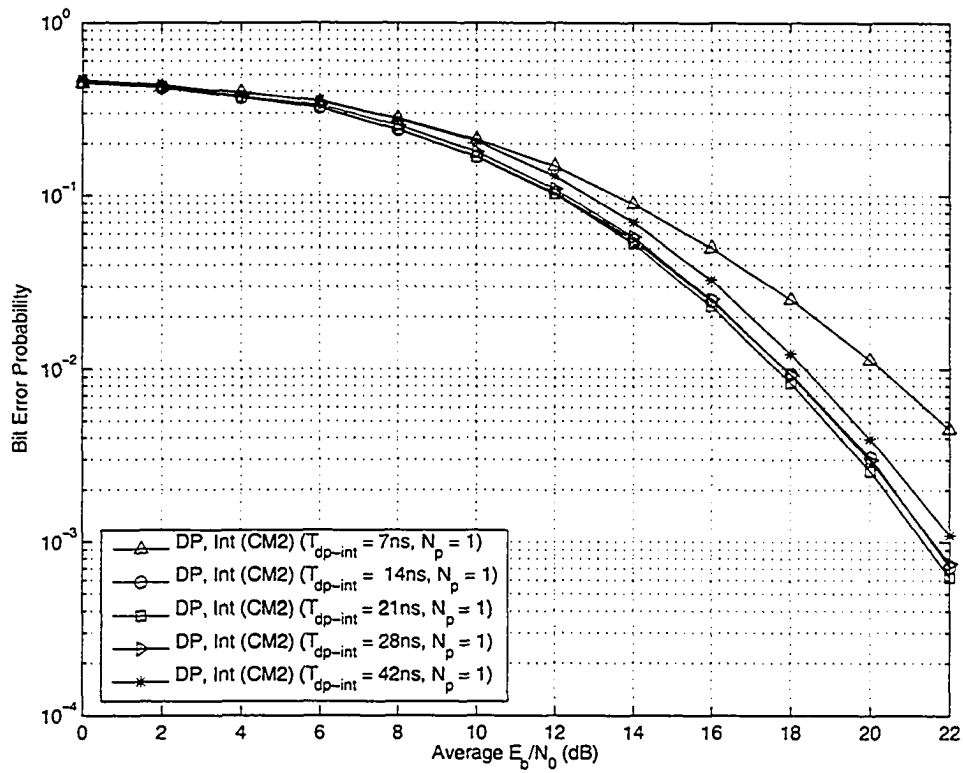


Figure 3.50: Effect of T_{dp-int} on DP-Int systems in CM2

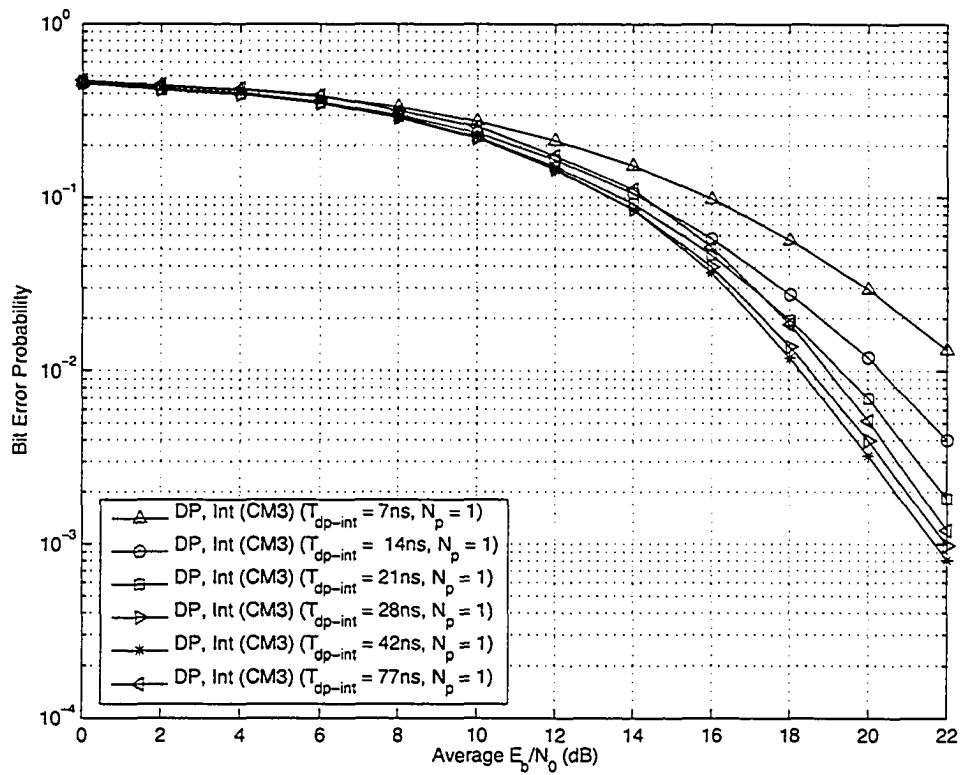


Figure 3.51: Effect of T_{dp-int} on DP-Int systems in CM3

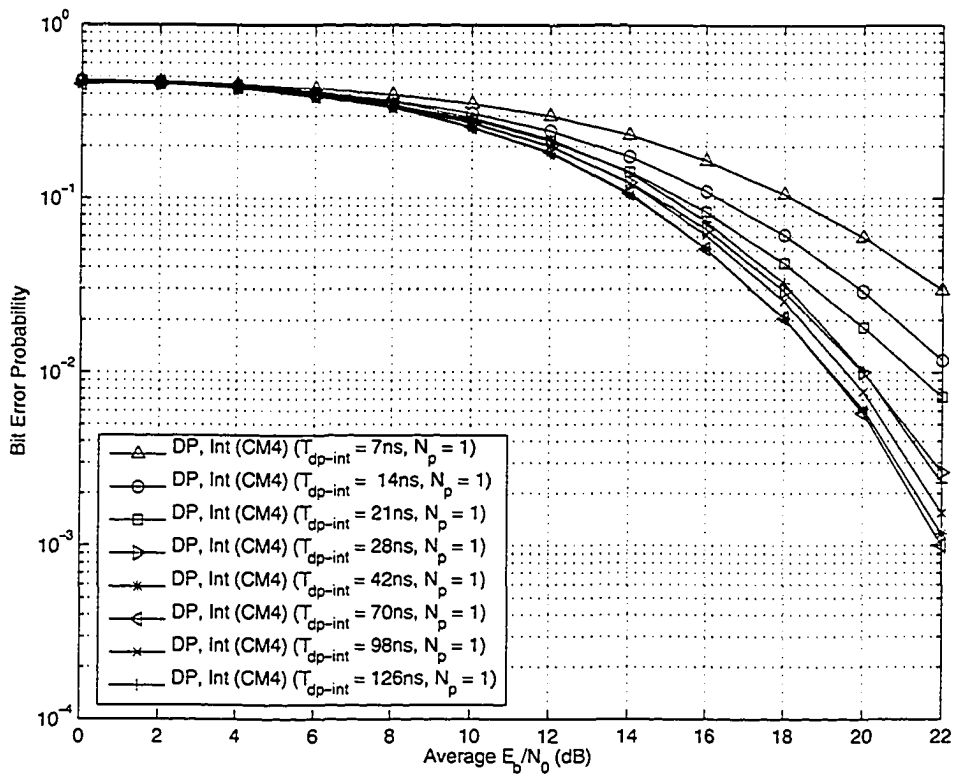


Figure 3.52: Effect of T_{dp-int} on DP-Int systems in CM4

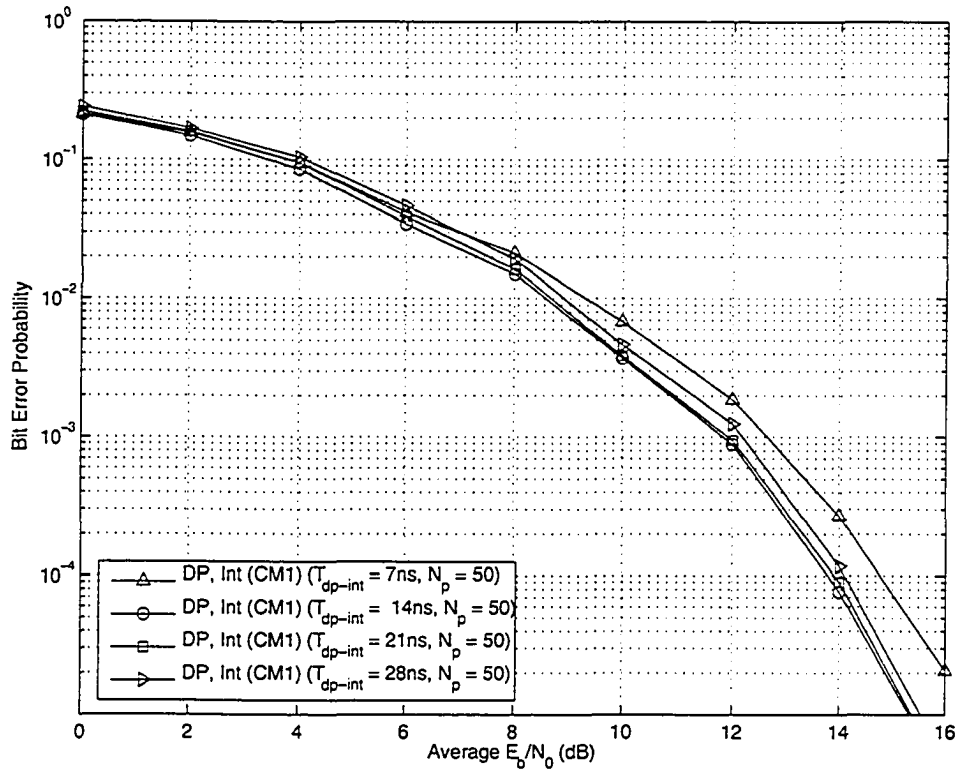


Figure 3.53: Effect of T_{dp-int} on DP-Int systems with noise averaging in CM1

This is because at sufficiently high SNR, the more paths the receiver collects even if it is a weaker path, would still increase the signal to noise ratio of the decision variable and thus increase the performance of the system.

3.4.13 Performance Comparison between TR, GSC, AT-GSC, NT-GSC and DP-Int Receivers

In this section, the DP system with different combining schemes and the DP-Int system are compared with the TR system of Chapter 2 over CM1-CM4. The integration length T_{tr} and T_{dp-int} of the TR system and DP-Int system respectively are set to equal to the maximum delay spread T_{mds} defined in Section 2.5. The GSC receiver scheme is set to collect about half of all the autocorrelator results (i.e. $L \approx \frac{L_t}{2}$). The AT-GSC scheme is simulated with

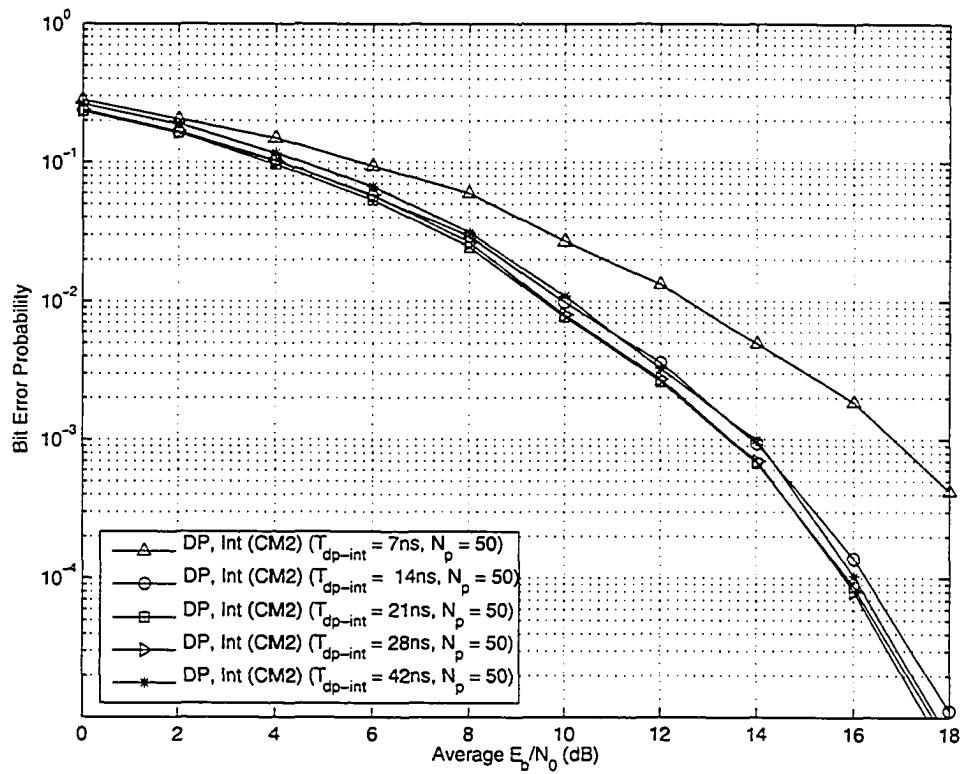


Figure 3.54: Effect of T_{dp-int} on DP-Int systems with noise averaging in CM2

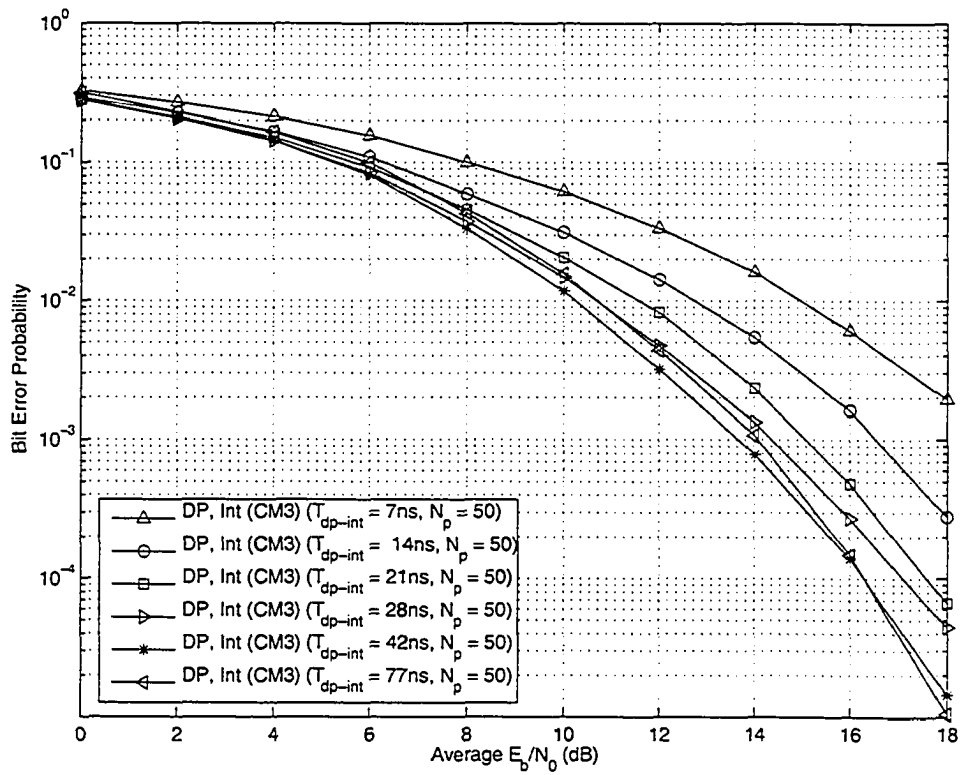


Figure 3.55: Effect of T_{dp-int} on DP-Int systems with noise averaging in CM3

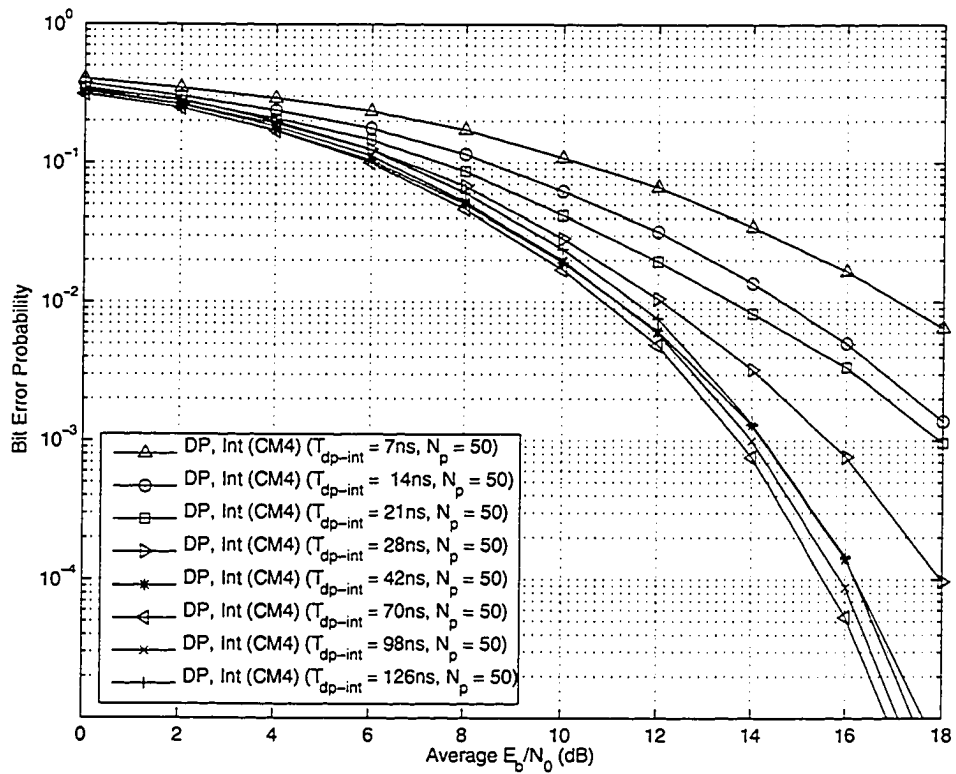


Figure 3.56: Effect of T_{dp-int} on DP-Int systems with noise averaging in CM4

the absolute threshold $D_{th} = 1.5$ for the receiver without noise averaging and $D_{th} = 0.1$ for the $N_p = 50$ case. Finally, the NT-GSC uses a threshold fraction $\eta_{th} = 0.1$. The settings for the DP systems are selected based on best overall performance achievable for that scheme in CM1-CM4.

Fig. 3.57 shows that the TR system slightly outperforms the DP system with and without noise averaging for CM1. This is likely due to the channel property of CM1, where the strong paths arrive at tightly packed groups, an example shown in Fig. 2.8. These closely spaced paths will create interference between the reference and data signals. As mentioned in Section 3.3.2 that the noise averaging will reduce the interference on the reference sub-pulse, hence the performance gap between the DP receiver and the TR receiver with $N_p = 50$ is closer than when $N_p = 1$. However the data pulse still suffers from certain degree of interference, and therefore the performance is still a bit worse than the TR system. Figs. 3.58-3.60 demonstrate that the performance of the DP system with GSC, AT-GSC, and NT-GSC combining, as well as DP-Int receiver is slightly inferior to the TR receiver when noise averaging is not applied. At $\text{BER} = 10^{-3}$ the performance gap between the DP system regardless of the receiver types and the TR system is 0.5 to 1 dB for CM2-CM4. However, for CM2-CM4, the DP receivers with noise averaging in Figs. 3.58-3.60 show performances that are very close to the TR system, with the gap being less than 0.5 dB at $\text{BER} = 10^{-3}$.

3.5 Conclusion

In this chapter, a novel signalling technique named DP is presented and thoroughly analysed together with three selection combining schemes. The new DP scheme retained the desirable properties of the TR system such as circumventing the need to estimate the multipath gains and the multipath delays and relaxed timing requirement. The DP scheme also doubles the data rate of the conventional TR system. It is less sensitive to time variation of the chan-

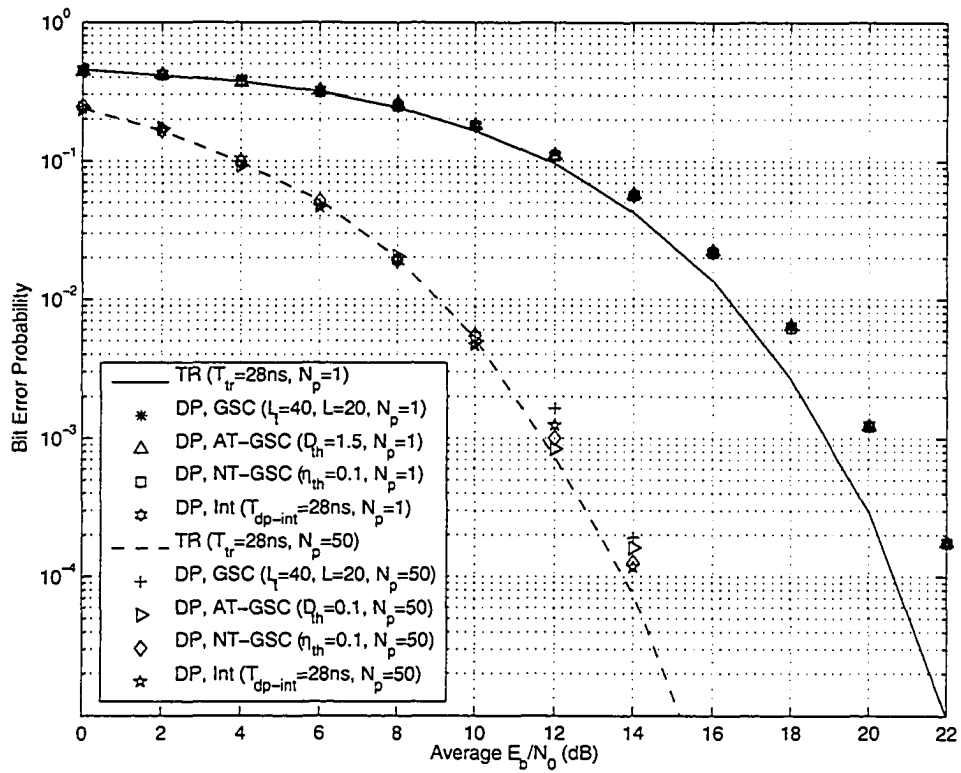


Figure 3.57: Comparison between TR and proposed DP systems for CM1

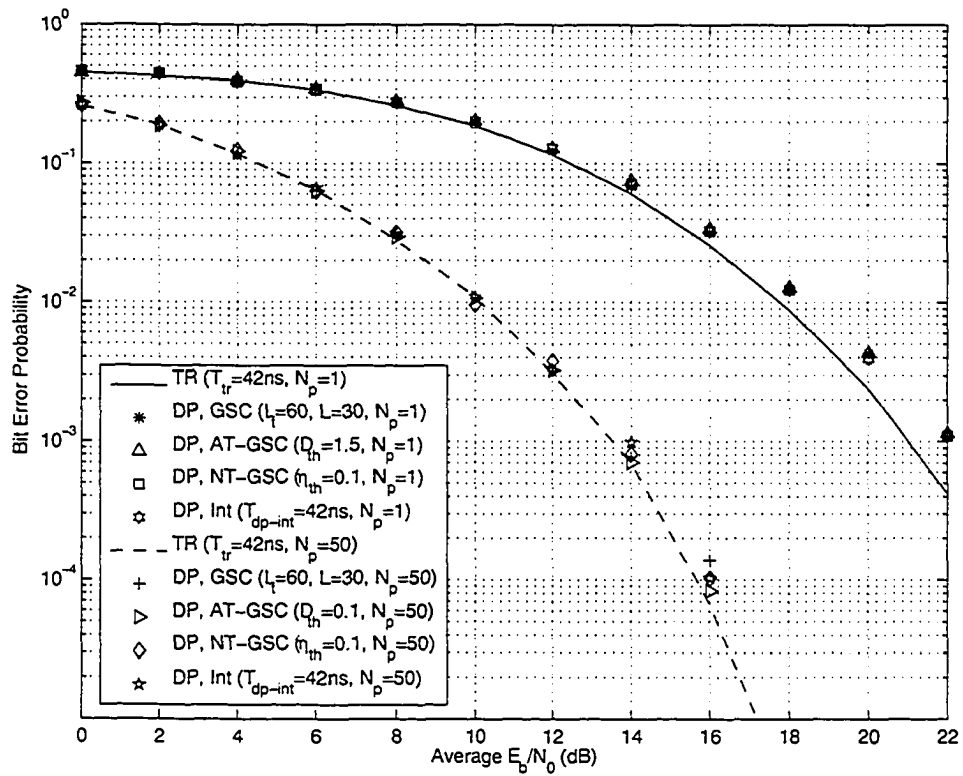


Figure 3.58: Comparison between TR and proposed DP systems for CM2

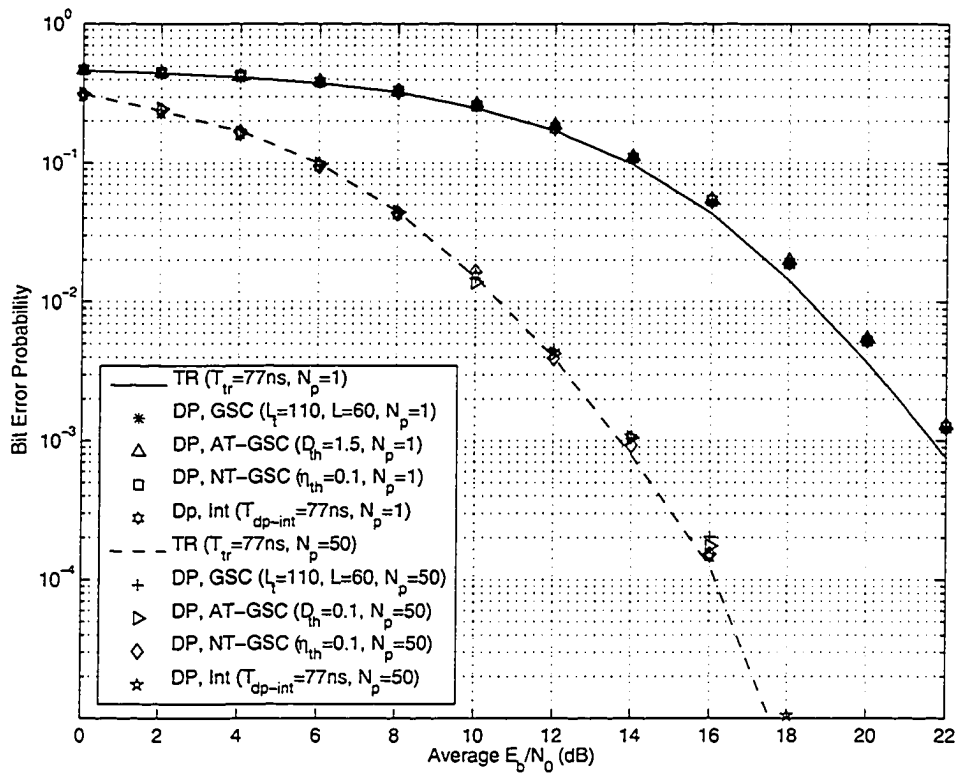


Figure 3.59: Comparison between TR and proposed DP systems for CM3

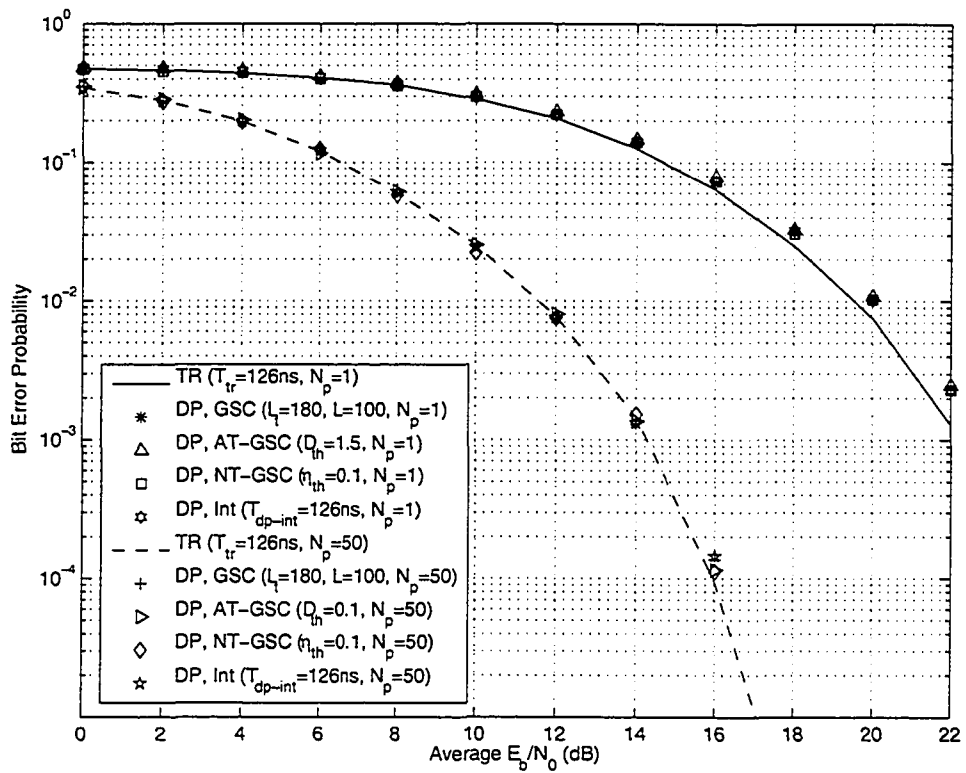


Figure 3.60: Comparison between TR and proposed DP systems for CM4

nel than the TR system because there is no time gap between the reference sub-pulse and data sub-pulse. On top of that the DP system needs shorter delay than the TR system. Each combining scheme shown in this chapter has its own unique properties. The GSC scheme offers consistent performance with minimal autocorrelator results combined regardless of channel properties. The AT-GSC scheme provides easy implementation with an absolute threshold, whose value varies with channel properties, while the NT-GSC scheme like the GSC scheme is well adapted to different channel scenarios. The DP-Int autocorrelator receiver however is able to achieve similar performance as the “GSC” receivers while providing a simpler receiver design. When the DP systems are compared with the TR system, it shows that their performances are very similar in most cases, especially in channels with high number of paths such as CM3 and CM4. In conclusion, the DP system proposed is a better solution than the TR system with the doubled data rate, easier implementation, smaller latency, and greater robustness to channel time variation, while keeping the similar performance to the TR system.

Chapter 4

The Improved DP System

4.1 Introduction

In the previous chapter, a transmission and detection scheme based on the DP pulse was introduced and compared with the conventional TR system. The proposed DP scheme has been shown with various degree of performance gaps when compared to the TR system for all the channel models presented. While system without noise averaging in general have a larger performance gap than the system with noise averaging. This is because in practice, some of the channel paths are spaced much closer than the pulse width T_w which leads to self interference between the reference sub-pulse and the data sub-pulse, also referred to as interpath interference. In this chapter, an improved system based on the DP scheme is proposed and compared with the TR system. Similar to the TR and DP scheme, the improved DP (*iDP*) scheme does not require the knowledge of either channel path delays or path strengths. This eliminates the need for channel estimation in the system design. The *iDP* scheme is a modified version of the DP scheme with $N_s = 2$. This modification allows the *iDP* scheme to cancel out the self interference between the reference sub-pulse and the data sub-pulse due to closely spaced channel paths. The result is a received reference sub-pulse and a received data sub-pulse that are free from interference caused by each other. Without the self interference between the reference sub-pulse and data sub-pulse, a better performance can be achieved.

In Section 4.2, the proposed *i*DP transmission scheme is described in detail. The receiver design of the DP scheme is modified for the *i*DP scheme in Section 4.3. The three proposed combining schemes (GSC, AT-GSC and NT-GSC) together with the autocorrelator receiver design (DP-Int) are also adopted in the *i*DP scheme. Section 4.4 presents the performance simulation of the *i*DP scheme and compares the results with the conventional TR system. To illustrate the performance improvement of the *i*DP system over the DP system of Section 3, the performance of the *i*DP system is compared with the DP system with $N_s = 2$ in Section 4.4.3.

4.2 Improved DP System Overview

As mentioned in the introduction, the *i*DP scheme requires the modified DP signal pulse to be transmitted twice (i.e., $N_s = 2$). This scheme, however, will not only double the received SNR for detection, but it will also eliminate the interference between the received reference sub-pulse and data sub-pulse. Using binary PAM, the *i*DP scheme works by transmitting two pulses, $g_1(t)$ and $g_2(t)$. The first pulse $g_1(t)$ has the identical pulse shape as $g_{dp}(t)$ (3.2) of the DP scheme. However, the reference sub-pulse of the second pulse $g_2(t)$ is inverted while the data sub-pulse left unchanged as in $g_1(t)$. An illustration of the *i*DP pulses is presented in Fig. 4.1, where the two pulses, $g_1(t)$ and $g_2(t)$ are processed as one unit. The *i*DP pulses are given by

$$g_1(t) = p(t) + b_1 \cdot p\left(t - \frac{T_w}{2}\right), \quad 0 \leq t \leq T_w \quad (4.1)$$

$$g_2(t) = -p(t) + b_1 \cdot p\left(t - \frac{T_w}{2}\right), \quad 0 \leq t \leq T_w. \quad (4.2)$$

The resulting information processing unit for the *i*DP scheme is

$$g_{idp}(t) = g_1(t) + g_2(t - T_f). \quad (4.3)$$

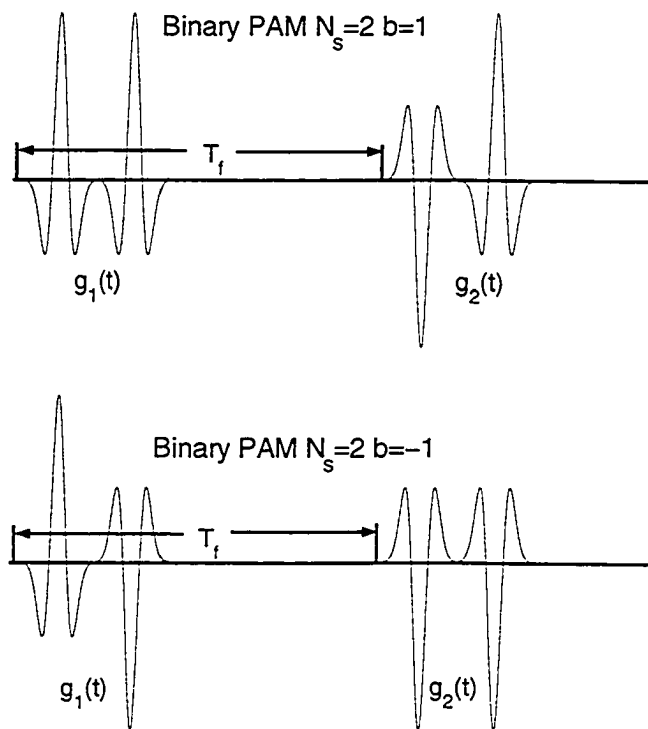


Figure 4.1: Illustration of binary PAM modulated iDP signal set $g_1(t)$ and $g_2(t)$

The received processing unit of the i DP scheme can be represented as

$$\begin{aligned}
r_{idp}(t) &= g_{idp} * h(t) + n(t) \\
&= g_1(t) * h(t) + g_2(t - T_f) * h(t) + n(t) \\
&= p(t) * h(t) + b_1 p(t - \frac{T_w}{2}) * h(t) \\
&\quad - p(t - T_f) * h(t) + b_1 p(t - T_f - \frac{T_w}{2}) * h(t) + n(t) \quad (4.4)
\end{aligned}$$

where the channel response $h(t)$ is assumed to be static for at least two time frame $2T_f$ and $n(t)$ is a filtered zero mean white Gaussian noise. The received signal $r_{idp}(t)$ can then be generalised into two received signal $r_1(t)$ and $r_2(t)$ given by

$$\begin{aligned}
r_{idp}(t) &= r_1(t) + r_2(t) \\
r_1(t) &= g_1(t) * h(t) + n_1(t), 0 \leq t \leq T_f \quad (4.5)
\end{aligned}$$

$$r_2(t) = g_2(t - T_f) * h(t) + n_2(t), T_f \leq t < 2T_f. \quad (4.6)$$

The received signal is then demodulated with a modified DP receiver shown in next section.

4.3 Receiver Design

The receiver design of the i DP scheme is similar to the DP receiver aside from an added structure that is used to cancel out the interference between the reference sub-pulse and data sub-pulse. To cancel the interference between sub-pulses, a T_f -delayed copy of the first received pulse $r_1(t)$ is added to the second received pulse $r_2(t)$ to obtain the interpath interference free data sub-pulse $r_{dat}(t)$. Since the reference sub-pulse of the second pulse $r_2(t)$ is inverted at the transmitter, therefore adding $r_1(t)$ and $r_2(t)$ together given they have the same channel response $h(t)$ would result in complete destructive addition of the two reference sub-pulses and complete constructive addition of the two data sub-pulses. With the same idea, the interpath interference free reference sub-pulse $r_{ref}(t)$ is then obtained by adding the T_f -delayed first pulse $r_1(t)$

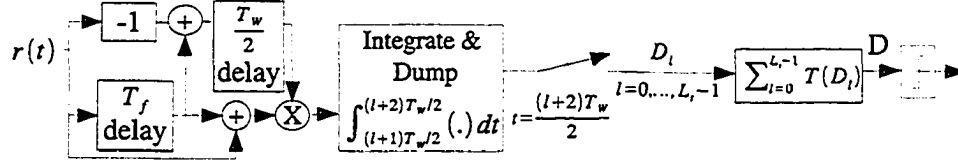


Figure 4.2: Block diagram for *i*DP receiver design

to an inverted second pulse $-r_2(t)$. The block diagram of the *i*DP scheme receiver is shown in Fig. 4.2. As shown in the diagram, once $r_{ref}(t)$ and $r_{dat}(t)$ are obtained, the rest of the receiver is the same as the receiver for the DP scheme in Chapter 3. Since the channel impulse response is assumed to be static for two time frames (i.e., $h(t) = h(t - T_f)$, $T_f \leq t < 2T_f$), therefore the interpath interference free reference sub-pulse $r_{ref}(t)$ and data sub-pulse $r_{dat}(t)$ are given by

$$\begin{aligned}
 r_{ref}(t) &= r_1(t - T_f) - r_2(t) \\
 &= [g_1(t - T_f) * h(t - T_f) + n_1(t - T_f)] - [g_2(t - T_f) * h(t) + n_2(t)] \\
 &= [p(t - T_f) * h(t) + b_1 p(t - T_f - \frac{T_w}{2}) * h(t) + n_1(t - T_f)] \\
 &\quad - [-p(t - T_f) * h(t) + b_1 p(t - T_f - \frac{T_w}{2}) * h(t) + n_2(t)] \\
 &= 2p(t - T_f) * h(t) + n_1(t - T_f) + n_2(t), \quad T_f \leq t < 2T_f \quad (4.7)
 \end{aligned}$$

and

$$\begin{aligned}
 r_{dat}(t) &= r_1(t - T_f) + r_2(t) \\
 &= [g_1(t - T_f) * h(t - T_f) + n_1(t - T_f)] + [g_2(t - T_f) * h(t) + n_2(t)] \\
 &= [p(t - T_f) * h(t) + b_1 p(t - T_f - \frac{T_w}{2}) * h(t) + n_1(t - T_f)] \\
 &\quad + [-p(t - T_f) * h(t) + b_1 p(t - T_f - \frac{T_w}{2}) * h(t) + n_2(t)] \\
 &= 2b_1 p(t - T_f - \frac{T_w}{2}) * h(t) + n_1(t - T_f) + n_2(t), \quad T_f \leq t < 2T_f. \quad (4.8)
 \end{aligned}$$

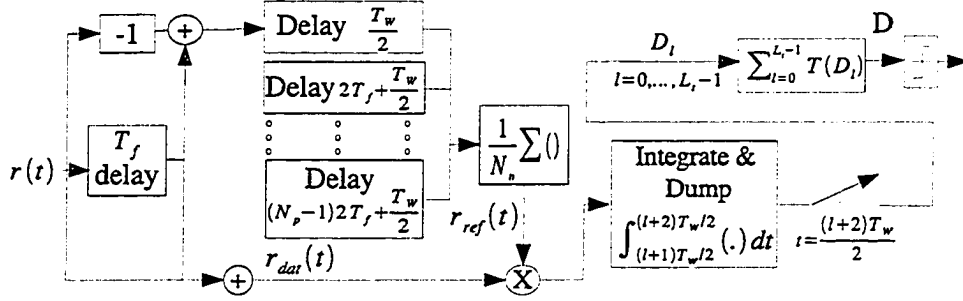


Figure 4.3: Block diagram for iDP receiver design with noise averaging

The autocorrelator result for each $\frac{T_w}{2}$ interval, D_l , is then represented by

$$D_l = \int_{l\frac{T_w}{2} + \frac{T_w}{2}}^{(l+1)\frac{T_w}{2} + T_w} r_{ref}(t - \frac{T_w}{2}) r_{dat}(t) dt. \quad (4.9)$$

The resulting D_l 's can then be combined with one of the three proposed combining methods (GSC, AT-GSC and NT-GSC) in Chapter 3 to create the decision variable D . The decision variable D can also be generated by defining $D = \int r_{ref}(t - \frac{T_w}{2}) r_{dat}(t) dt$ and integrating over the whole time frame as in the TR and DP-Int receiver design.

In both the TR system and the DP system proposed in earlier chapters, the noise averaging technique was applied to the received signal to lower the noise variance of the reference signal, and thus improves the system performance. The noise averaging technique can also be used in the iDP system to improve the system performance. A receiver block diagram with noise averaging is presented in Fig. 4.3. The noise averaging in this case is applied to the reference signal $r_{ref}(t)$. In next section, the performances of the iDP receiver with and without noise averaging are simulated and compared to the TR system as well as the DP system with $N_s = 2$.

4.4 Simulation Results and Discussion

In the simulation, the iDP signals are transmitted over the four realistic IEEE channel models (CM1-CM4). The GSC, AT-GSC and NT-GSC combining

schemes together with an autocorrelator design are used in the *i*DP receivers. The performance of the *i*DP receiver with different combining schemes is then simulated and compared to the TR system with $N_s = 2$. The *i*DP receiver with the noise averaging technique is also studied. The performances of the *i*DP and the DP scheme with $N_s = 2$ are also compared head to head to show the improvement obtained with the *i*DP scheme.

4.4.1 Simulation Setup

For the simulation, the parameters are defined the same as in Section 3.4.1 except that the maximum number of bits simulated is increased to 4×10^6 from 2×10^6 for improved accuracy. Note that the receiver design of the *i*DP system is a modified DP system with $N_s = 2$ with noise averaging applied on $r_{ref}(t)$. In order to compare with the TR and the DP system fairly, the transmitter and receiver design of the TR and the DP system are modified, respectively. The TR system for the simulation is set to transmit with $N_s = 2$, so the same reference and data signal pair is transmitted twice. At the receiver, the first received signal pair (i.e., reference pulse and data pulse occupying $2T_f$) will be delayed by $2T_f$ and added to the second received signal pair. The resultant value will be used as input to the TR receiver shown in Fig. 2.3. The noise averaging technique for the TR system will then be applied to the summed received TR signal. This resulted in delay tap changes of the noise averaging module in Fig. 2.6. While the number of delay tap T_p would stay the same, the delay different between taps for the noise averaging module is now $4T_f$ instead of $2T_f$. The adjustment in the delay tap is to reflect the fact that N_s is now equal to two. For the DP receiver, the transmitter will transmit the same DP pulse in two time frames, and the receiver will be similar to the *i*DP receiver without applying the inverter when calculating the reference receiver signal $r_{ref}(t)$. For the simulation, the pulse length of the TR systems is defined as 0.7 ns and the DP and *i*DP systems have pulse length T_w defined at 1.4 ns. The SNR is defined as E_p/N_0 where $E_p = \frac{E_b}{N_s}$.

4.4.2 Comparison between Improved DP systems of various combining schemes and the TR system

The performance of the *i*DP scheme with GSC, AT-GSC, NT-GSC and DP-Int receiver in CM1-CM4 are plotted against the TR system in Figs. 4.4-4.7. The $N_s = 1$ results (i.e. the DP scheme) are plotted on the same graphs as well for comparison between the $N_s = 2$ case and the $N_s = 1$ case. The performances of the *i*DP receivers and the TR receiver with and without noise averaging ($N_s = 2$) are all shown in Figs. 4.4-4.7. Figs. 4.4-4.7 indicate that the performance of the *i*DP scheme is very close to the TR scheme for both receivers with noise averaging and receivers without noise averaging. This is an improvement over the DP scheme, as expected. The performance differences among the GSC, AT-GSC and NT-GSC combining schemes and the autocorrelation receiver design for the *i*DP scheme as shown in the figures are very minor. When comparing the TR systems of $N_s = 1$ and $N_s = 2$ in Figs. 4.4-4.7, the performance difference is roughly 3 dB for both receivers with and receivers without noise averaging technique in CM1 to CM4. This is expected because when the data is transmitted twice, it effectively doubles the transmission power used for each data, and thus should result in roughly 3 dB gain.

4.4.3 Comparison between Improved DP and DP systems

This subsection compares the performance of the DP system with $N_s = 2$ to the *i*DP system with $N_s = 2$ employing or not employing the noise averaging technique. The comparison is made with all the receiver designs presented so far (i.e. GSC, AT-GSC, NT-GSC, and DP-Int). Figs. 4.8-4.11 show the performance comparison between the DP scheme and the *i*DP scheme for CM1 to CM4 respectively. For all the plots, it is evident that *i*DP scheme is able to get better performance than the DP scheme, especially in receiver without noise averaging technique. In Fig. 4.8 for CM1, it shows that the *i*DP

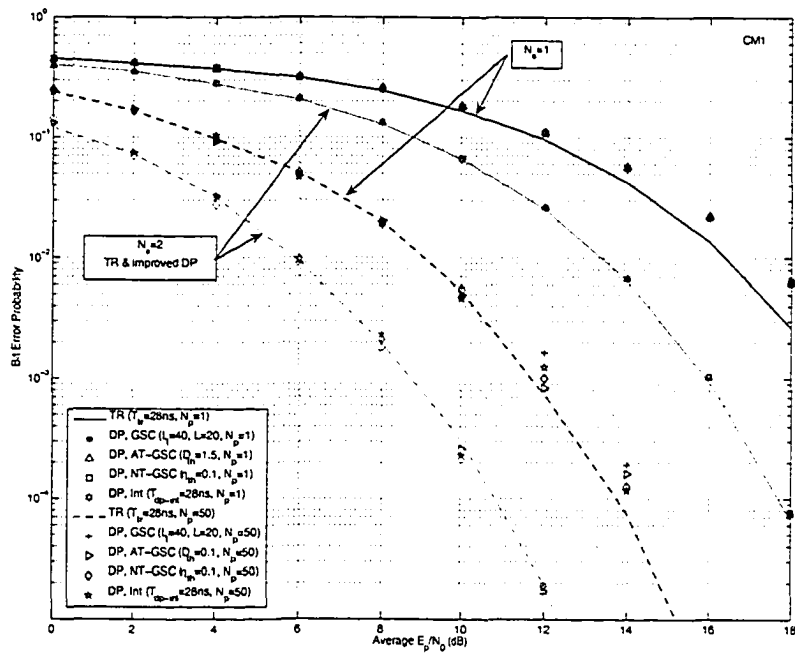


Figure 4.4: Comparison between TR and proposed *i*DP systems for CM1

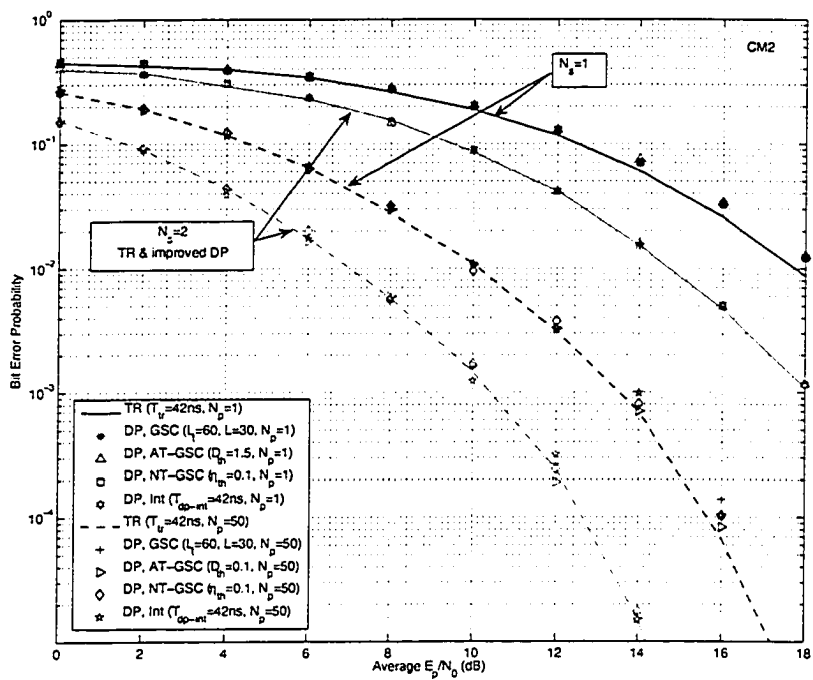


Figure 4.5: Comparison between TR and proposed *iDP* systems for CM2

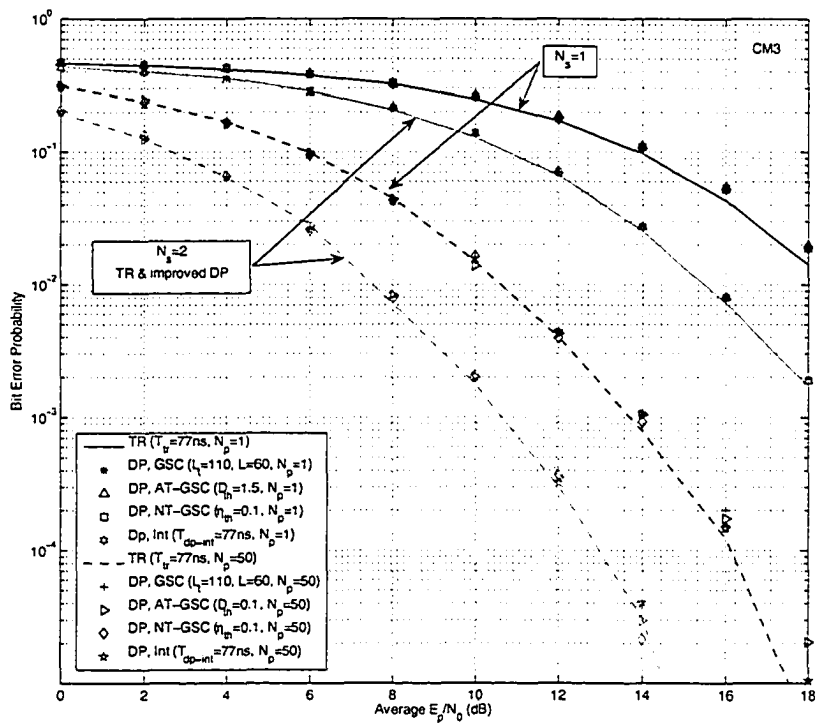


Figure 4.6: Comparison between TR and proposed iDP systems for CM3

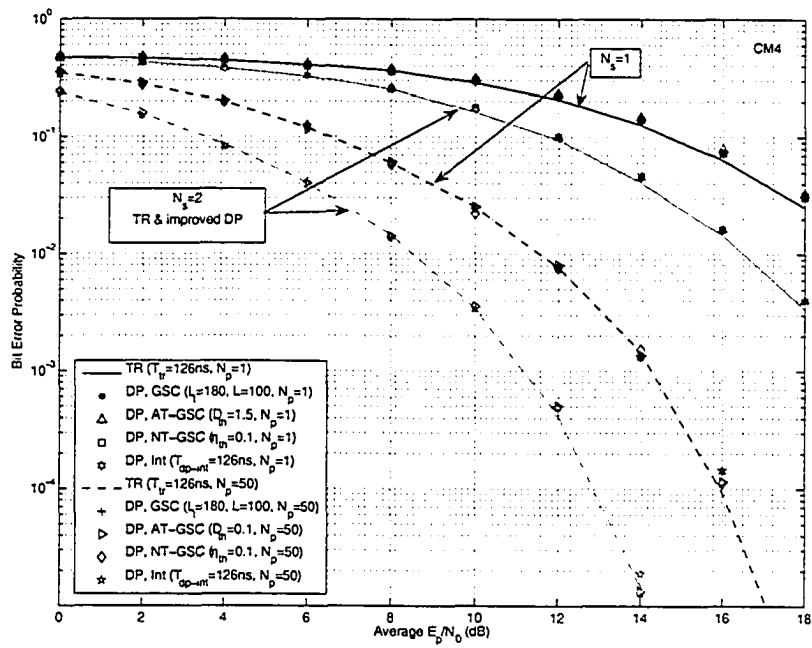


Figure 4.7: Comparison between TR and proposed iDP systems for CM4

scheme outperforms the DP scheme by as much as 1 dB at $\text{BER} = 10^{-2}$ for receivers without noise averaging. This performance improvement is due to the cancellation of the interference between the reference sub-pulse and the data sub-pulse. Fig. 4.11 shows that in CM4, the *i*DP scheme outperforms the DP scheme by only 0.5 dB at $\text{BER} = 10^{-2}$ for receivers without noise averaging. This is less than in CM1, which indicates that the interference between the reference sub-pulse and data sub-pulse is less severe in CM4 than CM1. The plots also show that with noise averaging, the performance improvement of the *i*DP scheme to the DP scheme is generally less than receivers without noise averaging for all channel models. This re-enforces the previous observation in Section 3.3.2 that noise averaging helps to reduce the interference between the reference and the data sub-pulses. Overall, these figures indicate that the interpath interference in the DP system is not very severe, especially for CM2-CM4. It is also expected that the performance gaps among different combining methods will be more pronounced at high SNR's.

4.5 Conclusion

In this chapter, an improved version of the proposed DP scheme is presented. The *i*DP scheme retains all the advantages of the DP scheme, except that it now requires to transmit with $N_s = 2$ or N_s equals multiples of two. The *i*DP scheme also requires a receiver design that is a bit more complicated. However, with this modification, the possible interference between the received reference sub-pulse and the data sub-pulse is eliminated, resulting in better performance. The simulation results show that the BER performance of the *i*DP system relative to the TR system is better than the regular DP system. It is also shown that the *i*DP scheme achieves better performance than the DP scheme with $N_s = 2$. Overall, in channel models with large amount of closely packed paths arriving at intervals shorter than T_w , the *i*DP scheme will be a definite advantage over the regular DP scheme due to its interference

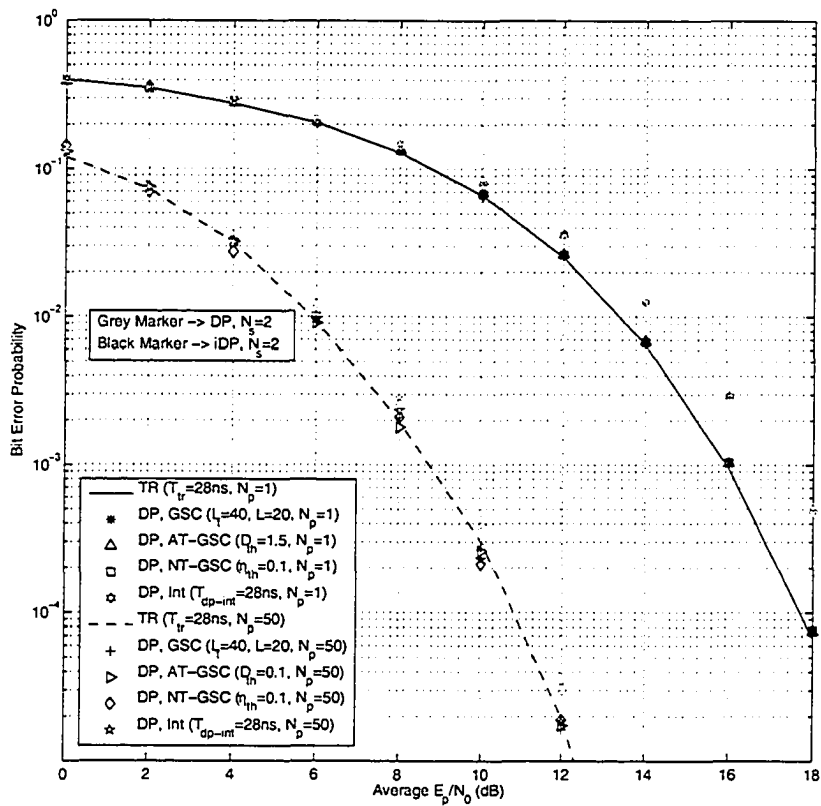


Figure 4.8: Comparison between DP and *i*DP systems for CM1

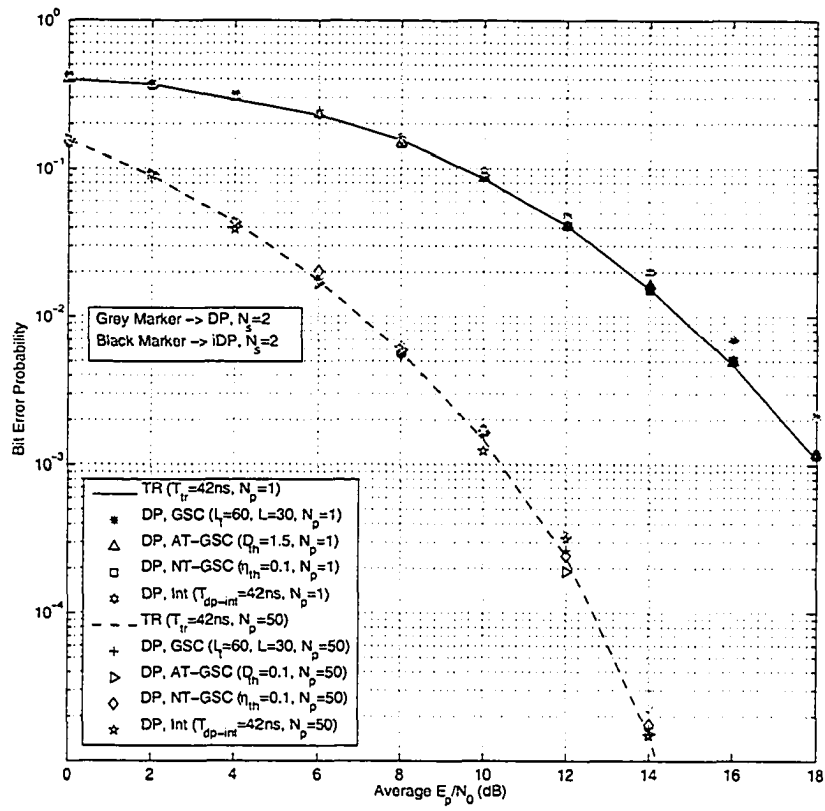


Figure 4.9: Comparison between DP and *i*DP systems for CM2

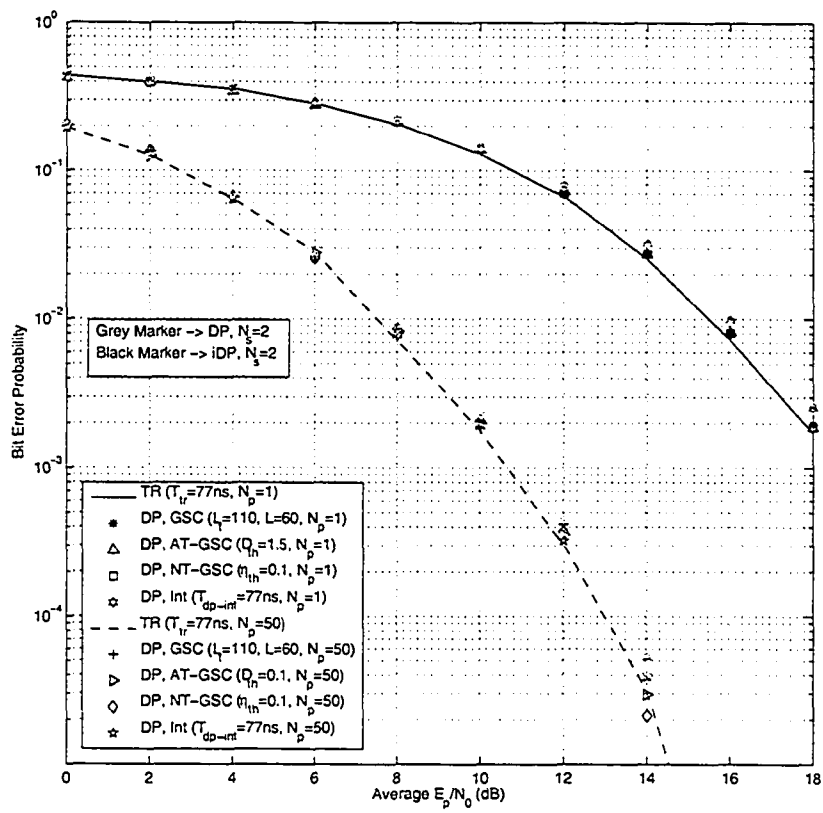


Figure 4.10: Comparison between DP and *i*DP systems for CM3

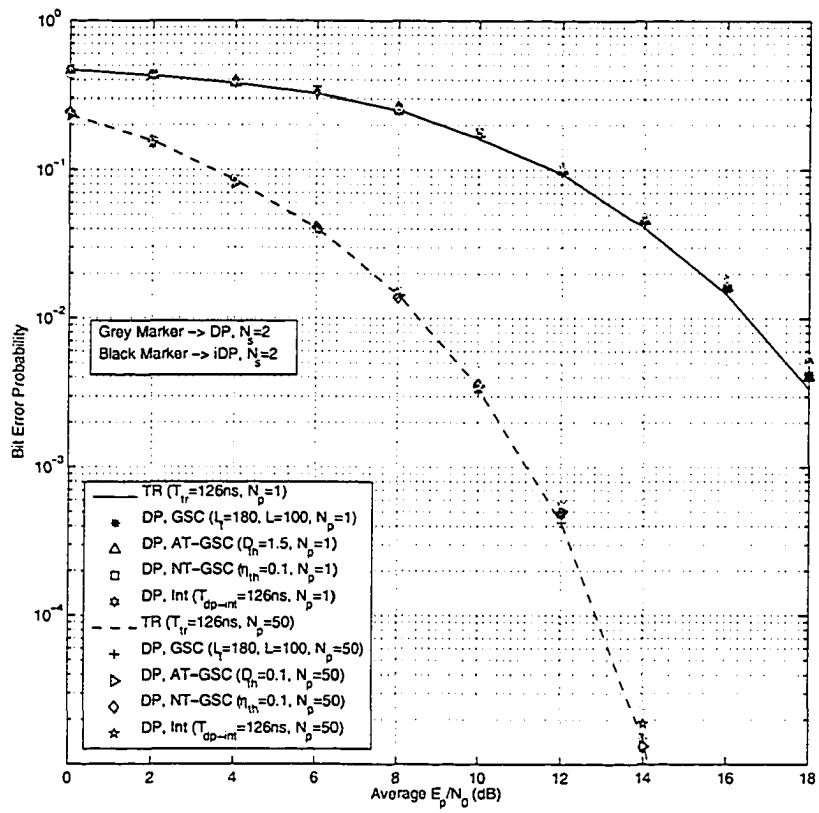


Figure 4.11: Comparison between DP and *i*DP systems for CM4

cancelling property.

Chapter 5

Summaries and Conclusion

The demand for high speed communication has driven communication systems to use wider bandwidth to accommodate the increased data rate requirement. UWB is a promising physical layer candidate for future wireless communications systems because of the enormous bandwidth available. There is currently no clear choice of receiver design for UWB communication systems. The two distinguishable receiver types are rake type receiver designs and autocorrelation type receiver designs such as the TR transmission scheme. In this thesis, the error performances of the novel DP transmission scheme have been analysed, simulated and compared against the TR scheme. The error performances of the the *i*DP transmission scheme which represents an improved version of the DP scheme are also simulated and compared. A summary of conclusions followed by suggestions for further research are presented in this chapter.

5.1 Conclusion

1. The TR system has been presented and simulated with the IEEE UWB channel models. The integration length T_{tr} of the autocorrelation receiver has been shown to have a big impact on the performance of the TR system. The longer the integration length T_{tr} will yield better performance up to a certain point. Beyond that point, further increasing the integration length T_{tr} up to the entire time frame T_f will actually

lead to performance degradation, especially in lower SNRs.

2. The novel DP signalling scheme based on the TR scheme has been presented and discussed in detail. The DP scheme combines the reference sub-pulse and data sub-pulse into a DP pulse for transmission in one time frame T_f . Therefore, the DP scheme is able to double the data rate of the TR scheme.
3. Three non-coherent autocorrelation receivers based on different selection combining schemes (GSC, AT-GSC, and NT-GSC) have been presented for the DP UWB system. Each combining scheme is analysed and its error performance conditioned on the path delays and path strengths is formulated. The error performance has been shown to be comparable to the TR scheme in most channels.
4. The effect of L on the GSC receiver has been studied by extensive simulations. It is concluded that the performance of the GSC receiver is affected by L up to a certain degree. For example, the performance improvement from increasing L is hardly noticeable as L becomes greater than 20. Therefore, it has been shown that a low L value (i.e., $L = 10$) will result in close to optimum performance of the GSC receiver in CM1.
5. The error performance of the AT-GSC receiver while varying the absolute decision threshold D_{th} has been studied with simulations in realistic channel models. The results show that the decision threshold has a great influence on the performance of the AT-GSC system, since it directly affects the amount of energy that the system collects. It is concluded that at higher SNRs, the lower the D_{th} will result in better AT-GSC receiver performance.
6. The impact of the normalized threshold η_{th} on the performance of the NT-GSC receiver has been obtained from simulations. The results have

shown that lowering the η_{th} will result in better performance for the NT-GSC receiver in the high SNR case.

7. The effect of the integration length T_{dp-int} on the performance of the DP-Int receiver has been investigated. The simulation results conclude that the effect of integration length on the autocorrelation receiver is similar to that of the TR signalling scheme. This implies that increase of T_{dp-int} will increase the system performance. However, beyond certain T_{dp-int} value increase of T_{dp-int} would worsen the DP-Int receiver performance.
8. An improved version of the DP scheme called the *i*DP scheme has been proposed and examined. This scheme eliminates the sub-pulse interference which degrades the performance of the DP scheme when compared with the TR scheme. Results from the realistic channel simulation based on the IEEE channel models show the *i*DP scheme has performance that matches the equivalent TR system while doubling the data rate.
9. The effect of noise averaging on the reference signal has been studied for all the proposed receivers and signalling schemes. The simulation results show that when the noise averaging technique is applied to the TR, DP, and *i*DP signalling scheme, the receiver performance is improved. The biggest performance gain from the noise averaging technique is when it goes from no noise averaging ($N_p = 1$) to averaging over 10 received reference signals ($N_p = 10$).

5.2 Suggestions for Future Work

The performance analysis and simulation in this thesis has been performed based on a single user scenario with binary PAM modulation. A multiuser access analysis will be a possible next step for this novel signalling scheme. The performance of the DP scheme with different signal modulation formats will also be an interesting topic to investigate.

Bibliography

- [1] *US Mobility Forecasts: 2004-2008*, Telecompetition, Inc., Mar. 2004. [Online]. Available: http://www.telecompetition.com/Products/ExecSum_Telecompetition_US_Mobility_Forecasts_2004.pdf
- [2] *Telecompetition Worldwide Mobility Report: 2003*, Telecompetition, Inc., Oct. 2003. [Online]. Available: http://www.telecompetition.com/Products/TOC_ExecSum_Telecompetition_IntlMobileRoaming2003.pdf
- [3] G. L. Stuber, *Principles of Mobile Communication*, 2nd ed. Norwell, MA: Kluwer Academic Publishers, 2001.
- [4] (2000, Apr.) Radiocommunications Agency UK. [Online]. Available: http://www.ofcom.org.uk/static/archive/spectrumbauctions/auction/auction_index.htm
- [5] (2004, Feb.) Canadian table of frequency allocations. Industry Canada. [Online]. Available: http://strategis.ic.gc.ca/epic/internet/insmt-gst.nsf/en/h_sf01678e.html
- [6] IEEE P802.11 Working Group for Wireless Local Area Networks. [Online]. Available: <http://grouper.ieee.org/groups/802/11/>
- [7] IEEE 802.15 WPAN Task Group 1 (TG1). [Online]. Available: <http://www.ieee802.org/15/pub/TG1.html>
- [8] Bluetooth - The official Bluetooth website. [Online]. Available: <https://www.bluetooth.com/>
- [9] Blueunplugged - wireless solution. [Online]. Available: http://www.blueunplugged.com/Products/Bluetooth_Phones.aspx
- [10] Apple Computer Inc. [Online]. Available: <http://www.apple.com/bluetooth/>
- [11] (2002, Apr.) Microsoft reveals world's first commercially available bluetooth desktop solution. Microsoft. [Online]. Available: <http://www.microsoft.com/presspass/press/2002/apr02/04-18BluetoothPR.asp>

- [12] The bluetooth car weblog. [Online]. Available: <http://bluetoothcar.typepad.com/main/>
- [13] M. Cetto. (2004, Dec.) Bluetooth gains speed. *Wireless Business & Technology*. [Online]. Available: <http://www.syscon.com/story/?storyid=47398&DE=1>
- [14] IEEE 802.15 WPAN High Rate Alternative PHY Task Group 3a (TG3a). [Online]. Available: <http://www.ieee802.org/15/pub/TG3a.html>
- [15] (2005, Jan.) Alereon introduces advanced 480 mbps ultra-wideband evaluation kit. Alereon, Inc. [Online]. Available: <http://www.alereon.com/press-room/press-releases/?pid=37>
- [16] L. Yang and G. B. Giannakis, "Ultra-wideband communications an idea whose time has come," *IEEE Signal Processing Magazine*, pp. 26–54, Nov. 2004.
- [17] M. Z. Win and R. A. Scholtz, "Impulse radio: How it works," *IEEE Communication Letters*, vol. 2, pp. 36–38, Feb. 1998.
- [18] *FCC First Report and Order: In the matter of Revision of Part 15 of the Commission's Rules Regarding Ultra-Wideband Transmission Systems, FCC 02-48*, FCC, Apr 2002. [Online]. Available: <http://www.fcc.gov>
- [19] K. Siwiak and D. McKeown, *Ultra-Wideband Radio Technology*. John Wiley & Sons, Ltd, 2004.
- [20] *Assessment of Ultra-Wideband (UWB) Technology, OSD/DARPA, Ultra-Wideband Radar Review Panel, R-6280*, July 1990.
- [21] G. Aiello and G. D. Rogerson, "Ultra-wideband wireless systems," *IEEE microwave magazine*, pp. 36–47, June 2003.
- [22] T. Barrett, "History of ultra wideband (uwb) radar and communications: Pioneers and innovators," *Proc. Progress in Electromagnetics Symposium 2000 (PIERS 2000)*, Cambridge, MA, July 2000.
- [23] F. Ramirex-Mireles, "Signal design for ultra-wide-band communications in dense multipath," *IEEE Transactions on Vehicular Technology*, vol. 51, pp. 1517–1521, Nov. 2002.
- [24] C.-C. Chui and R. A. Scholtz, "Optimizing tracking loops for uwb monocyces," in *Proceedings of the IEEE Global Telecommunications Conference, 2003*, vol. 1, Dec. 2003, pp. 425–430.
- [25] L. Zhao and A. M. Haimovich, "Capacity of m-ary ppm ultra-wideband communications over awgn channels," in *Proceedings of the IEEE 54th Vehicular Technology Conference, 2001*, vol. 2, Oct. 2001, pp. 1191–1195.
- [26] M. Z. Win, R. A. Scholtz, and M. A. Barnes, "Ultra-wide bandwidth signal propagation for indoor wireless communications," in *Proceedings of the IEEE 47th Vehicular Technology Conference, 1997*, vol. 3, May 1997, pp. 2243–2247.

- [27] L. Rusch, C. Prettie, D. Cheung, Q. Li, and M. Ho. Characterization of uwb propagation from 2 to 8 ghz in a residential environment. Intel Corporation, Intel Research Labs. [Online]. Available: <http://www.intel.com/technology/comms/uwb/docs.htm>
- [28] D. Cassioli, M. Z. Win, and A. F. Molisch, "The ultra-wide bandwidth indoor channel: From statistical model to simulations," *IEEE Journal on Selected Areas in Communications*, vol. 20, pp. 1247–1257, Aug. 2002.
- [29] A. F. Molisch, J. R. Foerster, and M. Pendergrass, "Channel models for ultrawideband personal area networks," *IEEE Wireless Communications*, vol. 10, pp. 14–21, Dec. 2003.
- [30] J. Foerster. (2003, Feb.) Channel modeling subcommittee report final. IEEE P802.15 Working Group for Wireless Personal Area Networks. [Online]. Available: http://grouper.ieee.org/groups/802/15/pub/2003/Mar03/02490r1P802-15_SG3a-Channel-Modeling-Subcommittee-Report-Final.zip
- [31] A. Saleh and R. Valenzuela, "A statistical model for indoor multipath propagation," *IEEE Journal on Selected Areas in Communications*, vol. SAC-5, pp. 128–137, Feb. 1987.
- [32] R. Scholtz, "Multiple access with time-hopping impulse modulation," in *MILCOM*, vol. 2, Oct. 1993, pp. 447–450.
- [33] F. Ramirez-Mireles, "Signal design for ultra wideband ppm communications," in *MILCOM*, vol. 2, Oct. 2002, pp. 1085–1088.
- [34] J. D. Choi and W. E. Stark, "Performance of ultra-wideband communications with suboptimal receivers in multipath channels," *IEEE Journal on Selected Areas in Communications*, vol. 20, pp. 1754–1766, Dec. 2002.
- [35] B. Berksoy and L. Wei, "Pulse waveform optimization for uwb systems with ppm on gaussian channels," in *Proceedings of the IEEE 58th Vehicular Technology Conference 2003, (VTC'03-Fall)*, vol. 5, Oct. 2003, pp. 3174–3178.
- [36] J. D. Choi and W. E. Stark, "Performance analysis of rake receivers for ultra-wideband communications with ppm and ooc in multipath channels," in *Proceedings of the IEEE International Conference on Communications (ICC 2002)*, vol. 3, 2002, pp. 1969–1973.
- [37] A. R. Forouzan, M. Nasiri-Kenari, and J. A. Salehi, "Performance analysis of ultrawideband time-hopping code division multiple access systems: Uncoded and coded schemes," in *Proceedings of the IEEE International Conference on Communications (ICC 2001)*, vol. 10, 2001, pp. 3017–3021.
- [38] P. Runkle, J. McCorkle, T. Miller, and M. Welborn, "Ds-cdma: The modulation technology of choice for uwb communications," in *Proceedings of the IEEE Conference on Ultra Wideband Systems and Technologies 2003*, Nov. 2003, pp. 364–368.

- [39] J. Balakrishnan, A. Batra, and A. Dabak, "A multi-band ofdm system for uwb communication," in *Proceedings of the IEEE Conference on Ultra Wideband Systems and Technologies 2003*, Nov. 2003, pp. 354–358.
- [40] M. Hamalainen, V. Hovinen, R. Tesi, J. H. J. Linatti, and M. Latva-aho, "On the uwb system coexistence with gsm900, umts/wcdma, and gps," *IEEE Journal on Selected Areas in Communications*, vol. 20, pp. 1712–1721, Dec. 2002.
- [41] L. D. Nardis, G. Giancola, and M.-G. Di Benedetto, "Power limits fulfillment and mui reduction based on pulse shaping in uwb networks," in *IEEE International Conference on Communications*, vol. 6, 2004, pp. 3576–3580.
- [42] A. C. Gordillo, G. T. F. de Abreu, and R. Kohno, "Band-limited frequency efficient orthogonal pulse shape modulation for uwb communications," in *IEEE Eighth International Symposium on Spread Spectrum Techniques and Applications*, 2004, pp. 498–502.
- [43] W. M. Lovelace and J. Townsend, "The effects of timing jitter and tracking on the performance of impulse radio," *IEEE Journal on Selected Areas in Communications*, vol. 20, pp. 1646–1651, Dec. 2002.
- [44] M. Z. Win and R. A. Scholtz, "Characterization of ultra-wide bandwidth wireless indoor channels: A communication-theoretic view," *IEEE Journal on Selected Areas in Communications*, vol. 20, pp. 1613–1627, Dec. 2002.
- [45] N. Boubaker and K. Letaief, "A low complexity mmse-rake receiver in a realistic uwb channel and in the presence of nbi," in *Wireless Communications and Networking, 2003*, vol. 1, 2003, pp. 233 – 237.
- [46] A. Rajeswaran, V. Somayazulu, and J. R. Foerster, "Rake performance for a pulse based uwb system in a realistic uwb indoor channel," in *Proceedings of the IEEE International Conference on Communications, (ICC'03)*, vol. 1, May 2003, pp. 2879 – 2883.
- [47] D. Cassioli, M. Z. Win, F. Vatalaro, and A. F. Molisch, "Performance of low-complexity rake reception in a realistic uwb channel," in *Proceedings of the IEEE International Conference on Communications, (ICC'02)*, vol. 2, May 2002, pp. 763–767.
- [48] B. Mielczarek, M.-O. Wessman, and A. Svensson, "Performance of coherent uwb rake receivers using different channel estimators," in *Proceedings of the IEEE 58th Vehicular Technology Conference 2003, (VTC'03-Fall)*, vol. 3, Oct. 2003, pp. 1880–1884.
- [49] Y.-L. Chao and R. A. Scholtz, "Optimal and suboptimal receivers for ultra-wideband transmitted reference systems," in *Proc. IEEE Global Telecommunications Conference 2003, (GLOBECOM'03)*.
- [50] L. Yang and G. B. Giannakis, "Optimal pilot waveform assisted modulation for ultrawideband communications," *IEEE Transactions on Communications*, vol. 3, pp. 1236–1249, July 2004.

- [51] IEEE 802.15 WPAN Low Rate Alternative PHY Task Group 4a (TG4a). [Online]. Available: <http://www.ieee802.org/15/pub/TG4a.html>
- [52] R. Hoor and H. Tomlinson, "Delay-hopped transmitted-reference communications," in *Proc. IEEE Conference on Ultra Wideband Systems and Technologies*, May 2002, pp. 265–269.
- [53] N. v. Stralen, A. Dentinger, K. Welles II, R. Gaus Jr., R. Hoor, and H. Tomlinson, "Delay-hopped transmitted-reference experimental results," in *Proc. IEEE Conference on Ultra Wideband Systems and Technologies*, May 2002, pp. 93–98.
- [54] H. Zhang and D. L. Goeckel, "Generalized transmitted-reference uwb systems," in *Proc. IEEE Conference on Ultra Wideband Systems and Technologies 2003*, Nov. 2003, pp. 147 – 151.
- [55] S. Franz and U. Mitra, "On optimal data detection for uwb transmitted reference systems," in *Proc. IEEE Global Telecommunications Conference 2003, (GLOBECOM'03)*.
- [56] A. Trindade, Q. H. Dang, and A.-J. van der Veen, "Signal processing model for a transmit-reference uwb wireless communication system," in *Proc. IEEE Conference on Ultra Wideband Systems and Technologies 2003*.
- [57] A. Papoulis and S. U. Pillai, *Probability, Random Variables and Stochastic Processes*, 4th ed. Boston: McGraw Hill, 2002.
- [58] M. K. Simon, S. M. Hinedi, and W. C. Lindsey, *Digital Communication Techniques: Signal Design and Detection*. Upper Saddle River, NJ: Prentice Hall, 1995.
- [59] M. Z. Win and R. A. Scholtz, "Ultra-wide bandwidth time-hopping spread-spectrum impulse radio for wireless multiple-access communications," *IEEE Transactions on Communications*, vol. 48, pp. 679–689, Apr. 2000.
- [60] S. K. Mitra, *Digital Signal Processing: A Computer-Based Approach, 2nd edition*. McGraw-Hill, 2001.
- [61] M. Ho, V. Somayazulu, J. Foerster, and S. Roy, "A differential detector for an ultra-wideband communications system," in *Proceedings of the IEEE 55th Vehicular Technology Conference 2002, (VTC'02-Spring)*, vol. 4, May 2002, pp. 1896–1900.
- [62] L. Xiao and X. Dong, "Probability space partition based unified analysis on generalized selection combining with normalized threshold test per branch over generalized fading channels," submitted.
- [63] X. Dong, A. Lee, and L. Xiao, "A new uwb dual pulse transmission and detection technique," submitted.
- [64] C. W. Helstrom, "Calculating error probabilities for intersymbol and cochannel interference," *IEEE Transactions on Communications*, vol. COM-34, pp. 430–435, May 1986.

- [65] J. Weideman, "Computation of the complex error function," *SIAM J. Numerical Analysis*, vol. 31, pp. 1497–1518, Oct. 1994.
- [66] M. K. Simon and M.-S. Alouini, "Performance analysis of generalized selection combining with threshold test per branch (t-gsc)," *IEEE Transactions on Vehicular Technology*, vol. 51, pp. 1018–1029, Sept. 2002.